Russian Original Vol. 30, No. 6, June, 1971

Translation published December, 1971

ILLEGIB

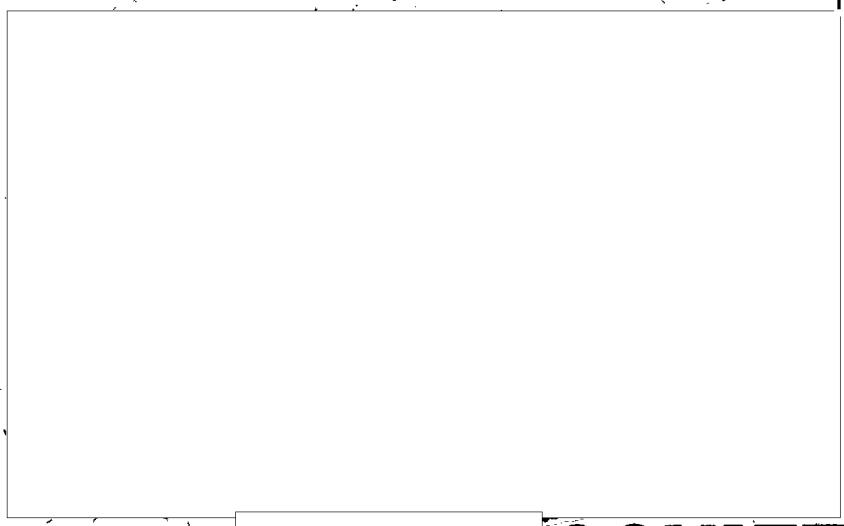

ILLEGIB

SOVIET ATOMIC ENERGY

АТОМНАЯ ЭНЕРГИЯ
(ATOMNAYA ÉNERGIYA)

TRANSLATED FROM RUSSIAN

c/b CONSULTANTS BUREAU, NEW YORK

SOVIET ATOMIC ENERGY

Soviet Atomic Energy is a cover-to-cover translation of *Atomnaya Énergiya*, a publication of the Academy of Sciences of the USSR.

An arrangement with Mezhdunarodnaya Kniga, the Soviet book export agency, makes available both advance copies of the Russian journal and original glossy photographs and artwork. This serves to decrease the necessary time lag between publication of the original and publication of the translation and helps to improve the quality of the latter. The translation began with the first issue of the Russian journal.

Consultants Bureau journals appear about six months after the publication of the original Russian issue. For bibliographic accuracy, the English issue published by Consultants Bureau carries the same number and date as the original Russian from which it was translated. For example, a Russian issue published in December will appear in a Consultants Bureau English translation about the following June, but the translation issue will carry the December date. When ordering any volume or particular issue of a Consultants Bureau journal, please specify the date and, where applicable, the volume and issue numbers of the original Russian. The material you will receive will be a translation of that Russian volume or issue.

Subscription
$67.50 per volume (6 issues)
2 volumes per year
(Add $5 for orders outside the United States and Canada.)

Single Issue: $30
Single Article: $15

CONSULTANTS BUREAU, NEW YORK AND LONDON

227 West 17th Street
New York, New York 10011

Davis House
8 Scrubs Lane
Harlesden, NW10 6SE
England

Second-class postage paid at Jamaica, New York 11431.

SOVIET ATOMIC ENERGY

A translation of *Atomnaya Énergiya*
Translation published December, 1971

Volume 30, Number 6 June, 1971

CONTENTS

	Engl.	Russ.
Andrei Kapitonovich Krasin (on His Sixtieth Birthday)	607	489
Improvement of Physical Characteristics of Fast Plutonium Reactors by Using U^{233} and Thorium – A. I. Leipunskii, L. N. Yurova, S. B. Bobrov, V. M. Murogov, L. V. Tochenyi, M. F. Troyanov, and A. N. Shmelev	609	491
Experimental Determination of the Starting Conditions for a Single-Circuit Loop with Natural Circulation – V. M. Selivanov, V. G. Konochkin, N. P. Dormidontov, and V. N. Smyslov	616	498
The Principal Neutron-physical Lattice Parameters of a VVR-SM Type Reactor – E. T. Józefewicz	621	503
Noise Associated with Inhomogeneities in the Heat Carrier of a Reactor – – A. I. Mogil'ner	629	510
Design of the JINR Four-Meter Isochronous Cyclotron with Smoothly Regulated Heavy-Ion Energies – I. A. Shelaev, E. D. Vorob'ev, B. A. Zager, S. I. Kozlov, V. I. Kuznetsov, R. Ts. Oganesyan, Yu. Ts. Oganesyan, K. I. Semin, A. N. Filipson, and V. A. Chugreev	635	514
System for Slow Steering of Accelerated Beam onto Internal Targets in the IHEP 70-GeV Accelerator – V. I. Gridasov, A. A. Kardash, K. M. Kozlov, O. V. Kurnaev, V. V. Lapin, S. V. Lobanov, L. L. Moizhes, K. P. Myznikov, and A. A. Naumov	641	520
REVIEWS		
Nuclear Power Engineering and Thorium Resources – I. V. Chirkov	647	526
ABSTRACTS		
Determination of the Dynamic Characteristics of Fuel Cells – I. I. Morozov and V. P. Kaz'min	655	534
The Viscosity of Heavy Water at High Pressures in the 100-275°C Temperature Range – N. A. Agaev, A. M. Kerimov, and Azad Abas-Zade	655	534
Simultaneous Determination of Lead, Copper, and Zinc in Samples of Polymetallic Ores and Products of Their Processing by an Activation Method – L. V. Navalikhin, V. A. Kireev, Yu. N. Talanin, and G. S. Nikonorov	656	535
Distribution of Neutrons Emitted from a Point Source and Slowed Down in a System of Two Media with a Plane Interface – I. A. Kozachok, V. V. Kulik, and V. I. Pirogov	657	536
Optimization of the Shape of a Shadow Shield Against Neutrons from a Surface Source by the Monte Carlo Method – V. L. Generozov and V. A. Sakovich	658	536
Neutron Threshold Detector RH^{103} – I. L. Lomonosov, E. I. Firsov, and N. G. Cherenda	659	537

CONTENTS

(continued)

	Engl.	Russ.
Effective Cross Sections of Proton and Alpha Particle Tracks in Ionic Crystal – D. I. Vaisburd, A. A. Vorob'ev, and L. A. Melikyan	660	538
LETTERS TO THE EDITOR		
Minimization of the Coefficient of Variation of Energy Release in a Slab Reactor With a Reflector – E. G. Sakhnovskii	662	539
Calculation of Heat Transfer under Conditions of Bubble Boiling – V. F. Prisnyakov	665	540
Use of Resistance Thermometers in Nuclear Reactors – É. Ya. Gorodetskaya, A. I. Kits, and V. Ya. Kotel'man	668	542
The Transition-Region Function for Beryllium and Some Examples of Its Use – V. N. Bogomolov and L. A. Chernov	670	543
Thermodynamics of Extraction of Pu(IV) from Nitric Acid Solutions by Tri-n-Butyl Phosphate (TBP) – A. S. Solovkin	673	545
Determination of Thorium Concentration with the Aid of Cascade Emission – G. S. Semenov, A. P. Grumbkov, and V. P. Kuptsov	676	547
NEWS OF SCIENCE AND TECHNOLOGY		
Measurement of Neutron Spectra in Fast Reactors – Yu. A. Kazanskii	678	549
The Leipzig Conference and Exhibition on Nuclear Instrumentation of the Council for Mutual Economical Assistance – L. N. Krylov	680	550
International Conference on Laser Plasma – G. V. Sklizkov	683	552
Symposium on New Developments in Physical and Biological Detectors of Radiation – V. I. Ivanov	686	554

The Russian press date (podpisano k pechati) of this issue was 5/27/1971. Publication therefore did not occur prior to this date, but must be assumed to have taken place reasonably soon thereafter.

ANDREI KAPITONOVICH KRASIN

(ON HIS SIXTIETH BIRTHDAY)

On May 21, 1970, Andrei Kapitonovich Krasin, Academician of the Academy of Sciences of the Belorussian SSR, honored scientist and technologist of the Belorussian SSR, Director of the Institute of Nuclear Energetics of the Academy of Sciences of the Belorussian SSR, member of the Editorial Board of the Journal Atomnaya Énergiya and Laureate of the Lenin Prize, celebrated his sixtieth birthday.

A. K. Krasin was born in 1911 in Tomsk. In 1934 he graduated from the physicomathematical department of Tomsk State University. From 1934 to 1940 he worked in the Siberian Physicotechnical Institute. Together with scientific work as a docent, he carried on pedagogical activity at Tomsk State University.

From 1940 to 1945 A. K. Krasin served at the fronts of the Second World War; he was awarded the Order of the Patriotic War Second Degree and two medals for his military services. In January 1945 he was sent to work in the Laboratory of Academician I. V. Kurchatov.

From 1946 to 1956 A. K. Krasin worked as Deputy Director of the Scientific Section, and from 1956 to 1960 as the Director of the Physicoenergetics Institute of GKAÉ* of the USSR. At the same time Andrei Kapitonovich supervised and participated directly in the creation of the first atomic electric power plant in the world; he participated in the development of reactors with nuclear superheating of steam for the Beloyarskii Atomic Electric Power Plant, and the creation of the TES-3 mobile atomic electric power plant.

*State Committee for the Use of Atomic Energy.

Translated from Atomnaya Énergiya, Vol. 30, No. 6, pp. 489-490, June, 1971.

For the creation of the first atomic electric power plant in the world, he was awarded the highest government award – the Order of Lenin, and was given the honorary title of Laureate of the Lenin Prize.

At Obninsk Physicoenergetics Institute, A. K. Krasin was the initiator of investigations of the use of beryllium as a moderator in atomic reactors. A. K. Krasin reported data on the investigation and operation of an experimental reactor in 1958 at Geneva at the Second International Conference on the Peaceful Uses of Atomic Energy and received the high esteem of foreign scientists.

In 1960 A. K. Krasin was elected Member of the Academy of Sciences of the Belorussian SSR. Moving to Minsk, A. K. Krasin headed the department of Atomic Energetics of the Power Engineering Institute of the Academy of Sciences of the Belorussian SSR.

In June, 1965, A. K. Krasin was named Director of the newly organized Institute of Nuclear Energetics of the Academy of Sciences of the Belorussian SSR. Under his supervision this institute was converted to one of the greatest scientific institutions of the Belorussian SSR. With the direct participation of Andrei Kapitonovich, two essentially new scientific directions were formulated in the institute: the use of dissociating coolants in nuclear energetics and the utilization of the energy of nuclear fuel for the accomplishment of radiation chemical processes and radiation ratification of materials.

An experimental base, providing the possibility of conducting experimental investigations at the modern level, was also created at the institute:

an IRT-2000 atomic reactor with loop devices for conducting investigations in the field of nuclear energetics and radiation chemistry;

the largest universal irradiating γ installation in the USSR, with a capacity of 500,000 gram radium equivalents, permitting the wide introduction of atomic energy into the national economy of the republic, and in particular, into agricultural production;

a radiochemical laboratory providing for work with radioactive substances and studies of the radiation chemical synthesis of substances of value to the national economy;

more than 30 different installations for investigating the properties of new coolants for atomic electric power plants;

a laboratory of physical assembly plants, in which operating models of reactors under development are being investigated.

As a result of theoretical and experimental investigations conducted under the supervision of A. K. Krasin, the scientific and technical bases for the use of essentially new coolants – dissociating gases – in nuclear energetics were developed.

The results of A. K. Krasin's scientific activity have made an important contribution to atomic science and technology. Andrei Kapitonovich is the author and coauthor of more than 300 scientific works. He is active in the training of scientific personnel.

A. K. Krasin is a Member of the Editorial Board of the Journal "Atomnaya Énergiya" and "Inzhenerno-Fizicheskii Zhurnal," and Editor-in-Chief of the Journal "Izvestiya AN BSSR" (Physical Energetics Sciences Series).

In connection with the sixtieth birthday of Andrei Kapitonovich Krasin, the editors of the journal "Atomnaya Énergiya on behalf of the scientific and technical community at large, cordially congratulate the hero of the day and wish him good health and further successes for the welfare of Soviet atomic science and technology.

IMPROVEMENT OF PHYSICAL CHARACTERISTICS OF FAST PLUTONIUM REACTORS BY USING U^{233} AND THORIUM

A. I. Leipunskii, L. N. Yurova,
S. B. Bobrov, V. M. Murogov,
L. V. Tochenyi, M. F. Troyanov,
and A. N. Shmelev

UDC 621.039.5/6

Research in the physics of fast reactors performed in the USSR [1-3] and abroad [4, 5] has shown that the requirements for achieving a high breeding rate and ensuring safety (sodium and Doppler reactivity coefficients) can be contradictory. For example an attempt to guarantee negative values of the sodium reactivity coefficient leads to worsening of the economics of the fuel cycle.

We discuss some ways of resolving these contradictions. We investigate the possibility of constructing a high-power fast reactor, operating in a mixed-fuel cycle using U^{238}, thorium, plutonium, and U^{233} simultaneously, with effective flattening of the heat release distribution, varying with time and permitting an increase in the power density and the breeding rate. At the same time we succeed in obtaining negative sodium and Doppler reactivity coefficients which are large in comparison with those in a plutonium fast multiplier in which two regions with different enrichments are used to flatten the heat release distribution.

Basic Physical Characteristics of Mixed-fuel Fast Reactors with Flattening of the Heat Release Distribution. Optimizing reactor characteristics from the point of view of breeding, taking account of technical possibilities, requires increasing the ratio of core diameter to height and flattening the heat release distribution.

We consider the flattening of the heat release distribution by creating regions of different enrichment while retaining a constant fuel fraction in the core. This method has been extensively studied and is specified for the fast power reactors BN-350 and BN-600.

Flattening the heat release distribution by enrichment while maintaining core power and volume makes it possible to increase the fuel element diameter and the fuel content of the core. If the breeder material in the core is U^{238} its fission increases the breeding ratio. Although the critical mass is increased by such flattening, the amount of fuel in the cycle is not increased because of the lengthening of the operating period, and therefore the decisive factor is the increase in the breeding ratio. Flattening also decreases the doubling time.

It is known that flattening of the heat release distribution in fast thorium reactors does not lead to a significant change in the breeding characteristics since the contribution of thorium fission is small [6].

Calculations have shown that the flattening of the heat release distribution by enrichment in a fast reactor fueled with a mixture of U^{233} and plutonium can lower the ratio of maximum to average power density in the radial direction from 1.7-1.8 to 1.2-1.3. At the same time the breeding ratio is increased from 1.2 to 1.4 and the doubling time is decreased from ~15 to ~10 years.

Further significant improvement of the physical characteristics of large fast power reactors can be obtained by increasing the ratio of the cylindrical core diameter to height. In a reactor of a given power and constant power density such a change permits a significant increase in the fuel volume, the operating time of the reactor, and the breeding ratio. Since the critical mass is increased also, there is an optimum value of this ratio for each reactor [2, 7].

Translated from Atomnaya Énergiya, Vol. 30, No. 6, pp. 491-498, June, 1971. Original article submitted January 13, 1971.

TABLE 1. Characteristics of Various High-Power Fast Reactors

Parameter	Plutonium reactor	Mixed-fuel cycle				Thorium reactor
		in two reactors		in one reactor		
		type 9 reactor	type 3 reactor	fuel in the form of a homogeneous mixture of $Pu^{239} + U^{233} + U^{238}$	separate use of uranium and plutonium fuel	
Core volume V_C, liters	5600	5600		5600	5000	5600
Ratio of radius of inner subregion to radius of core R_1/R	0,73	0,73		0,73	0,73	0,73
Average power density Q, kW/liter	400	400		400	450	400
Core composition:						
ε_T	0,40	0,40		0,40	0,44	0,42
ε_{Na}	0,36	0,36		0,36	0,34	0,35
ε_{St}	0,24	0,24		0,24	0,22	0,23
Initial loading, kg:						
U^{233}	—	—	1800	850	700	2500
Pu^{239}	2250	2260	—	1350	1300	—
Breeding ratio:						
in core BRC	0,82	0,82	0,75	0,78	0,80	0,65
in blanket BRB	1,38	1,36	1,30	1,34	1,34	1,1
Breeding ratio in regions of different enrichment:						
BRC_1	0,94	0,94	0,87	0,90	0,90	0,75
BRC_2	0,70	0,70	0,65	0,68	0,70	0,50
Maximum to average power density:						
K_V	1,70	1,70	1,65	1,68	1,50	1,55
K_r	1,35	1,35	1,30	1,34	1,20	1,25
Specific loading, kg·cycle/MW (e) for $T_F = 0.5$ yr	2,8	2,8	2,25	2,75	2,5	1
Doubling time T_2, yr for $T_F = 0.5$ yr	9	10		10	9	38

Note: T_F is the time of the outer fuel cycle.

The foregoing determined the choice of the initial parameters of a high-power fast reactor [8] serving as a prototype for the various mixed-fuel reactors considered. The initial parameters of these reactors are listed below:

Power	1000 MW (e)
Fuel	Oxide
Coolant	Sodium
Ratio of core diameter to height	D/H = 3
Maximum sodium velocity	10 m/sec
Thickness of radial and axial blankets	40 cm
Composition of radial blanket $\varepsilon_T/\varepsilon_{Na}/\varepsilon_{St}$	0.60/0.25/0.15
Fuel density, g/cm^3	
in core	8.5
in blanket	9.5
Thickness of fuel element cladding	0.4 mm
Initial isotopic composition of plutonium	100% Pu^{239}

The calculated characteristics of mixed-fuel and plutonium reactors are shown in Table 1. We have considered the following possible mixed-fuel cycles:

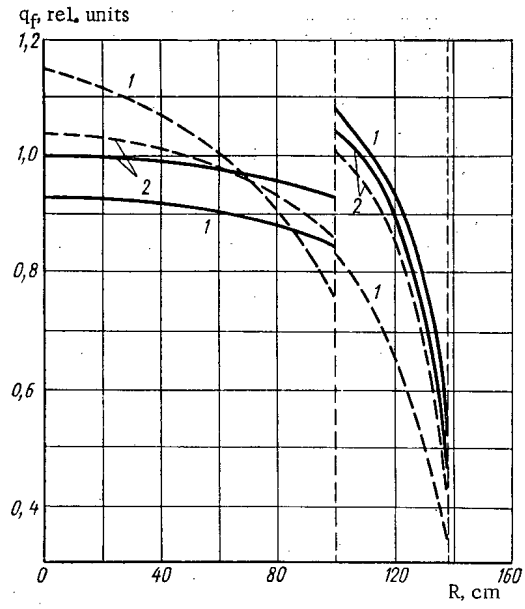

Fig. 1

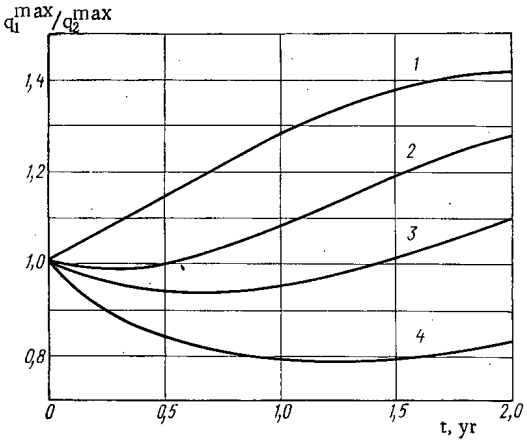

Fig. 2

Fig. 1. Change in radial distribution of volumetric heat release rate in a fast reactor with operation: ———) beginning of operation; - - - -) end of operation: 1) plutonium reactor flattened by creating regions of different enrichments ($R_1/R = 0.73$); 2) reactor using $U^{233} + U^{238}$ at the core center and plutonium + U^{238} at the periphery ($R_1/R = 0.73$).

Fig. 2. Change in the ratio of maximum heat release in regions of different enrichment (q_1^{max}/q_2^{max}) as a function of the time t of continuous operation: 1) plutonium reactor ($R_1/R = 0.73$); 2) reactor fueled with $U^{233} + U^{238}$ at core center and plutonium + U^{238} at pheriphery ($R_1/R = 0.80$); 3) the same for $R_1/R = 0.73$; 4) the same for $R_1/R = 0.60$.

1) Reactors operating in parallel – type 3 with $U^{233} + U^{238}$ core fuel, and type 9 with $Pu^{239} + U^{238}$ core fuel; the blankets of both reactors contain thorium.

2) a reactor fueled with a mixture of $U^{233} + U^{238} + Pu^{239}$ and having thorium in the blanket.

3) a reactor with a regional distribution of fissionable isotopes; in the central region the fuel is $U^{233} + U^{238}$ and in the peripheral region it is plutonium + U^{238}; the blanket contains thorium.

Calculations were performed with computer programs [9, 10] using multigroup constants [11] which take account of the latest refinements of the nuclear constants of Pu^{239} and U^{238} [12].

A detailed study enabled us to find the characteristics of high-power mixed fuel fast reactors with a regional distribution of fissionable isotopes. The arrangement having $U^{233} + U^{238}$ in the central region of the core and $Pu^{239} + U^{238}$ in the peripheral region not only decreased the nonuniformity of the heat release distribution and improved certain safety characteristics, but also improved the time behavior of the heat release distribution.

Change in Shape of the Heat Release Distribution during Operation of a High-power Mixed-fuel fast Reactor. If the same fissionable isotope is burned and reproduced in the reactor the change in shape of the heat release distribution is determined mainly by the change in the ratio of the concentrations of fissionable isotopes in the regions. Assuming that the breeding ratios within the regions of different enrichments are constant, the change with time of the ratio of the maximum heat release in the regions q_1^{max}/q_2^{max} is determined mainly by the ratio of the breeding ratios in these regions. Since the breeding ratio has its largest value in the region with the smaller enrichment, i. e., in the central region of the core, the heat release will become relatively large at the center of the reactor and relatively small in the outer regions of the core. In other words the nonuniformity of the heat release distribution will be increased.

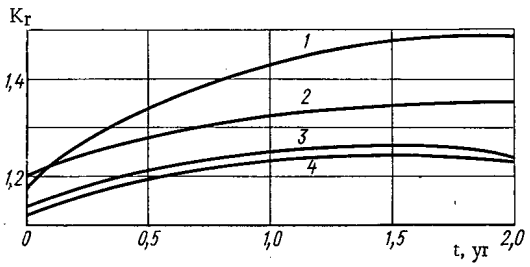

Fig. 3. Change in ratio of maximum to average power density during operation for various large fast reactors as a function of the time of continuous operation: 1) plutonium reactor ($R_1/R = 0.73$); 2) reactor fueled with $U^{233} + U^{238}$ at center and plutonium + U^{238} at periphery ($R_1/R = 0.60$); 3) the same for $R_1/R = 0.80$; 4) the same for $R_1/R = 0.73$.

Figure 1 shows that the situation is very different for mixed fuel when different isotopes are burned and bred in the core. For example, in a mixed-fuel reactor using a regional distribution of fissionable isotopes U^{233} is burned up in the central region and Pu^{239} is bred. In this case the change in shape of the heat release distribution with time is determined not only by the ratio of the regional breeding ratios BRC_1/BRC_2 but also by the difference in fission cross sections of the isotopes which are burned up and accumulated. Qualitatively the shape of the heat release distribution in the reactor core in the latter case can be characterized by the change in the ratio of the maxima of the heat release in the first and second reactor regions. For each of these stages the so-called heat release breeding ratio HBR is introduced and defined as the ratio of the rate of increase of the volumetric heat release rate as a result of the formation of new fissionable isotopes to the rate of decrease of the volumetric heat release rate as a consequence of the burnup of the principal fissionable isotopes. In the case under discussion the HBR can be written in the form

$$\mathrm{HBR} = \frac{\bar{\sigma}_f^{\mathrm{Pu}}(\bar{r})\,\frac{d\rho_{\mathrm{Pu}}}{dt}(\bar{r})}{\sigma_f^{\mathrm{U^{233}}}(\bar{r})\left|\frac{d\rho_{\mathrm{U^{233}}}}{dt}(\bar{r})\right| + \sigma_f^{\mathrm{Pu}}(\bar{r})\left|\frac{d\rho_{\mathrm{Pu}}(\bar{r})}{dt}\right|} \approx \frac{\overline{\sum}_c^{\mathrm{U^{238}}}(\bar{r})\cdot\bar{\sigma}_f^{\mathrm{Pu}}(\bar{r})}{\overline{\sum}_{cf}^{\mathrm{U^{233}}}(\bar{r})\cdot\bar{\sigma}_f^{\mathrm{U^{233}}}(\bar{r}) + \overline{\sum}_{cf}^{\mathrm{Pu}}(\bar{r})\cdot\bar{\sigma}_f^{\mathrm{Pu}}(\bar{r})}, \quad (1)$$

where $\bar{\sigma}_f$, $\overline{\Sigma}_c$, and $\overline{\Sigma}_{cf}$ are respectively the microscopic fission cross section and the macroscopic capture and fission cross sections of the indicated isotopes averaged over the neutron spectrum. Then the change in the ratio of the heat release maxima will be determined by the ratio HBR_1/HBR_2.

In a plutonium reactor HBR ≈ BRC and the relative change of shape of the heat release distribution is determined mainly by the ratio of the regional breeding ratios $HBR_1/HBR_2 = BRC_1/BRC_2$. In a mixed-fuel reactor the change in shape of the heat release distribution is given by the expression

$$\frac{\mathrm{HBR_1}}{\mathrm{HBR_2}} = \frac{\mathrm{BRC_1}}{\mathrm{BRC_2}}\cdot\frac{\bar{\sigma}_f^{\mathrm{Pu}}}{\bar{\sigma}_f^{\mathrm{U^{233}}}}$$

at the outset when the effect of secondary fuel in the region with U^{233} and U^{238} is small. In large reactors the ratio of the regional breeding ratios BRC_1/BRC_2 is almost always greater than unity (1.0-2.0) and depends on the ratio of the enrichments in the regions. The ratio of the microscopic fission cross sections of plutonium and U^{233} in such reactors is always less than unity (0.6-0.7) and practically constant. Thus by varying the ratio of the regional breeding ratios, e. g. by changing the boundaries of the regions and the enrichments in them, it is possible in principle to achieve equality of the heat release breeding ratios in the two regions. In this case the heat release distribution preserves its shape practically unchanged for some time.

A similar situation arises when regions with different enrichments of the same fissionable isotope contain two different breeding materials, e. g. U^{238} at the center and thorium on the periphery. Such combinations of isotopes make it possible to produce a core in which the heat release shape changes with time according to a given law depending on the ratio of the regional heat release breeding ratios.

If BRC_1 is sufficiently larger than BRC_2 to compensate for the decrease in the fission cross section of the secondary fissionable isotope (Pu^{239} in comparison with the fission cross section of U^{233}), $HBR_1/HBR_2 > 1$ and there will be a relative increase in heat release at the center of the reactor – a case analogous to the behavior of the heat release distribution in a plutonium reactor.

If the difference in regional breeding ratios does not make up for the change in fission cross section, i. e., $HBR_1/HBR_2 = (BRC_1/BRC_2)(\bar{\sigma}_f^{\mathrm{Pu}}/\bar{\sigma}_f^{\mathrm{U^{233}}}) < 1$, after a certain time there will be a relative increase in heat release in the peripheral zone which, except in a plutonium reactor, is flattened by enrichment.

The intermediate case corresponds to an unchanged shape of the heat release distribution for a certain length of time.

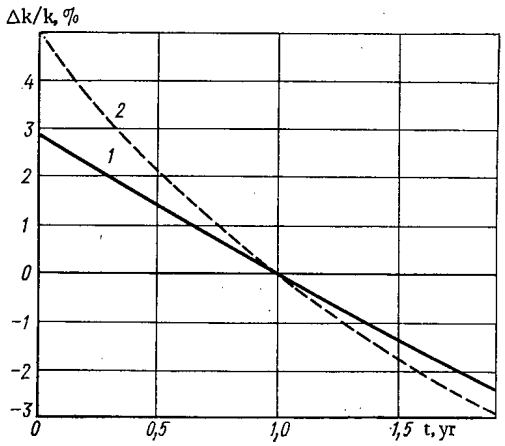

Fig. 4

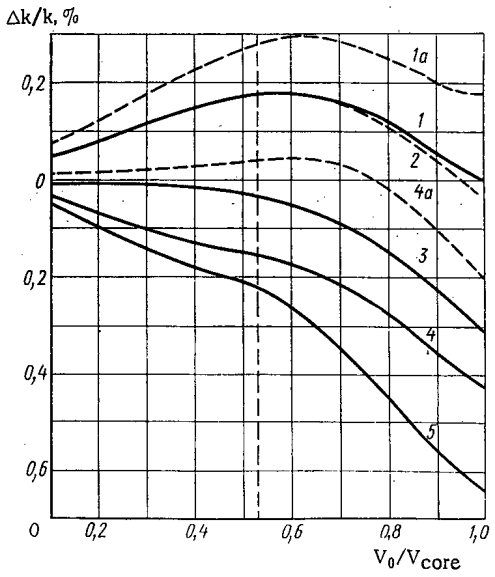

Fig. 5

Fig. 4. Change in reactivity during operation of a high-power fast reactor: 1) plutonium reactor ($R_1/R = 0.73$); 2) mixed-fuel reactor ($R_1/R = 0.73$).

Fig. 5. Reactivity as a function of the fraction of the core volume from which 50% of the sodium is removed: 1) plutonium reactor; 1a) plutonium reactor with average isotopic fuel composition for a burnup of 50,000 MW days/metric ton; 2) plutonium reactor with thorium blanket; 3) mixed-fuel reactor $U^{233} + U^{238} + Pu^{239}$ with a thorium blanket; 4) mixed-fuel reactor having $U^{233} + U^{238}$ at the center and $Pu^{239} + U^{238}$ at the periphery with a thorium blanket, 4a) mixed-fuel reactor with regional distribution of fissionable isotopes for a burnup of 50,000 MW days/metric ton; 5) reactor fueled with $U^{233} + U^{238}$ and having a thorium blanket.

The results of the investigation of the behavior of the heat release distribution during the operation of a large 1000 MW(e) fast reactor are shown in Figs. 1-3. The calculation takes account of the change in isotopic composition of the fuel and the change in the neutron flux distribution during operation.

Figure 2 shows that in mixed-fuel reactors, in contrast with plutonium reactors, the time dependence of the ratio of the heat release maxima in the regions is not a monotonic function. This is because $HBR_1/HBR_2 < 1$ at the beginning of operations and there is a relative decrease of heat release in the central region. With the burnup of U^{233} and the accumulation of Pu^{239} in the central region the ratio HBR_1/HBR_2 approaches the ratio BRC_1/BRC_2, i. e., it becomes larger than unity, and therefore the heat release in such a reactor approaches the distribution in a plutonium reactor with a certain a priori specified "overshoot" of the heat release maximum in the second region ($q_1^{max}/q_2^{max} < 1$). We note that the overestimate of the maximum heat release in the second region in comparison with the central is considered as one method of decreasing the change in the nonuniformity of the heat release distribution during the operation of plutonium reactors [4, 8].

It is shown that it is possible to choose an optimum value of the radius of the inner region for a given operating time (burnup) of a mixed-fuel reactor.

Change in Reactivity during Operation of a High-power Mixed-fuel Fast Reactor. In a mixed-fuel fast reactor the secondary fuel in the core (Pu^{239}) is less effective than the fuel consumed (U^{233}). Therefore the change in reactivity during reactor operation is not characterized by BRC-1, but by the difference between the breeding ratio reactivity BRR [13] and unity, and for the case in hand takes the form

$$BRR \approx BRC \quad \frac{M_{cr}^{U^{233}}}{M_{cr}^{Pu^{239}}} - 1, \qquad (2)$$

TABLE 2. Comparison of Sodium and Doppler Effects in High-Power Plutonium and Mixed-Fuel Reactors

Characteristic	Plutonium fuel: $PuO_2 - UO_2$	Mixed fuel: $UO_2 + U^{233}O_2$ at center of core and $PuO_2 + UO_2$ at periphery; ThO_2 in blanket
Reactivity change, $\Delta k/k$ %, due to the uniform removal of 50% of the sodium from the central part of the core	+0,17	−0,16
Doppler effect in Pu^{239} (U^{233}) in inner region	+0,09	+0,005
Doppler effect in core	−0,7	−0,8

Note: T = 900-2100 °K.

where M_{cr} is the critical mass.

Since $M_{Cr}^{U^{233}}/M_{Cr}^{Pu^{239}}$ is almost always about 0.8-0.9 in fast reactors the change in reactivity in a mixed-fuel reactor with BRC ≈ 1 is larger after operation than is the case for a plutonium reactor.

Figure 4 shows that continuous operation of a plutonium reactor of conventional composition and size for a year requires an excess reactivity of ~3%, while a mixed-fuel reactor requires ~5%. This can lead to considerable difficulties since it is necessary either to decrease the time of continuous reactor operation to ~0.5 year, which worsens the power plant economics, or to increase the control rod capacity, which decreases the breeding ratio. An increase in the number of absorbing rods can change the behavior of the heat release distribution during operation. These difficulties can be resolved in mixed-fuel reactors with BRR ≈ 1. Satisfaction of this condition is guaranteed by going to reactor powers of 2,000 MW(e) and more with carbide or metallic fuels.

Doppler and Sodium Reactivity Coefficients in a Large Mixed-fuel Fast Reactor. It as been shown [5, 14, 15] that the introduction of U^{233} into the core, and thorium into the blanket, of a fast plutonium reactor, i. e., the creation of a mixed-fuel reactor, leads to an improvement of the sodium reactivity coefficient of a fast reactor. We have studied the reactivity as a function of the fraction of the core volume from which 50% of the sodium is removed uniformly. The volume and radius of the cylindrical region from which the sodium is removed increase gradually from the reactor center to the periphery. The height of this region is always equal to the core height. The results for the various reactors are shown in Fig. 5.

1. A plutonium reactor with regions of different enrichment (original version). The fuel in the core is $PuO_2 + UO_2$ and that in the blanket is UO_2; the integrated effect on reactivity of removing sodium from the whole core is close to zero.

2. A plutonium reactor with a thorium blanket (type 9 reactor). The difference between the sodium coefficient of this reactor and that of a plutonium reactor appears only in the core layers closest to the blanket since the densities of uranium and thorium in the blankets of both reactors are assumed the same.

3. A reactor using $U^{233}O_2 + U^{238}O_2 + PuO_2$ in both regions and ThO_2 in the blanket. The removal of sodium from the inner region has practically no effect. This effect is substantially negative for the removal of sodium from an inner volume larger than the first region.

4. A mixed-fuel reactor with a regional distribution of fissionable isotopes: U^{233} at the center and plutonium at the periphery. The effect of removing sodium is substantially negative over the whole core.

5. A reactor with uranium oxide fuel: $U^{233}O_2 + U^{238}O_2$ in the core and ThO_2 in the blanket (type 3 reactor). This reactor has the largest negative sodium coefficient.

Calculations show that the contribution to the power effect from decreasing the sodium density and from a partial loss of sodium, e. g. from boiling in certain channels, is very much less positive in a large mixed-fuel fast reactor using U^{233} in the central part of the core than in the plutonium version. This is explained by the weak energy dependence of $\alpha = \sigma_c/\sigma_f$ for U^{233}, the increased leakage from the outer part of the core due to the increased fuel enrichment, and the use of thorium in the blanket.

As U^{233} burns up and Pu^{239} and the U^{234} and Pu^{240} fission fragments accumulate, the positive sodium effect in a mixed-fuel reactor becomes larger. Calculations showed that for an average isotopic composition of the core corresponding to maximum burnup (100 kg of fragments per metric ton of fuel) there is a region of positive values of the sodium coefficient, but this positive effect is very much smaller in a mixed-fuel reactor than in the plutonium version (cf. curves 1a and 4a of Fig. 5).

Uranium 233 has a small temperature coefficient of reactivity. Therefore placing it in the central region makes the largest change in reactivity and decreases the positive component of the Doppler coefficient.

Table 2 shows that a mixed-fuel reactor with U^{233} in the central region has a somewhat larger negative Doppler coefficient than the plutonium version.

The following conclusions can be drawn from the discussion:

1. Flattening the heat release distribution by creating regions of different enrichments of $U^{233} + Pu^{239} + U^{238}$ fuel and increasing the ratio of core diameter to height reduce the maximum to average power density ratio in the radial direction from ~1.8 to ~1.2, increase the breeding ratio from ~1.2 to ~1.4, and decrease the doubling time from ~15 to ~10 years.

2. The most attractive way of arranging fissionable isotopes is to place U^{233} in the central region and plutonium at the periphery. This regional distribution of fissionable isotopes has the following advantages:

a) the heat release distribution can be flattened more effectively and its change with reactor operating time is more favorable. As a consequence it is possible to increase the power density in the fuel by ~10% in a mixed-fuel reactor. Thus in spite of a somewhat worse value of the breeding ratio the rate of accumulation of new fuel will not be lower in mixed-fuel reactors than in plutonium reactors;

b) a mixed-fuel reactor is characterized by larger negative values of the sodium and Doppler coefficients of reactivity.

3. The advantages of a mixed-fuel cycle can be vitally important in high-power fast reactors (2000 MW(e) and higher), when the loss in reactivity $\Delta k/k$ during operation is small, the time of continuous operation is one year or more, and certain safety problems become more complicated.

Thus the use of U^{233} and thorium with U^{238} and plutonium in high-power fast reactors can increase the power density and the rate of breeding fuel, and at the same time ensure the safety of a sodium cooled fast reactor.

The authors thank V. Ya. Makartsevaya, A. I. Nevinitsa, A. V. Rudnev, and V. Ya. Serovaya for their great help in performing the calculations.

LITERATURE CITED

1. A. I. Leipunskii et al., Atomnaya Énergiya, 18, 342 (1965).
2. A. I. Leipunskii et al., Paper No. 369, presented at the Third International Conference on the Peaceful Uses of Atomic Energy [in Russian], Geneva (1964).
3. A. I. Leipunskii, V. M. Murogov, and M. F. Troyanov, paper presented at a conference of experts on the Use of Thorium [in Russian], MAGATÉ, Vienna (1966); cf. also Nuclear Reactor Physics Problems [in Russian], Vol. 1, Obninsk (1968), p. 20.
4. C. Zaleski and D. Smidt, ANS-100, 275 (1965).
5. D. Okrent, Nuclear Safety, 6, 340 (1965).
6. R. Hankel et al, NDA 2164-3 (1962).
7. V. V. Khromov et al., Atomnaya Énergiya, 17, 3 (1964).
8. A. I. Novozhilov et al., CMÉA Symposium on the State and Prospects of Constructing Power Plants with Fast Reactors [in Russian], Obninsk (1967).
9. V. V. Khromov et al., in: Nuclear Reactor Physics [in Russian], L. N. Yurova (editor), Vol. 1, Atomizdat, Moscow (1968), p. 159.
10. G. I. Marchuk et al., Critical Parameters of Homogeneous Multiplying Systems [in Russian], Atomizdat, Moscow (1965).
11. L. P. Abagyan et al, Group Constants for Nuclear Reactor Calculations [in Russian], Atomizdat, Moscow (1964).
12. L. P. Abagyan et al., Nuclear Data for Reactors, Vol. 2, IAEA, Vienna (1970) p. 667.
13. A. N. Shmelev in: Reactor Engineering and Physics Problems [in Russian], Atomizdat, Moscow (1966), p. 85.
14. W. Loewenstein and B. Blumenthal, ANL-7120, 751 (1965).
15. W. Allen, D. Stoker, and A. Campise, Proceedings of Second International Thorium Fuel Cycle Symposium, Gatlinburg (1966), p. 81.

EXPERIMENTAL DETERMINATION OF THE STARTING CONDITIONS FOR A SINGLE-CIRCUIT LOOP WITH NATURAL CIRCULATION

V. M. Selivanov, V. G. Konochkin,
N. P. Dormidontov, and V. N. Smyslov

UDC 621.039.514.23

The starting conditions for a single-circuit channel reactor of the Bilibinsk ATÉTs type [1] have been studied experimentally in the natural-circulation water loop of the First Atomic Power Station.

The experimental loop (Fig. 1) constitutes a closed circuit formed by channels set in the reactor and also by uptaking and downcoming pipes, which are connected to a drum separator. The circuit is supplied with a steam-condensation system and supply and blowing systems. The loop arrangement provides for the possibility of feeding nitrogen into the vapor space of the drum separator in order to create a gas cushion. The motion of the heat carrier in the circuit is achieved by natural circulation; the circulation pump incorporated in the system is only used for preliminary experiments relating to the calibration of the power of the channels in the water mode. Figure 1 shows the heights at which the principal elements of the circuit are situated (in meters).

Experiments were carried out with five identically-constructed channels of the First Atomic Power Station type [2], distinguished by having an augmented number of fuel elements (five) and also a lower siting of the compensators in the uptaking pipes. The relative powers of the channels were 1.0; 0.81; 0.80; 0.76; 0.65.

The loop was supplied with a control and measuring system for measuring and recording the temperature of the heat carrier in various parts of the circuit, and also the flows, both in the individual channels and in the circuit as a whole. In order to monitor the temperature of the outer can of the fuel elements, three fuel elements in each channel were furnished with surface thermocouples.

The experiments relating to the starting conditions were aimed at solving the following problems: To determine the initial pressure in the circuit such as would ensure a stable mode of heating; to elucidate the effects of the initial conditions (in particular the reversed circulation in individual channels) on the development of the motion of the heat carrier in the circuit; to determine the influence of the level of the start-up power on the manner in which the circulation developed; to compare various methods of starting the loop, e.g., with a gas cushion or with the circuit completely filled with water.

Three methods of starting the loop in natural circulation were studied:

starting with a completely filled circuit ($p = 20$-50 abs. atm);

starting with a gas cushion ($p = 5$-30 abs. atm);

starting from atmospheric pressure (a particular case of a gas cushion, $p = 1$ abs. atm).

The experiments on the starting conditions were carried out for two initial states of the reactor: 1) cold, with a temperature of 40-50°C in the loop and a graphite temperature of ~50°C; 2) hot, with a temperature of 70-100°C in the loop and a graphite temperature of ~190°C.

In the course of starting the system, the reactor power was raised in accordance with normal service requirements [2]. After reaching the specified power, further heating was continued at constant power; the

Translated from Atomnaya Énergiya, Vol. 30, No. 6, pp. 498-502, June, 1971. Original article submitted April 6, 1970, revision submitted August 20, 1970.

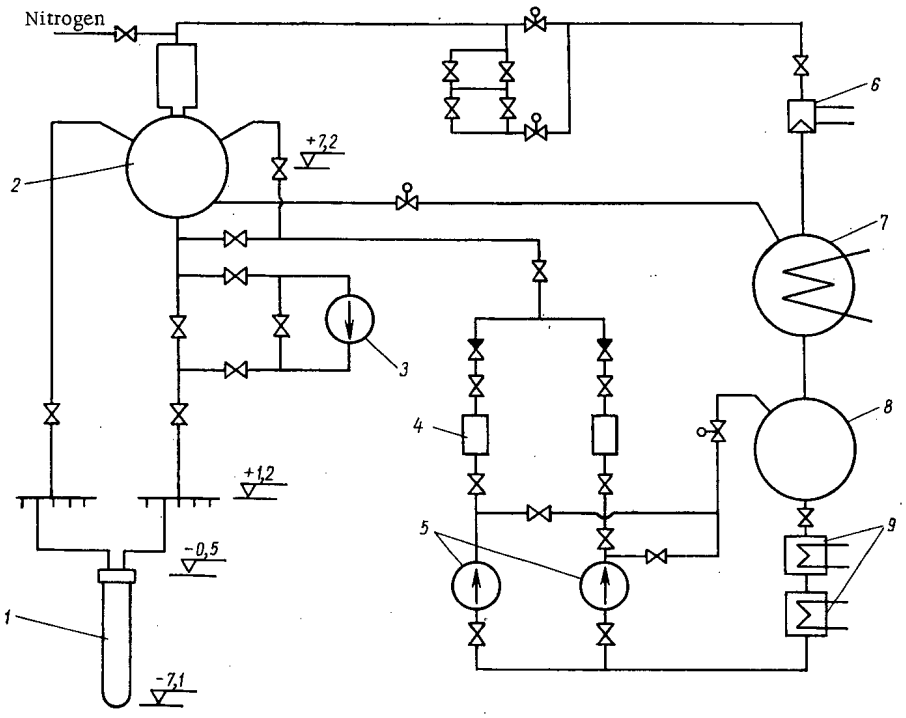

Fig. 1. Principal arrangement of the loop. 1) Experimental channel; 2) drum separator; 3) circulation pump; 4) mechanical filter; 5) supply (feed) pump; 6) reducing–cooling system; 7) condenser; 8) storage tank; 9) condensate cooler.

value of this power was chosen on the basis of the maximum permissible degree of pre-heating in the channels, ~100°C in the water mode (in accordance with the working conditions of the compensators).

The starting procedure with a completely filled circuit was carried out at constant pressure in a system which was maintained by feeding and blowing from a drum separator; the temperature of the feeding water in these experiments was ~30°C. When the temperature had been raised to 5-8°C under boiling at the outlet from the most-stressed channel, the feed pump was stopped and the level in the drum separator was brought to the normal position by smoothly increasing the rate of blowing, after which blowing was stopped and the pressure in the loop was raised to the nominal value (60 abs. atm). On reaching the nominal pressure, the steam valve was opened, the feed pump switched on, and the loop brought to its steady-state condition.

An analogous method of heating and establishing the level in the evaporators was employed in starting the first unit of the Beloyarsk atomic power station in the second circuit [3].

Figure 2 shows the change in the main parameters of the circuit for the case of hot starting, with water under a pressure of ~50 abs. atm and a reactor power of 7%. We see from the figure that the temperature of the fuel elements and the temperature at the outlet from the channels start rising ~6 min after the initial rise in power while the rise in the water temperature at the channel inlet starts after a period of ~12 min. This is due to the time required for heating the water in the drum separator and the transport delay in the downcoming and uptaking pipes.

The change taking place in the rates of flow in the channels and in the loop for the single-phase mode of flow is determined by the nature of the change in power and by the temperature field in the circuit. The slight rise in the pressure of the system in the initial period of starting is due to inaccuracy in regulating the feeding and blowing rates of flow.

At the instant of time $\tau = 48$ min, on reaching a temperature of $\Delta t_H \approx 20$°C under boiling at the outlet from the channel, the rate of flow G in the most loaded channel increases. This may be explained as being due to the appearance of vapor bubbles, resulting from surface boiling. As Δt_H diminishes, the intensity of the surface boiling increases and so does the proportion of the cross section occupied by the steam; the

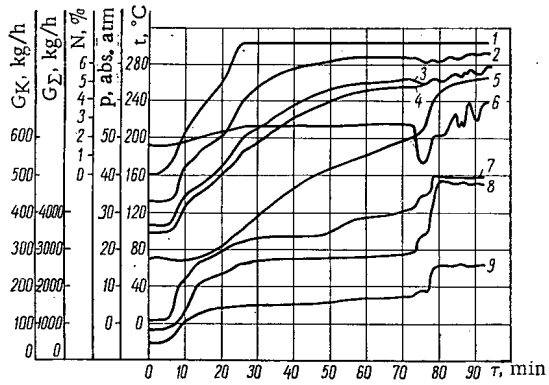

Fig. 2. Change in the main parameters of the loop on starting with a filled circuit. 1) Reactor power N; 2) temperature of the fuel elements of the most loaded channel; 3) temperature at the outlet from the most loaded channel; 4) temperature at the outlet from the least loaded channel; 5) temperature at the inlet to the channels; 6) pressure in the circuit; 7) rate of flow in the most loaded channel; 8) rate of flow in the least loaded channel; 9) total rate of flow in the circuit.

life-time of the steam increases, hence so do the moving head and the rate of flow of the heat carrier through the channel. For $\Delta t_H \approx 10°C$, pulsations at a frequency of ~0.08 cps appear in the most stressed channel ($\tau = 57$ min), the amplitude of the pulses being as great as $\pm 0.12\ G_{av}$; after the loop has passed into a state of volume boiling, the pulsations die out (Fig. 3). The nature of these pulsations is clearly associated with the surface-boiling process, in which an unstable generation of steam bubbles sets in at the hot wall of the channel, the bubbles then being condensed in the flow of underheated liquid.

It should be noted that, when the pulsations begin, the underheating at the outlet from the heated section is smaller than $\Delta t_H = 10°C$ (the value measured at the outlet from the channel), since a certain loss of heat always occurs in the section leading from the active zone to the upper head (the upper reflector and the roof of the reactor); according to approximate calculations, the underheating at the outlet from the heated section of the channel is ~3°C. Starting from the instant at which the fluctuations in rate of flow commence, the temperature of the fuel elements preserves a constant value right up until the instant at which a sharp fall in circuit pressure occurs as a result of the stopping of the supply (feed) pump ($\tau \approx 73$ min), after which all the channels in the loop are brought to a state of volume boiling, and further changes in the temperature of the fuel elements are determined by changes in circuit pressure. The transition to volume boiling and the appearance of the vapor phase in the uptaking tracts of the circuit cause a sharp increase in the rate of flow in the channel ($\tau \approx 73$ min).

The change in the parameters of the heat carrier in the slightly-loaded channel has the same qualitative character as that in the channel of maximum power; the rate-of-flow pulsations in the period of transition to the two-phase mode of flow start later in time (but at the same degree of underheating) and have a smaller amplitude (~0.08 G_{av}). The pulsations die out after the transition to volume boiling. The total rate of flow in the loop varies in accordance with the same laws as those governing the flow in the channels. No pulsations of the total flow occur in the mode under consideration.

As the loop heats further ($\tau > 80$ min), the degree of blowing creating the level in the drum separator is adjusted, and the temperature and pressure in the circuit change accordingly.

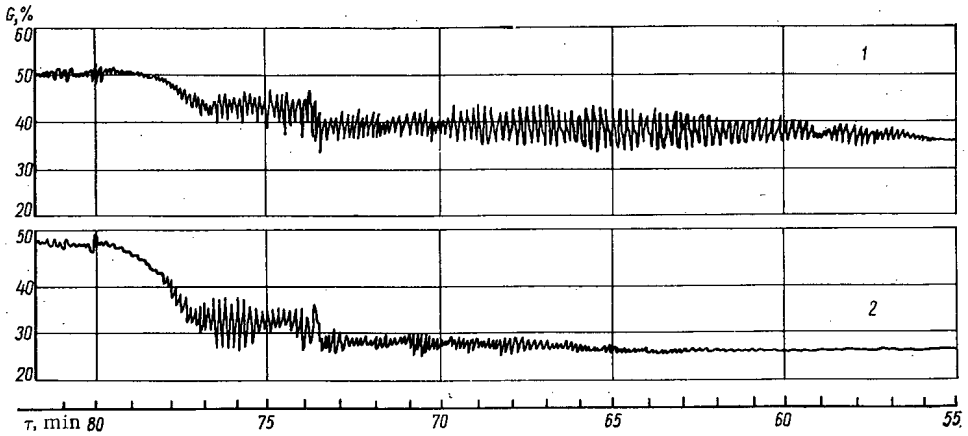

Fig. 3. Pulsations in the rates of flow during start-up from a pressure of $p \approx 50$ abs. atm. 1) Most loaded channel; 2) least loaded channel.

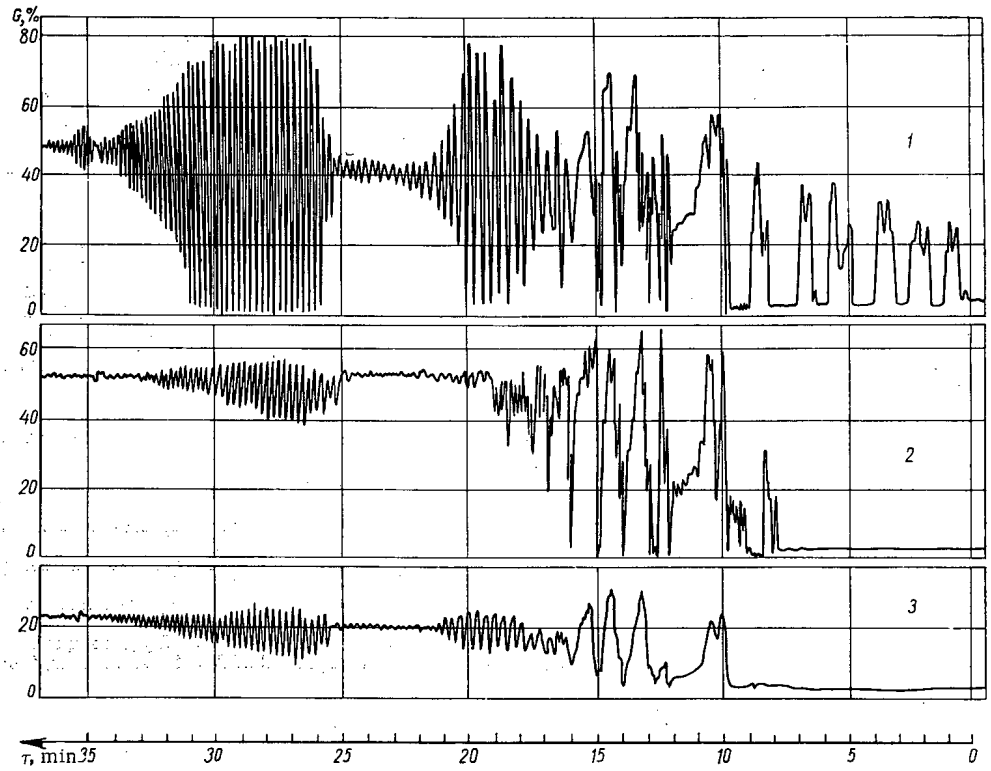

Fig. 4. Rate-of-flow pulsations on starting from p = 1 abs. atm. 1) Most loaded channel; 2) least loaded channel; 3) total rate of flow in the loop circuit.

Starting modes based on a completely-filled circuit with other pressures and powers have the same general character as the mode based on a pressure of p = 50 abs. atm, but differ in respect of the following aspects: the extent of the temperature drop between the fuel-element can and the water, which is determined by the power level; the time required for the circuit to pass to the state of volume boiling, which depends on the power, the initial parameters, and the feeding and blowing rates of flow; the amplitude of the rate-of-flow pulsations as boiling commences. The amplitude of the rate-of-flow pulsations increases on reducing the pressure in the circuit; the pulsation amplitude does not appear to depend on the thermal flux.

The start-up procedures incorporating a gas cushion were conducted with the pressure in the circuit gradually rising until reaching the nominal value. The changes in the main loop parameters during the heating process were of the same general nature as those just indicated. The degree of underheating at the outlet from the channels at the onset of pulsations in the rate of flow was the same; the frequency of the pulsations was also 0.08 cps in all operating modes. On reducing the pressure in the circuit, the amplitudes of the pulses increased; at $p \approx 10$ abs. atm, pulsations appeared in the total rate of flow.

In start-up procedures involving a low initial pressure (5 and 1 abs. atm) and $t_{out} \approx t_s$, the effect of spontaneous evaporation (due to the reduction in the hydrostatic pressure as the heat carrier moved upward along the tracts of the circuit) began to make itself appreciably felt. The spontaneous evaporation manifested itself as substantial fluctuations in the rate of flow, the temperature of the fuel elements falling in the instants at which the rate of flow rose. With increasing power of the reactor, the intensity of vapor formation by virtue of the access of heat from the fuel elements increased, and the part played by spontaneous evaporation diminished, the flow becoming more regular.

Figure 4 presents sections of the recordings giving the rates of flow in the tracts on starting the system from atmospheric pressure. The fluctuations in the rates of flow during the period 0-16 min are due to spontaneous evaporation. The pulsations of large amplitude in the periods 16-22 and 25-33 min are due to the fact that the power of the most loaded channel has exceeded the stability limit [4] (these periods coincide with the gradual rise in reactor power to 3 and 5%). As the pressure in the circuit rises, the channel passes out of the unstable mode and the pulsations are damped out.

In certain start-up modes involving a gas cushion, reversed circulation appears in the initial state in one or two slightly loaded channels of the loop. Some 10-12 min after raising the power, the circulation in these channels assumes itsnormal direction. The working of the channels with reversed circulation has no effect in the temperature characteristics of the fuel elements.

In the case of starting from the cold state of the reactor, before the power is raised there is hardly any circulation at all in the circuit; as the reactor power increases, however, this develops in the normal order.

Comparison of the results obtained from the experiments with various start-up procedures leads to the following conclusions:

1. The development of the circulation takes place in a stable manner on starting the system from p > 10 abs. atm. Natural circulation in the circuit imposes no limitations on the rate of increasing the power, which is determined simply by the permissible rate of heating the circuit (in the experiments this reached 200°C/h). If reversed circulation occurs in individual channels before starting, the motion of the heat carrier in these rapidly comes into order as power increases, not being accompanied by any deviations in fuel-element temperature.

2. In starting modes with $p < 10$ abs. atm, a spontaneous-evaporation effect appears, this being expressed in the form of periodic fluctuations of the rate of flow in the channels (the fluctuations are the greater, the lower the pressure in the circuit), leading to fluctuations in the temperature of the fuel elements.

3. The rise in the temperature of the fuel elements during the heating process (for $p > 10$ abs. atm) occurs quite smoothly, in accordance with the rise in the temperature of the heat carrier at the outlet from the channel. The pulsations in the rates of flow on passing to the boiling mode have no effect on the temperature of the fuel elements.

4. The starting mode involving a gas cushion is simpler; however, remembering that this method of starting the reactor requires a considerable amount of nitrogen, and also special arrangements for discharging and holding the active vapor–gas mixture, it would appear preferable to adhere to the starting procedure based on a circuit filled completely with water.

LITERATURE CITED

1. G. V. Ermakov, Énergeticheskoe Stroitel'stvo, No. 10-11, 64 (1967).
2. G. N. Ushakov, First Atomic Power Station [in Russian], Gosénergoizdat, Moscow (1959).
3. V. N. Smolin et al., At. Énerg., 19, 261 (1965).
4. V. V. Dolgov and O. L. Sudnitsyn, Ten Years of the World's First Atomic Power Station in the USSR [in Russian], Atomizdat, Moscow (1964), p. 107.

THE PRINCIPAL NEUTRON – PHYSICAL LATTICE PARAMETERS OF A VVR-SM TYPE REACTOR

E. T. Józefowicz

UDC 621.039.51

In this paper are reported the results of measurements of the static neutron–physical lattice parameters of a VVR-SM type reactor, undertaken at the Institute of Nuclear Research in the Polish Peoples' Republic. These results are analyzed by means of the multiplication factor of an infinite medium. An attempt is made also to determine the parameters of a two-group criticality equation, taking into account the results of the experiments, and to estimate the reliability of the calculations. Certain of the results obtained are used for verification of the design programs.

Lattice Characteristics

A fundamental cell of a VVR-SM type lattice was represented by a hexagon with a water moderator and a fuel element consisting of three coaxial tubes, the outside one of which was hexagonal (Fig. 1). The fuel was a dispersion of 36%-enriched uranium in aluminum. The volume fractions of the components of the elementary cell and of their atom density (in units of 10^{20} atoms/cm^3) were: 1) fuel (0.1255) 14.04 U^{235}; 24.96 U^{238}, 78.05 oxygen, 488.5 aluminum; 2) cladding (0.3226), 602 aluminum; 3) water (0.5519), 668 hydrogen, 334 oxygen.

The core configuration was varied in the experiments (this will be discussed in more detail later), but in order that the measurements could be interpreted as if they had been carried out in an infinite medium, the investigations were made in a cell remotely located from a lattice discontinuity and the core boundary.

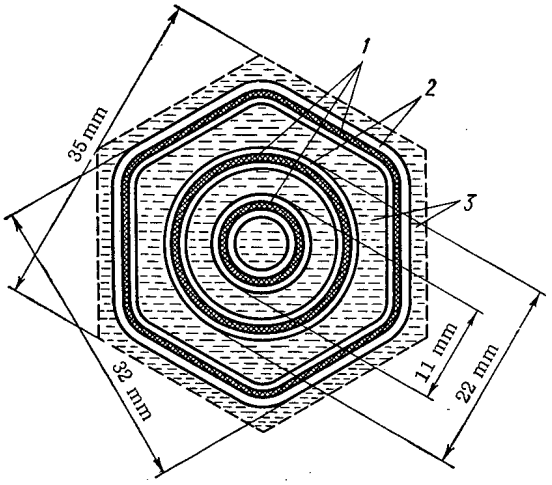

Fig. 1. Cross-section of an elementary VVR-SM cell: 1) fuel (0.7 mm thick); 2) aluminum cladding (0.9 mm thick); 3) water.

Multiplication Factor of an Infinite Medium

The multiplication factor of an infinite medium can be expressed by the following formula

$$\kappa_\infty = \kappa_t + \kappa_e = \kappa_t (1 + \delta^{25}), \qquad (1)$$

where $K_t = \eta_t f p^{25} p^{28} \varepsilon$; $K_e = \eta_e (1 - p^{25}) p^{28} \varepsilon$; $\delta^{25} = K_e/K_t$ is the ratio of the number of fissions by epithermal neutrons to the number of fissions by thermal neutrons; η_t and η_e are the average values of the ratio $\nu\Sigma_f/\Sigma_a$ for thermal and epithermal neutrons respectively (f is the thermal neutron utilization factor); p^{25} and p^{28} are the probabilities of resonance escape in U^{235} and U^{238} respectively, and ε is the fast neutron fission factor.

This approach is described in [1], where it is assumed that the main part of the resonance absorption in U^{235} takes place with a lower neutron energy than resonance absorption in U^{238}. Resonance absorption in the cladding material can be neglected. The small error

Institute of Nuclear Research, Swierck, Polish Peoples' Republic. Translated from Atomnaya Énergiya, Vol. 30, No. 6, pp. 503-509, June, 1971. Original article submitted February 11, 1970; final revision October 2, 1970.

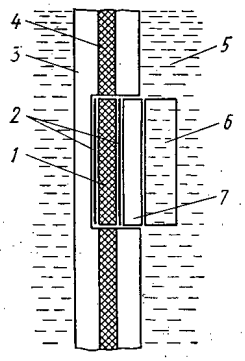

Fig. 2

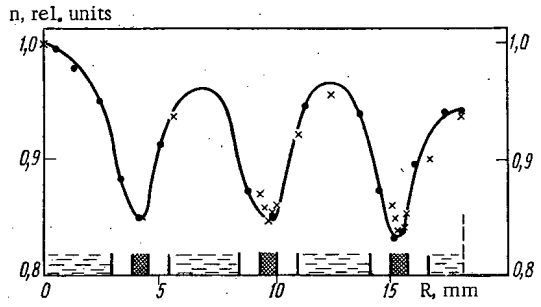

Fig. 3

Fig. 2. Disposition of detectors for measuring the epithermal parameters of the cell: 1) fuel pellet; 2) dysprosium foils; 3) aluminum; 4) fuel; 5) water; 6) plastic disc; 7) aluminum disc.

Fig. 3. Macrodistribution of thermal neutrons in the elementary VVR-SM cell: X) experiment; ●) calculation.

due to neglecting the effect of neutron leakage on the lattice parameters is compensated by the inseparability of K_t and K_e in the two-group criticality equation, which is admissible for water lattices. In this case, the probability of resonance escape can be written in the following form:

$$p^{28} = \frac{1}{1+\rho^{28}p^{25}f\dfrac{\sum_{a,\,t}^{28}}{\sum_{a,\,t}^{f}}}; \tag{2}$$

$$p^{25} = \frac{1}{1+\delta^{25}\eta_t f/\eta_e}, \tag{3}$$

where ρ^{28} is the ratio of the number of epithermal to thermal absorptions in U^{238}; $\Sigma_{a,t}^{28}$ and $\Sigma_{a,t}^{f}$ are the macroscopic absorption cross-sections of thermal neutrons in the U^{238} located in the fuel element and the fuel respectively.

Number of Neutrons Produced by a Single Absorbed Thermal Neutron

The thermal neutron utilization factor, defined as the ratio of thermal neutrons absorbed in the fuel to the total number of neutrons absorbed in the cell, can be calculated by means of the average cross-sections:

$$\frac{1}{f} = 1 + \frac{\sum_a^c V_c}{\sum_a^f V_f}\delta_c + \frac{\sum_a^m V_m}{\sum_a^f V_f}\delta_m, \tag{4}$$

where

$$\delta_c = \frac{\bar{n}_c}{\bar{n}_f};\ \delta_m = \frac{\bar{n}_m}{\bar{n}_f};\ \bar{n}_i = \frac{1}{V_i}\int_{V_i} n(\mathbf{r})\,d\mathbf{r};$$

f, c and m denote the fuel, cladding and water respectively.

When measuring the thermal neutron distribution in the cell, openings drilled in one of the fuel elements were used. An assembly of materials simulating fuel layers and foil-detectors (an alloy of manganese and nickel) were installed in these, as shown in Fig. 2. However, instead of one fuel pellet, two pellets were installed with a foil between them or only the foils were used; the effective absorption cross-section of these was equal to the absorption cross-section of the fuel. A foil was also positioned along the axis of the cell. Although the flux perturbation in the cell under these conditions was quite small, it is necessary to estimate the possible sources of error, for example: the effect of macrodistribution, installation of the absorbing foil in the moderator, etc. The measurements were carried out in different core configurations and in different openings in order to eliminate possible errors due to nonuniform distribution of the fuel in the fuel element. No systematic deviations were observed in these experiments. The procedure is described in more detail in [2, 3].

The experimental measurement results of the thermal neutron macrodistribution in an elementary cell of the VVR-SM were compared with calculations by the S-II-THERMOS program [2, 4]. Figure 3 shows the excellent agreement between these data. In order to obtain the parameters of the thermal neutron spectrum, the spectral indexes (SI) determined by the formula

$$SI = \frac{a^i_{Lu}/a^i_{Dy}}{a^t_{Lu}/a^t_{Dy}},$$

were measured and compared with the calculations, where a_{Lu} and a_{Dy} are the relative activities of the isotopes formed in the reactions $Lu^{176}(n, \gamma)Lu^{177}$ and $Dy^{164}(n, \gamma)Dy^{165}$, of which the former has considerable resonance in the thermal region of the spectrum. The spectral index is a quantity which is sensitive to changes of the neutron temperature. The indexes i and t correspond to exposures in the thermal spectrum being studied and in the standard thermal spectrum. The method of measurement is described in [5] and is similar to that described above. Thus, the neutron temperature in the fuel obtained was 430 ± 20°K (this parameter is essential for estimating the magnitude of the deviation of the U^{235} cross-section from the 1/v [6] by Westcott's formalism). For the thermal neutron utilization factor, the value of $f = 0.8652^{+0.0020}_{-0.0035}$ was obtained. In the error shown, in addition to others, the error resulting from the unknown detailed activation distribution of manganese by epithermal neutrons is also included. Very good agreement was obtained between the calculations of this parameter carried out by means of the S-II-THERMOS program (f = 0.8656).

Using the cross-section values from [6] and the currently recommended value of $\nu_t = 2.422 \pm 0.005$ [7], we obtain $\eta_t = 2.046$ and the "experimental" parameter $\eta_t = 1.749^{+0.005}_{-0.007}$; from the calculations we obtain $\eta^f_t = 1.747$ (for $\nu_t = 2.43$).

Fast Neutron Multiplication Factor

As the parameter ε is insignificant for fuel with a relatively high absorption, measurements of this parameter were not undertaken. The calculated estimate of the parameter ε was determined by the semi-empirical formula [8] for a homogenized cell:

$$\varepsilon = \frac{\nu_f - (1+\alpha_f)\sum_{if}}{\sum_{cf} + \sum_{if} - (\nu_f - 1)\sum_{ff}} + 1, \quad (5)$$

where Σ_{cf}, Σ_{if} and Σ_{ff} are the cross-sections of absorption, inelastic scattering, and fission respectively, averaged over the fission spectrum. The most important parameters are taken from [8] and the others (U^{235} and aluminum) have been obtained by averaging 26-group effective cross-sections [9] over the fission spectrum. The value of ε obtained by these calculations is equal to 1.0020.* We have used this result in future calculations and it shows that the contribution from fast neutrons to the multiplication factor is insignificant.

Epithermal Parameters of the Cell, δ^{25}, ρ^{28} and the ICR

The determination of the epithermal neutron fission coefficient δ^{25} and the resonance absorption coefficient ρ^{28} are given below. The ICR (initial coefficient of reproducibility), defined as the ratio of the number of neutrons absorbed in U^{238} to the total number of neutrons absorbed in U^{235} was obtained directly from the results of the measurements of the so-called modified initial coefficient of reproducibility (MICR), which is defined as the ratio of the total number of neutrons absorbed in U^{238} to the total number of neutrons created by the fission of U^{235}. This value was measured simultaneously with δ^{25} and ρ^{28}. It is obvious that

$$ICR = MICR \frac{1}{1+\alpha^i}, \quad (6)$$

so that the value of α must be averaged over the spectrum of neutrons in the reactor; the error in its determination will affect the accuracy of the determination of ICR.

Many possibilities exist for the choice of method of measuring the parameters listed above. The quantity measured must be β- or γ-active, proportional to the total and subcadmium absorption in U^{238} and to the fissioning in U^{235}. It is desirable that the detector used should not disturb the geometry of the cell and should have a uranium nuclei density similar to the density of the fuel nuclei, as resonance absorption is very sensitive to this quantity. Therefore, it is best to use a detector of the same composition as the fuel composition in the cell.

*Recently, K. Yuzefovich obtained by the method of track detectors, a result which confirms the value quoted, within the limits of error.

The subcadmium absorption and fission were not measured in the lattice being studied because of the complex structure of the cell and the perturbations introduced into it. This difficulty has been overcome by measuring the number of absorptions and fissions in the thermal neutron spectrum in the thermal column of the "EVA" reactor. These two measurements were normalized by means of a thermal neutron detector.

Because of the high fuel enrichment, which leads to a high ratio of the fission product activity to the activity proportional to resonance absorption in U^{238}, it is necessary to separate chemically the activated detectors. The measurements were made only in the outer tube of the fuel element. The possible difference of these parameters in different tubes is considerably less than the experimental errors. In the external cladding to the layer of fuel of the outer fuel element tube, openings were made with diameter ~5 mm, into which the assembly shown in Fig. 2 was introduced, with additional aluminum foils for shielding the foil-detectors from fission fragments.

In order to prevent the influx of water to the fuel element and the detector, covers of a water-impermeable adhesive tape were used. In order to eliminate any possible error due to nonuniformity of distribution of the fuel in the fuel element layer, the measurements were carried out at several points of the outer tube. The fuel pellets with dysprosium foil in the thermal spectrum were irradiated in the thermal column of the "EVA" reactor.

The gamma-activity of the dysprosium foils was measured by a well-scintillation counter. The average activity of the dysprosium foil, corresponding to the position of the pellet in the fuel element, was calculated by the known distribution of the neutron density within the cell [3]. The total γ-activity of the fission products, proportional to the number of fissions in the uranium, was determined with a threshold of ~1.3 MeV in order to discriminate the γ-radiation and the bremsstrahlung from isotopes of uranium and neptunium, also by a well-scintillation counter.

After measuring the activity of the fission products from the fuel pellet, the Np^{239} was separated chemically. The method of separating the neptunium is based on two chromatographic separations, with 2-thenoyltrifluoroacetone (TTA) as the stationary phase. This separation method is described in [10], trivial changes were introduced. The activity of the liquid neptunium samples was measured by a scintillation counter and a multichannel analyzer by the Np^{239} peak (106 keV, over the range 60-160 keV), with subtraction of the background due to other activities.

Thus, in the lattice studied and the thermal spectrum respectively, the following relative activities were obtained: dysprosium a^i_{Dy} and a^t_{Dy}; neptunium a^i_{Np} and a^t_{Np} and fission products a^i_{FP} and a^t_{FF}. By means of these values δ^{25}, ρ^{28} and MICR can be determined.

The number of epicadmium fissions in U^{235} to the number of thermal fissions in U^{235} in this case will be equal to

$$\delta^{25} = R\left(\frac{FP}{Dy}\right)_{cor} - 1. \tag{7}$$

In the experimentally obtained relation $R(FP/Dy) = (a^i_{FP}/a^i_{Dy})/(a^t_{FP}/a^t_{Dy})$ it is necessary to introduce corrections for the activation of the dysprosium by epithermal neutrons and also for the difference between the effective thermal cross-sections in a pure thermal spectrum and in the thermal neutron spectrum of the lattice being studied.

The first correction is introduced by measuring the cadmium ratio for dysprosium in the lattice being studied, and the second by using the effective cross-sections averaged over the spectrum ($\bar{\sigma}^{Dy}_a$, $\bar{\sigma}^{25}_a$) and calculated by the S-II-THERMOS program. Finally, we obtain

$$\delta^{25} = \left[R\left(\frac{FP}{Dy}\right)\frac{Cd\,R\,(Dy)}{Cd\,R\,(Dy)-1}\cdot\frac{g^{25}_f(T_t)\,\sigma^{25}_{f,0}\cdot\bar{\sigma}^{Dy}_a}{g^{Dy}_a(T_t)\,\sigma^{Dy}_{a,0}\cdot\bar{\sigma}^{25}_f}\right] - 1. \tag{8}$$

The differences between the isotope yields in the case of fission by neutrons with nonidentical energies and subsequent differences in the total activities can be neglected.

The number of epithermal absorptions in U^{238} to the number of thermal absorptions of U^{238} is

$$\rho^{28} = R\left(\frac{Np}{Dy}\right)_{cor} - 1. \tag{9}$$

It is necessary to introduce certain corrections into the experimentally measured ratio $R\left(\frac{Np}{Dy}\right)$. These corrections, as in the previous case, are obtained as a result of measurements of the cadmium ratio and the effective cross-sections based on calculations by the S-II-THERMOS program:

$$\rho^{28}=\left[R\left(\frac{Np}{Dy}\right)\frac{Cd\,R\,(Dy)}{Cd\,R\,(Dy)-1}\cdot\frac{g_c^{28}(T_t)\,\sigma_{c,0}^{28}\cdot\bar{\sigma}_a^{Dy}}{g_a^{Dy}(T_t)\,\sigma_{a,0}^{Dy}\cdot\bar{\sigma}_c^{28}}\right]-1. \tag{10}$$

By obtaining the numerical values of the corresponding corrections Q_1 and Q_2 from [11], we can determine also

$$\rho^{28}=\left[R\left(\frac{Np}{Dy}\right)Q_1Q_2\frac{Cd\,R\,(Dy)}{Cd\,R\,(Dy)-1}\right]-1. \tag{11}$$

These corrections are trivial.

The modified initial coefficient of reproducibility can be obtained directly:

$$MICR=\left(\frac{\sum_a^{28}}{\sum_f^{25}}\right)_{sp}^{th}\quad\frac{a_{Np}^i/a_{FP}^i}{a_{Np}^t/a_{FP}^t}, \tag{12}$$

and also by an indirect method:

$$MICR=\frac{1+\rho^{28}}{1+\delta^{25}}\left(\frac{\sum_a^{28}}{\sum_f^{25}}\right)_{\substack{\text{subcadmium}\\ \text{spectrum in cell}}}. \tag{13}$$

The ratios of the effective cross-sections are determined by means of Westcott's formalism (this is not entirely accurate in the second case) or by a numerical method.

Results of Measurements of the Cell Parameters

The directly measured quantities in this paper are: density distribution of thermal neutrons and loss coefficients, $\delta_m = 1.104 \pm 0.015$, $\delta_c = 1.044 \pm 0.010$; the spectral indexes for estimating the neutron temperature $\rho^{28} = 5.41\ ^{+0.17}_{-0.41}$, $\delta^{25} = 0.137 \pm 0.008$; MICR $= 0.0481 \pm 0.0013$.

The derived quantities: $f = 0.8652\ ^{+0.0020}_{-0.0035}$; $\eta_t f = 1.749\ ^{+0.005}_{-0.007}$; $\varepsilon = 1.002$; $p^{28} = 0.971\ ^{+0.002}_{-0.001}$; $p^{25} = 0.871\ ^{+0.007}_{-0.012}$; $k_e = 0.203^{+0.019}_{-0.011}$; $k_t = 1.482^{+0.019}_{-0.028}$; $K_\infty = 1.685\ ^{+0.010}_{-0.020}$; ICR $= 0.0394 \pm 0.0015$.

More detailed results are given in [12]. The relatively large error in ρ^{28} consists of a systematic error, due to the penetration of resonance neutrons through the gaps between the pellet and the walls of the opening in the fuel element. The value of η_e is assumed equal to 1.62 [1]. The effect of the inaccuracy in determining δ^{25} at K_∞ is small, as it is cancelled out to a considerable degree in the expressions $1 + \delta^{25}$ and p^{25}.

The methods described above were developed specially for investigations of complex lattices with average and high enrichments. This permits us to obtain data about the lattice parameters within the limits of applicability of the multiplication factor for an infinite medium.

Similar measurements were made for lattices of the VVR-SM type with increased ratio of the water and fuel volumes [13].

The Material Parameter of the Reactor

Whilst carrying out the program of criticality experiments with VVR-SM lattices, a large number of core configurations was chosen. In one of them, the geometry of which was close to cylindrical, with a water or beryllium reflector, with and without a dry part of the lattice, the horizontal and vertical flux distributions of thermal and epithermal neutrons were measured in detail. For this purpose copper foils and copper wires, bare or in a cadmium sheath were used and also threshold detectors of nickel and sulfur. The procedure for these experiments and their results is described in detail in [14]. The results of the measurements of the vertical distributions of the neutron fluxes carried out close to the core axis, were fitted to the relation $\Phi = A \cos B_z (z - z_0)$. The majority of the measurement results of the horizontal distributions was sufficiently accurate for fitting to a Bessel function: $\Phi' = A' J_0(B_r r)$. Thus, the axial and radial components of the material parameter of the reactor were determined.

The results of these measurements are given also in [14]. The value of the total parameter varies considerably, depending on the core configuration and the range of energies in which the distributions were determined. The dry part of the lattice, if it exists, affects the total parameter of the reactor obtained in practice from the distributions measured below the water level. Consequently, in order to estimate the experimental value of the material parameter of a pure lattice, only the results of the experiments conducted in zones without a dry part were used. The value of the material parameter of the reactor, determined by the epithermal neutron distributions obviously is nearer in all to the true value, as the epithermal neutron distributions are less sensitive to perturbations from the water channels for the control rods. As a result, the material parameter of the reactor obtained is $B^2 = 0.115 \pm 0.0003$ cm^{-2}.

Mean-Square Diffusion Length and Neutron Age

The mean-square diffusion length of thermal neutrons $\overline{L}^2$ is determined by means of the average effective cross-sections $\overline{\Sigma}_{tr}$ and $\overline{\Sigma}_a$ by the usual method:

$$\overline{L}^2 = \frac{1}{3\,\overline{\Sigma}_{tr}\,\overline{\Sigma}_a}, \tag{14}$$

where $\overline{\Sigma}_{tr}$ and $\overline{\Sigma}_a$ are obtained by weighting the corresponding cross-sections of the individual media with respect to flux:

$$\overline{\Sigma}_{tr} = \frac{\sum_i \Phi_i \Sigma^i_{tr}}{\sum_i \Phi_i} \approx \frac{\sum_i \delta_i V_i \Sigma^i_{tr}}{\sum_i \delta_i V_i};$$
$$\overline{\Sigma}_a = \frac{\sum_i \Phi_i \Sigma^i_a}{\sum_i \Phi_i} \approx \frac{\sum_i \delta_i V_i \Sigma^i_a}{\sum_i \delta_i V_i}. \tag{15}$$

Here, the loss coefficients δ_i are taken from the measurements mentioned above and the neutron temperatures for determining the effective cross-sections are taken from measurements of the Lu/Dy spectral index [5]. These values lead to $\overline{L}^2 = 2.7$ cm^2. Probably, it is better to take $\overline{L}^2 = 2.6$ cm^2, obtained from calculations by the S-II-THERMOS program [4]. The determination of this quantity is not required to a high accuracy as the mean-square diffusion length is small in comparison with the neutron age.

In principle, no direct experimental method has been developed for determining the neutron age in such a lattice. Therefore, in this paper the neutron age τ has been obtained by somewhat indirect methods based on the results of experiments and calculations.

1) Results are available of the measurements and calculations of neutron age up to indium resonance in mixtures of aluminum and water for different ratios of V_{Al}/V_{H_2O}. As, from the point of view of neutron retardation, the lattice being studied is in practice a mixture of water and aluminum (the corresponding fractions by volume are 0.552 and 0.424), interpolation of the age τ_{In} is possible from a series of results for the Al – H_2O mixture. Thus, based on the data from [15] we obtain $\tau_{In} = 65$ cm^2. This value does not coincide with the most recent measurements. Thus, for example, in [16] the value of 53 ± 1 cm^2 is obtained by the same method and in [17] $\tau_{In} = 49 \pm 1$ cm^2.

2) From calculations for these same mixtures, carried out by the MUFT-4 program [18], the one-group age can be determined. Interpolation of the results, using this, gives $\tau_{In} = 51.5 \pm 1$ cm^2.

3) Using the results of calculations by the Monte-Carlo method obtained in [19] by interpolation, we determine the value of τ_{In} equal to ~ 51 cm^2 (this latter value was obtained for a heterogeneous mixture).

4) A. D. Galanin [21] derives a formula for determining the neutron age in a mixture of several components:

$$\frac{1}{\tau} = \sum_i \frac{c_i^2}{\tau_i} + \sum_i \sum_{j>i} A_{ij} c_i c_j, \tag{16}$$

where τ_i is the neutron age in the i-th component and c_i is the fraction by volume of the i-th component. Using this formula for the lattice being investigated and considering it as a homogeneous mixture, we obtain $\tau_{In} = 66.7$ cm^2, which differs considerably from the results given above. It should be borne in mind that formula (16) has been derived for components with identical dependence of the effective cross-sections on energy. Only in this case are the A_{ij} well-defined by the functions τ, μ and ξ of the components. In the

case being considered, this condition is not fulfilled and it is more effective to use the coefficients A_{ij} for matching parameters of the calculated results to the experimental data. In practice, the sole purpose in this case is to determine the coefficient A_{ij} for i (water) and j (aluminum), as it is only important for the lattice being investigated. For example, if we calculate this coefficient by the data from [22], in which the age was measured in many mixtures of $H_2O-Al-Th$ (where it is not possible to use simple interpolation), we obtain $\tau_{In} = 53.8 \pm 2$ cm^2. This same coefficient can be determined by the other measurements mentioned (in very good agreement with the coefficient from [22]).

5) Finally, in order to obtain the neutron age, 26-group constants are used [9] according to the following formula:

$$\tau = \int_{E}^{E_0} \frac{l_s l_t}{3\xi} \frac{dE}{E} + \frac{l_{s,0} \cdot l_{t,0}}{3} \approx \sum_{\kappa} \frac{l_{s,\kappa} \cdot l_{t,\kappa}}{3\xi_\kappa} \ln \frac{E_\kappa}{E_{\kappa+1}} + \frac{l_{s,0} \cdot l_{t,0}}{3}, \tag{17}$$

where K is the index of the group corresponding to the upper energy boundary. In each group the following relations are valid:

$$\left.\begin{aligned} \frac{1}{l_{s,\kappa}} &= \sum_i N_i (\sigma^i_{e,\kappa} + \sigma^i_{in,\kappa}); \\ \frac{1}{l_{t,\kappa}} &= \sum_i N_i [\sigma^i_{e,\kappa}(1 - \mu^i_{e,\kappa}) + \sigma^i_{in,\kappa}]; \\ \xi_\kappa &= l_{s,\kappa} \sum_i N_i \xi^i_\kappa (\sigma^i_{e,\kappa} + \sigma^i_{in,\kappa}). \end{aligned}\right\} \tag{18}$$

The initial groups are weighted with respect to the fission spectrum and the correction due to the first transmit (before the first collision of the neutron) also was averaged over the fission spectrum. The effect of inelastic scattering was not considered in more detail, but the effect should be trivial as the layers of fuel are very thin. As a result of the calculations carried out we obtain $\tau = 50.8$ cm^2.

The neutron age calculated by this same method up to indium resonance in water is equal to 27.0 cm^2, which is found to be in very good agreement with the data of report [23]. The errors derived together with the results are due only to the method of determining the neutron age for the lattice being investigated. By means of such a choice of values, we can obtain a more reliable average. The weighted mean value of the neutron age up to indium resonance for a regular VVR-SM lattice is 51.5 ± 0.6 cm^2. A somewhat higher value of the neutron age (52.6 cm^2) is obtained for the very similar lattice of the VVR-M (a little greater fraction of aluminum than in the VVR-SM), as a result of matching to the experimentally measured critical mass [24].

The correction for the neutron age of indium resonance up to thermal energy is 2.4 ± 0.2 cm^2, so that the overall neutron age is 53.9 ± 0.7 cm^2. It should be noted that the results of the age calculations by the method described in Section 5 using 26-group constants [9], are very similar to the average value of the age. Obviously, this method can be used for estimating the age for a number of uranium – water lattices.

Effective Multiplication Factor

Let us consider the criticality equation in simple approximation for water systems:

$$\kappa_{eff} = \frac{\kappa_\infty}{(1 + \tau B^2)(1 + L^2 B^2)}. \tag{19}$$

Substituting the values derived above, the magnitude of the neutron escape probability can be obtained as 0.599 ± 0.009. Consequently, $K_{eff} = 1.010^{+0.021}_{-0.027}$, which is quite a good result.

The large error is distributed almost uniformly between $K_\infty (^{+0.6\%}_{-1.2\%})$, B^2 ($\pm 1.0\%$) and τ ($\pm 0.5\%$). It is possible that some sources of error in the multiplication factor of an infinite medium are overestimated, for example, because of the unknown nature of the distribtuion of epicadmium activity of the thermal neutron detector or the leakage of resonance neutrons during the measurements of ρ^{28}. Therefore, the resulting errors might be less. The material parameter of the reactor undoubtedly can be measured with a high accuracy by careful exclusion of lattice perturbations. Data from [20] show that the principal error of the final result is caused by neglecting the effect of heterogeneity of fission neutron sources when estimating

the age. Here, an addition to the value of τ of about 1 cm^2 is permissible. The possibilities of estimating this effect by a simple method are discussed in [25].

It is advantageous to proceed in reverse, i. e., to obtain the material parameter of the reactor by the use of the 2-group criticality equation, using the measured multiplication factor of an infinite medium, and the calculated age. In this case, $B^2 = 0.0118^{+0.003}_{-0.005}$ cm^{-2}, which is in good agreement with the results obtained by measurement of the macrodistributions [14].

The author takes this opportunity to express his thanks to Dr. S. Khvashchevskii and his co-workers L. Adamskii and K. Jozefowicz for valuable comments and constant assistance, and also to the operating group of the MARYLA reactor for their close cooperation.

LITERATURE CITED

1. D. B. Wehmeyer, Light Water Lattices, Technical Reports Series No. 12, IAEA, Vienna (1962), p. 177.
2. E. T. Józefowicz, L. Turi, and J. Valkó, Nukleonika, 14, 1171 (1969).
3. E. T. Józefowicz, Dokald IBJ No. 884/IXA/PR, Institute of Nuclear Research, Warsaw (1968).
4. K. Kowalska, see [3], Doklad IBJ No. 878/XXI/PR (1968).
5. E. T. Józefowicz, P. IBJ No. 895/IXA/PR (1968).
6. E. Critoph, Addendum to AECL-1101 (1964), CRRP-1191.
7. F. L. Fillmore, J. Nucl. Energy, 22, 79 (1968).
8. R. L. Hellens, WAPD-114 (1956).
9. L. P. Abagyan, N. O. Bazazyants, I. I. Bondarenko, and M. N. Nikolaev, Group Constants for the Calculation of Nuclear Reactors [in Russian], Atomizdat, Moscow (1964).
10. E. T. Józefowicz, Doklad No. 748/IXA/PR, Institute of Nuclear Research, Warsaw (1966).
11. O. S. Larvin et al., Symposium on Exponential and Critical Experiments, Vol. II, IAEA, Vienna, 161 (1964).
12. E. T. Józefowicz, P. IBJ No. 919/IXA/PR (1968).
13. E. T. Józefowicz, P. IBJ No. 1119/IXA/PR (1969).
14. L. Adamski, K. Józefowicz, and E. T. Józefowicz, Doklad IBJ No. 968/IXA/PR (1968).
15. J. B. Hill, L. D. Roberts, and T. B. Fitch, J. Appl. Phys., 26, 1013 (1955).
16. R. K. Paschall, Nucl. Sci. Engng, 26, 73 (1966).
17. J. D. Spencer and T. G. Williamson, Nucl. Sci. Engng, 27, 568 (1967).
18. D. H. Shaftman, Special Report on [23].
19. H. Goldstein et al, ORNL-2639 (1961) (Reported in [17]).
20. P. Palmedo, Trans. ANS, 10, 240 (1967).
21. A. D. Galanin, Theory of Thermal Neutron Reactors, Atomizdat, Moscow (1959).
22. W. G. Pettus, BAW-146 (1960).
23. Reactor Physics Constants, ANL-5800 (1963).
24. T. B. Ashrapov et al., Doklad 152, Fifth Conference on the Physics and Technology of Research Reactors [in Russian], 5RC/124, Warsaw, December (1968).
25. E. T. Józefowicz, Nukleonika, 15, 399 (1970).

NOISE ASSOCIATED WITH INHOMOGENEITIES IN THE HEAT CARRIER OF A REACTOR

A. I. Mogil'ner

UDC 621.039.51

The noise effects observed in power reactors contain a large number of components reflecting the characteristics of the technological processes. One of these components may be associated with inhomogeneity of the heat carrier due, for example, to the formation of gas or steam bubbles, solid corrosion products, and so forth.

Let us consider the contributions made to the neutron noise of a reactor by inhomogeneities distributed uniformly over the heat carrier, for example, gas (or steam) bubbles circulating together with the heat carrier in the first circuit. An approach of this kind is also valid when the effect of boiling (ebullition) on the reactor noise is under consideration.

Theory of Noise Due to Bubbles Circulating in the Heat Carrier

Let the heat carrier flow from bottom to top along the axis of the reactor. Let us suppose that the bubbles are uniformly distributed over the reactor cross section. Let us use q_j to denote the contribution to the reactivity due to the replacement of the j-th bubble by an equal volume of heat carrier, averaged over the volume occupied by the heat carrier. The quantity q_j is a random function of the index j. Moving along the z axis of the reactor, the bubble introduces different contributions into the reactivity; these may be described by means of a certain function $q_j\psi(z)$ averaged over the reactor cross section.

If the bubble moves at a velocity v_0, the time dependence of the change in reactivity may be expressed in the form

$$U_j(t) = q_j \varphi(t - t_j), \tag{1}$$

where t_j is the instant at which the j-th bubble crosses the central plane of the reactor with coordinate z = 0. The weighting functions $\psi(z)$ and $\varphi(t)$ are related by the expressions

$$\psi[v_0(t - t_j)] = \varphi(t - t_j). \tag{2}$$

We shall consider that the function $\varphi(t)$ possesses the properties

$$\varphi(t) = \begin{cases} \varphi_0(\tau) & \text{for } |\tau| = |t - t_j| \leqslant \frac{h}{2v_0}; \\ 0 & \text{for } |\tau| = |t - t_j| \geqslant \frac{h}{2v_0}, \end{cases} \tag{3}$$

where h is the effective height of the reactor.

Let us consider a fairly large time interval $-T/2$ to $T/2$ ($T \gg h/v_0$) during which $N \gg 1$ bubbles pass through the reactor. For a fairly large number of such realizations (aggregates), the reactivity noise considered over the specified interval may be expressed in the form of the following stochastic function for each (k-th) realization:

$$U^{(k)}(t) = \sum_{j=1}^{N} q_j^{(k)} \varphi(t - t_j). \tag{4}$$

The random process under consideration is regarded as being centered, stationary, and ergodic.

The spectrum of function (4) has the form

Translated from Atomnaya Énergiya, Vol. 30, No. 6, pp. 510-514, June, 1971. Original article submitted May 11, 1970, revision submitted July 22, 1970.

$$U^{(k)}(f) = \sum_{j=1}^{N} q_j^{(k)} \int_{-\infty}^{\infty} \varphi(t - t_j)\, e^{-i\omega t}\, dt, \quad \omega = 2\pi f. \tag{5}$$

The spectral density of the reactivity noise $S_1(f)$ is defined by averaging the realizations over the aggregate thus:

$$S_1(f) = \lim_{T\to\infty} \frac{2E_k |U^{(k)}(f)|^2}{T}. \tag{6}$$

We also suppose that the dimensions of the bubbles are not correlated with respect to the sequence of their passing into the reactor, so that

$$E_k [q_j^{(k)}] = \bar{q}; \tag{7}$$

$$E_k [q_j^{(k)} q_l^{(k)}] = \begin{cases} \bar{q}^2 & \text{for } j = l; \\ \bar{q}^2 & \text{for } j \neq l. \end{cases} \tag{8}$$

According to the theorem of lagging and relation (3)

$$\int_{-\infty}^{\infty} \varphi(t - t_j)\, e^{-i\omega t}\, dt = e^{-i\omega t_j} \int_{-\infty}^{\infty} \varphi(t)\, e^{-i\omega t}\, dt = e^{-i\omega t_j} \int_{-h/2v_0}^{h/2v_0} \varphi_0(\tau)\, e^{-i\omega\tau}\, d\tau. \tag{9}$$

We introduce the dimensionless function

$$\Phi(f) = \frac{v_0}{h} \int_{-h/2v_0}^{h/2v_0} \varphi_0(\tau)\, e^{-i\omega\tau}\, d\tau. \tag{10}$$

Then

$$|U^{(k)}(f)|^2 = \left(\frac{h}{v_0}\right)^2 |\Phi(f)|^2 \sum_{j,\, l=1}^{N} q_j^{(k)} q_l^{(k)}\, e^{-i\omega t_j}\, e^{i\omega t_l}. \tag{11}$$

After averaging the realizations over the aggregate, using relations (7) and (8), we obtain

$$E_k |U^{(k)}(f)|^2 = \left(\frac{h}{v_0}\right)^2 |\Phi(f)|^2 \left[N\bar{q}^2 + \bar{q}^2 \sum_{(j\neq l)=1}^{N} e^{i\omega(t_l - t_j)}\right]. \tag{12}$$

Supposing that the instants at which the bubbles cross the central plane of the reactor are quite random, we obtain

$$\sum_{(j\neq l)=1}^{N} e^{i\omega(t_l - t_j)} = \sum_{(j\neq l)=1}^{N} \cos\omega(t_l - t_j) + i \sum_{(j\neq l)=1}^{N} \sin\omega(t_l - t_j) = 0 \tag{13}$$

as a result of the uniform distribution of the values of $\cos\omega(t_l - t_j)$ and $\sin\omega(t_l - t_j)$ in the range -1 to $+1$.

Thus, on introducing the average frequency of access of the bubbles $n = N/T$, we may write down the following expression for the spectral density of the reactivity noise:

$$S_1(f) = 2n\bar{q}^2 \left(\frac{h}{v_0}\right)^2 |\Phi(f)|^2 \tag{14}$$

or

$$S_1 = 2rn\bar{q}^2 \left(\frac{h}{v_0}\right)^2 |\Phi(f)|^2, \tag{14a}$$

where $P = \bar{q}^2/\bar{q}^2$.

Relation (14) may also be obtained from the second Campbell theorem for random dimensions of the bubble (contribution to reactivity) and for a random time of its passage into the reactor. The Campbell theorem may be written in the form

$$\sigma_1^2 = n \int_0^{\infty} \bar{f}^2(t)\, dt, \tag{15}$$

where σ_1^2 is the mean square of the fluctuations in reactivity, while $f(t)$ is the reaction of the reactor (reactivity) to the bubbles which have passed into the reactor at the time $t = 0$. In the case under consideration

$$\int_0^{\infty} \bar{f}^2(t)\, dt = \int_{-\infty}^{\infty} \bar{q}^2 \varphi^2(t)\, dt, \tag{16}$$

where we have averaged over the aggregate in view of the random nature of the quantity q (the difference from the canonical formulation of the Campbell theorem lies in the replacement of q^2 by $\overline{q^2}$).

Thus the mean square of the fluctuations in reactivity equals

$$\sigma_1^2 = n\overline{q^2} \int_{-\infty}^{\infty} \varphi^2(t)\, dt. \tag{17}$$

In accordance with the Parseval theorem and Eqs. (3) and (10)

$$\int_{-\infty}^{\infty} \varphi^2(t)dt = \left(\frac{h}{v_0}\right)^2 \int_{-\infty}^{\infty} |\Phi(f)|^2\, df = 2\left(\frac{h}{v_0}\right)^2 \int_0^{\infty} |\Phi(f)|^2\, df, \tag{18}$$

so that

$$\sigma_1^2 = 2n\overline{q^2}\left(\frac{h}{v_0}\right)^2 \int_0^{\infty} |\Phi(f)|^2\, df. \tag{19}$$

However, by definition

$$\sigma_1^2 = \int_0^{\infty} S_1(f)\, df, \tag{20}$$

whence

$$S_1(f) = 2n\overline{q^2}\left(\frac{h}{v_0}\right)^2 |\Phi(f)|^2,$$

which agrees with Eq. (14).

Equation (14) may easily be related to certain more convenient macroscopic quantities, the rate of flow of the heat carrier Q and the volume concentration of the bubbles in the heat carrier g:

$$S_1(f) = \frac{2r'}{\gamma Q}\alpha' g\overline{V}\,|\Phi(f)|^2. \tag{21}$$

Here $r' = \overline{V}^2/\overline{V}^2$; V is the volume of a bubble, $\alpha(r)$ is the contribution made to the reactivity on replacing the heat carrier by a bubble, referred to unit volume, $\alpha' = \overline{\alpha}^2 V_R^2$ is a dimensionless quantity depending on the character of the spatial dependence $\alpha(r)$; V_R is the volume of the heat carrier in the reactor, $\gamma = v_0/v_1$ is the ratio of the average velocity of the bubbles to the average velocity of the heat carrier in the reactor. If the nonuniformity $\alpha(r)$ is fairly small, α' may be expressed in terms of ρ_1, the contribution of the heat carrier filling the reactor to the reactivity:

$$\alpha' \approx \overline{\alpha}^2 V_R^2 = \left(\frac{\rho_1}{V_R}\right)^2 V_R^2 = \rho_1^2,$$

so that

$$S_1(f) = \frac{2r'}{\gamma Q}\rho_1^2 g\overline{V}\,|\Phi(f)|^2. \tag{21a}$$

Expressions (21) and (21a) show that the fluctuations associated with the inhomogeneity of the heat carrier increase both with increasing concentration of the bubbles g and with increasing bubble size V. As $\overline{V} \to 0$ the heat carrier becomes inhomogeneous, and the noise component under consideration vanishes.

The spectral composition of the noise is a sensitive characteristic of the velocity of the bubbles in the reactor. The form of the spectral function $\Phi(f)$ is determined by the form of the weighting function $\varphi_0(t)$, which in turn depends on the manner in which the inhomogeneities act upon the reactivity. If we suppose that the contribution of the bubble to the reactivity is proportional to the flux and intensity of the neutrons at the site of the bubble, and that the weighting function $\varphi_0(t)$ may be approximated by

$$\varphi_0(t) = 2\cos^2\frac{v_0}{h}\pi t \tag{22}$$

(where the coefficient 2 is taken in accordance with the requirement that $\varphi_0(t) = 1$), then the corresponding frequency function $|\Phi(f)|^2$ will be expressed by

$$|\Phi(f)|^2 = \frac{\sin^2 b\pi}{\pi^2 b^2 (1-b^2)^2}, \quad b = \frac{h}{v_0} f. \tag{23}$$

Expression (23) tends to unity as $v_0 \to \infty$ and $f = 0$, and reaches zero at a frequency of $f = 2(v_0/h)$.

As indicated earlier, there may well be other forms of the $\varphi_0(t)$ and hence the $\Phi(f)$ relationship. However, the upper limit of the spectrum cannot change seriously, as it is determined by the average time spent by the bubble in the reactor $\tau_0 = h/v_0$.

The mean square of the fluctuations of reactivity due to the bubbles is described by the following expression, on the assumption that Eq. (22) remains valid:

$$\sigma_1^2 = \int_0^\infty S_1(f)\,df = \frac{3}{2} r'\alpha' g \frac{\overline{V}}{V_R}. \tag{24}$$

In practice we are concerned not with fluctuations in reactivity but with power noise. The spectral density of the power noise $S_n(f)$ is obtained by means of the transmission function of the reactor $R(f)$:

$$\frac{1}{N_0^2} S_n(f) = \frac{2r'}{\gamma Q} g\alpha' \overline{V} |\Phi(f)|^2 |R(f)|^2, \tag{25}$$

where N_0 is the steady-state reactor power. At low frequencies, in particular, on filtering the noise in a narrow band Δf around the frequency $f_0 \ll v_0/h$

$$\varepsilon_n^2 \approx \frac{2r'}{\gamma Q} g\alpha' \overline{V} |R(f_0)^2 \Delta f, \tag{26}$$

where $\varepsilon_n^2 = \{S_n(f_0)/N_0^2\}\Delta f$ is the relative mean square of the power noise.

The foregoing expressions relate to a critical reactor. For a subcritical system, the average power N_0 of which is given by the degree of subcriticality $\rho' = (1 - K_{eff})/K_{eff}$ and the intensity of the neutron source, we must use the corresponding expression for the transmission function of a subcritical reactor $R(\rho', f)$. In the particular case of fairly low frequencies, and with a narrow-band filter, the relative mean square power noise approximately equals

$$\varepsilon_n^2 \approx \frac{2r'}{\gamma Q} \cdot \frac{\alpha'}{\beta_{eff}^2} g\overline{V} \Delta f_{eff}. \tag{27}$$

We note that in the majority of practically-important cases we may approximately assume $r' \approx 1$, $\gamma \approx 1$. A more precise value of γ is obtained from the form of the spectrum $S_1(f)$ or from the Stokes law, when the application of this is justified.

A measurement of the relationship $S_1(f)$ enables us to find the form of the time function $\varphi(t)$ describing the effect of a bubble on the reactivity for various positions of the bubble relative to the height of the reactor. This may be done if we assume the symmetry of the function $\varphi(t)$. In this case the spectrum of the function $\varphi(t)$ does not contain any imaginary component, and the form of the original time function may be restored by means of an inverse Fourrier transformation

$$|\varphi_0(\tau)|^2 = 2\frac{v_0}{h_0} \int_0^\infty \left| \sqrt{\frac{S_1(f)}{S_1(0)}} \right| \cos 2\pi f\tau\, df; \quad \frac{-h}{2v_0} \leqslant \tau \leqslant \frac{h}{2v_0}. \tag{28}$$

Calculation of the relationship (28) enables us to determine the average time spent by the bubble in the reactor $\tau_0 = h/v_0$ and the mean velocity of the bubble in the reactor v_0. It should be noted that if the dimensions of the bubble change as it passes along the axis of the reactor, then this is reflected in the form of the weight function $\varphi(t)$.

Observation of Circulating Bubbles

In constructing a system for observing moving bubbles or other inhomogeneities it is important to optimize the frequency range of the recording. It is clearly preferable to choose a region of higher frequencies, since in this case the problems of measurement are simplified and the contribution of competing processes is less serious. If on the side of the reactor there are no competing processes in the frequency range chosen, then the possibility of observing bubbles will be limited by the intrinsic current fluctuations of the ionization chamber. The latter of course occupy a wide range of frequencies with a spectral density $S_0 = 2q_0J$, where J is the average current of the ionization chamber, while q_0 is the mean charge arising in the chamber on recording a neutron.

The possibility of observing bubbles by the method described is determined by the condition

$$\frac{S_n(f)}{S_0} = \frac{r'\alpha'}{\gamma Q} g\overline{V} |\Phi(f)|^2 |R(f)|^2 \frac{J}{q_0} \gtrsim 1. \quad (29)$$

On choosing the frequency range of the recording in the region $f \gtrsim 1$ cps $|R(f)|^2 \approx 1/\beta_{eff}^2$ and

$$\frac{S_n(f)}{S_0} \approx \frac{r'\alpha'}{\gamma Q \beta_{eff}^2} g\overline{V} |\Phi(f)|^2 \frac{J}{q_0} \gtrsim 1. \quad (30)$$

Let us consider an example (for the BR-5 reactor). We take $r' \approx 1$; $\gamma \approx 1$; $Q = 240$ m^3/h; $\alpha' \approx (4.5\beta_{eff})^2$; $h \approx 0.5$ m; $v_0 \approx 4$ m/sec; $q_0 \approx 10^{-14}$ C/neutron; $J \approx 10^{-4}$ A. Choosing $f \gtrsim 1$ cps we obtain $|\Phi(f)|^2 \approx 1$. Let us discover for what mean bubble sizes $\overline{V}$ the bubbles may be detected for a mean volume concentration of the gas in the heat carrier of 1% ($g \approx 10^{-2}$). Substituting the corresponding values in Eq. (30) we find

$$\overline{V} \gtrsim 0.03 \text{ mm}^3.$$

This effect of inhomogeneities on reactivity constitutes an analog of the well-known electronic shot effect, complicated by fluctuations in the sizes of the inhomogeneities and the finite time during which these move in the reactor.

Determination of Gas (Steam) Content in the Heat Carrier

The volume concentration of the gas in the heat carrier g may be determined experimentally by considering the effect of the pressure of the heat carrier on the reactivity. If in fact a change in the heat-carrier pressure in the reactor from p to p + Δp is accompanied by a change in the volume of the gas (uniformly distributed over the reactor) from V_1 to $V_1 + \Delta V_1$, then this will cause the reactivity to change by an amount

$$\Delta\rho = -\rho_1 \frac{\Delta V_1}{V_R}. \quad (31)$$

Assuming constancy of the temperature and the validity of the equation

$$pV_1 = (p + \Delta p)(V_1 + \Delta V_1), \quad (32)$$

we find that

$$\frac{\Delta V_1}{V_1} = -\frac{\Delta p}{p + \Delta p}. \quad (33)$$

Substituting expression (33) into (31) we obtain

$$\Delta\rho = \rho_1 g \frac{\Delta p}{p + \Delta p}. \quad (34)$$

Thus

$$g = \frac{\Delta\rho}{\rho_1}\left(1 + \frac{p}{\Delta p}\right). \quad (35)$$

We note that, generally speaking, the pressure in the bubbles themselves should be used in the foregoing examples, rather than the pressure in the heat carrier, the former being equal to

$$p_0 = p + \frac{2\varkappa}{r_0}, \quad (36)$$

where $2\varkappa/r_0$ is the additional pressure, which is determined by the surface tension of the film of heat carrier limiting the volume of the bubble, $\varkappa$ is the surface-tension coefficient, and r_0 is the radius of the bubble. However, this difference need only be allowed for in the case of very small bubbles ($2\varkappa/r_0 p \gg 1$), i. e., when the bubbles have dimensions of the order of 1 μ or under.

Effect of Pressure Fluctuations on Reactivity

The existence of pressure fluctuations in the presence of gas "vacancies" leads to additional fluctuations of reactivity. For small pressure fluctuations relation (34) may be written in the form

$$\Delta\rho = \rho_1 g \frac{\Delta p}{p}. \quad (37)$$

Assuming that in Eq. (37) the quantities $\Delta\rho$ and Δp describe a stationary, ergodic, random process, it is quite easy to transform to the spectral densities

$$S_2(f) = \rho_1^2 g^2 S_p(f). \tag{38}$$

Here S_2 is the reactivity noise component due to the pressure fluctuations in the presence of vacancies, and $S_p(f)$ is the spectral density of the relative pressure fluctuations.

Thus the additional component of reactivity noise associated with the pressure fluctuations reproduces the form of the spectral composition of the latter; it vanishes when the vacancies vanish from the reactor ($g=0$). For very small bubble sizes, Eq. (38) has to be corrected by allowing for the fact that the pressure in the bubble differs from that in the heat carrier surrounding it:

$$S_2(f) = \rho_1^2 g^2 S_p(f) \left(\frac{1}{1+\frac{2\varkappa}{r_0 p}}\right)^2. \tag{38a}$$

The latter expression shows that a reduction in bubble size leads to a gradual reduction in the contribution of the component in question, until it vanishes completely.

Equation (38) may be applied in order to determine the concentration of the vacancies in the heat carrier. In order to secure as high as possible an accuracy in separating out the component in question, it is convenient in Eq. (38) to transform to the mean square relative deviations $\sigma_p^2 = \int_0^\infty S_p(f)\,df$ и $\sigma_2^2 = \int_0^\infty S_2(f)\,df$:

$$g = \frac{\sigma_2}{\rho_1 \sigma_p}. \tag{39}$$

Combined Effect of Circulating Bubbles and Pressure Fluctuations on Reactivity

The two components mentioned usually act together, i. e., we observe a reactivity noise which, by virtue of the statistical independence of the effects of these random processes, is described by the expression

$$S(f) = \frac{2r'\alpha'}{\gamma Q} g\overline{V} |\Phi(f)|^2 + g^2 \rho_1^2 S_p(f). \tag{40}$$

However, the frequency composition of the two components usually differs. This difference may be used in order to separate the components (the first often has a wider frequency band than the second). In this case the S(f) relationship gives the concentration of vacancies in the heat carrier g and the average volume of the bubble $\overline{V}$ quite independently.

As already indicated, the components under consideration have different sensitivities to the sizes of the bubbles. Whereas the first component is only observed for fairly large bubbles, the second appears under far less rigorous conditions.

The foregoing relationships may prove useful in analyzing reactor noise, and in particular in studying the boiling of the heat carrier in the reactor.

In conclusion, the author wishes to thank S. A. Morozov and G. P. Krivelev for useful discussions.

DESIGN OF THE JINR FOUR-METER ISOCHRONOUS CYCLOTRON WITH SMOOTHLY REGULATED HEAVY-ION ENERGIES

I. A. Shelaev, E. D. Vorob'ev,
B. A. Zager, S. I. Kozlov,
V. I. Kuznetsov, R. Ts. Oganesyan
Yu. Ts. Oganesyan, K. I. Semin,
A. N. Filipson, and V. A. Chugreev

UDC 621.384.633

Further development in the physics of nuclear reactions between complex nuclei is bound up with the use of fast ion beams of even heavier elements in these reactions and also with an increase in their energy and intensity. For this purpose, a four-meter isochronous cyclotron (accelerator U-400) has been designed in the JINR Laboratory of Nuclear Reactions on the basis of the results obtained in the construction of the JINR two-meter isochronous cyclotron U-200 [1]. At the present time, work at JINR involves the fabrication of parts and sections of the U-400 accelerator, which is being built on the foundations of the existing 310-centimeter, classical heavy-ion cyclotron (accelerator U-300) [2].

The parameters of these accelerators are given in Table 1, from which it is apparent that practically all the systems of the U-400 accelerator differ significantly from those of the U-300. The U-400 cyclotron is very much like the U-200 accelerator, which can be considered as a model of the larger accelerator on

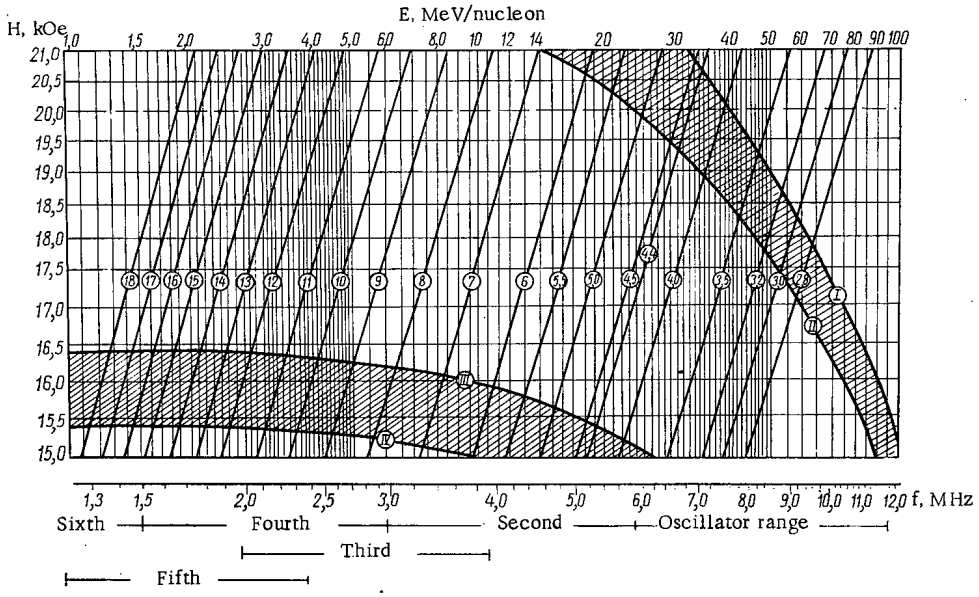

Fig. 1. Energy of ions with various values of A/Z (numbers in circles) in the operating range of the levels of the average field H and rotational frequency f of the ions at the final radius R_f = 180 cm for the U-400 cyclotron. The Roman numerals I-IV correspond to the values 0, 0.04, 0.21, and 0.25 for ν_z^2.

Translated from Atomnaya Énergiya, Vol. 30, No. 6, pp. 514-520, June, 1971. Original article submitted, May 13, 1970; revision submitted August 3, 1970.

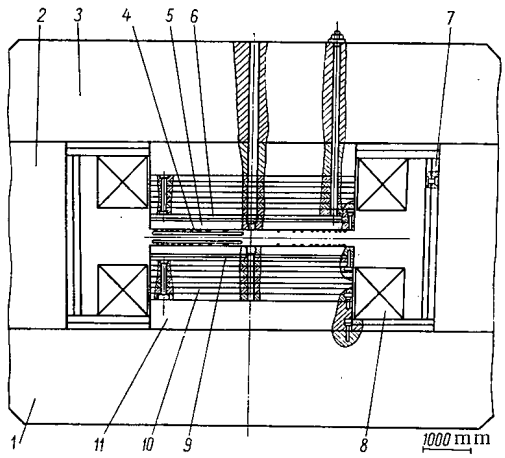

Fig. 2. Electromagnet of the U-400 cyclotron: 1, 3) upper and lower beams; 2) columns; 4) sector; 5) chamber cover; 6, 9) upper and lower spacer discs; 7) supplementary iron yoke; 8) excitation coils; 10, 11) new and old pole stacks.

a 1:2 scale. Some differences primarily concern the magnetic field structure in connection with the expansion of the mass and energy of the accelerated ions. Figure 1 shows the energy E for ions with different A/Z and the rotational frequency of these ions in the selected range of working levels of the average magnetic field in the cyclotron (16-20 kOe at the final radius of 180 cm). In the figure, the hatched regions correspond to the areas where the breakdown of betatron oscillation stability arises. Expansion of the range of final energies of the ions accelerated in the cyclotron from E = 5-10 to E = 1-50 MeV/nucleon and of the range A/Z ratios from 5-7 to 3.5-25 are ensured by an increase in the magnetic field level, by the introduction of azimuthal variations, and by other changes in the cyclotron structure.

Magnet Structure

To increase the level of the magnetic field to 20 kOe, the cross section of the magnetic circuit of the electromagnet (Fig. 2) was increased by 13%, and the spacing between the main excitation coils was reduced by 500 mm. The conical pole tips (D_{max} = 400 cm, D_{min} = 310 cm) were replaced by cylindrical ones 400 cm in diameter. The new pole tips were built up from separate discs using the same technology as for the U-200 cyclotron [3]. The average air gap between the poles was reduced from 540 to 200 mm.

Magnetic circuit calculations and extrapolation of experimental results obtained with the U-200 cyclotron showed that after completion of the changes listed above, an average magnetic field of 20-20.5 kOe could be obtained with an excitation current of 2200-2500 A in the main coils. This made it possible to keep the old electromagnet supply system without change.

The magnetic gap of the U-400 cyclotron is shown in Fig. 3. The spacing between the steel vacuum chamber covers is 300 mm. The elements for shaping the magnetic field (sectors, concentric coils, etc). and the dees are located in this gap. These elements were designed with the results obtained on the U-200 cyclotron kept in mind. The isochronous shape of the magnetic field is determined by the expression

$$H_{is} = \frac{H\bar{0}}{\sqrt{1-\frac{2W}{E\bar{0}}}},$$

where W is the ion kinetic energy per nucleon and E_0^- is the proton rest energy; this shape is ensured by circular shims and concentric coils. The calculation of the required configuration of the circular shims was done on a computer. As experiments performed on the U-200 showed, the accuracy of these calculations is about 10% of the total shim contribution (~ 1.5 kOe); consequently, further field correction will be

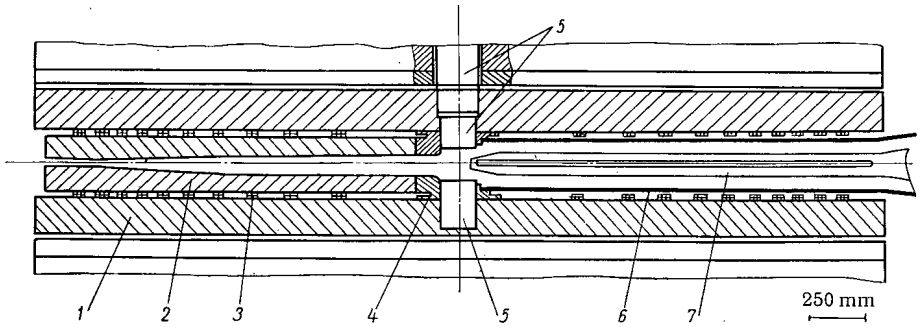

Fig. 3. Geometry of the air gap in the U-400 cyclotron: 1) steel chamber covering; 2) sector shim; 3) circular correction coil; 4) central shim; 5) removable central plugs; 6) chamber cladding; 7) dee.

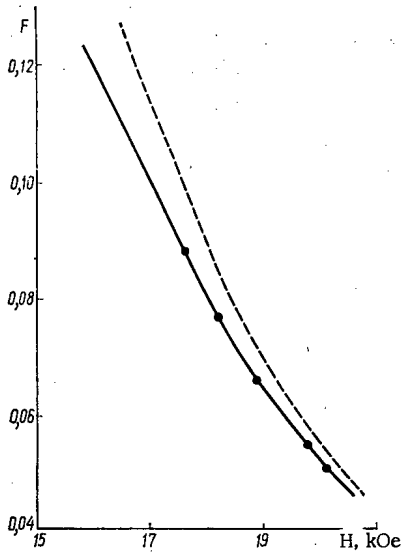

Fig. 4

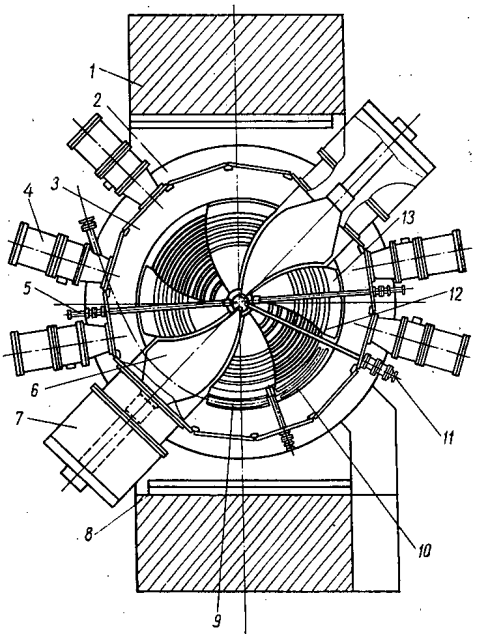

Fig. 5

Fig. 4. Dependence of the magnetic field flutter in the U-200 cyclotron (——) and of the U-400 cyclotron flutter corrected for sector height (- - - -) on the average field level at the final radius of the accelerator.

Fig. 5. Diagram of U-400 accelerator: 1) electromagnet column; 2) excitation coil; 3) vacuum chamber; 4) VA-8-4 high-vacuum pump; 5) transfer probe; 6) dee; 7) resonator; 8) supplementary iron yoke; 9) magnetic channel; 10) electrostatic deflector; 11) ion source; 12) concentric coil; 13) sector shim.

accomplished experimentally. In the U-400 cyclotron, such shims are located only in the sectors and are fabricated together with them. This type of shim arrangement complicates sector construction somewhat, but makes it possible at the same time to reduce the height of the circular shims and simplifies their fabrication technology.

Correction of the average magnetic field over the entire operating range of field levels is accomplished with concentric coils. Calculation of the ampere-turns required for correction was performed on a computer by the least-squares method for two versions of radial coil distribution – uniformly in r and r^2. To obtain an isochronous magnetic field shape and permissible radial gradients, the number of coil pairs was varied from 8 to 12. It should be noted that for a coil distribution uniform in r^2, the ampere-turns for each coil were nearly the same. The U-400 current-correcting system contains ten pairs of concentric coils (total number of ampere-turns IW = 22,500). Each circular coil consists of three turns of a hollow copper conductor 11.5 × 11.5 mm in size with a central opening 8 mm in diameter for cooling. The turns, which were insulated with a fiber-glass-epoxy compound, were put down in an aluminum housing located under the sectors (see Fig. 3).

Each concentric coil is fed from a six-phase silicon rectifier through a choke filter. Current regulation (from 0 to 900 A) is accomplished by a magnetic amplifier connected in the primary circuit of a step-down transformer. Separate supplies for the upper and lower coils are provided for three pairs of concentric coils in order to achieve median plane corrections. Amplitude and phase control of the lower harmonics of the magnetic field nonuniformity is accomplished by six pairs of azimuthal coils.

Azimuthal variation of the magnetic field is created by four sector pairs. The sector height and the magnetic field flutter was calculated with the results obtained on the U-200 in mind. The proposed magnitude

TABLE 1. Parameters of the U-300 and U-400 Cyclotrons

System characteristic	U-300	U-400
Electromagnet		
Diameter of pole tips, cm	310	400
Final acceleration radius, cm	138	180
Magnet weight, tons	1900	2260
Average air gap, mm	540	200
Number of turns in main excitation coils	2×224	2×224
Operating current in electromagnet coil, A	1870	1000 – 2500
Average magnetic field, kOe	16,7	16 – 20
Number of sectors	—	4
Angle of spiral	—	30°
Radial drop in magnetic field, %	0,8	Isochronous
Number of auxiliary coils	4	19
Hf-system		
Number of dees	2	2
Azimuthal extent of dee	180°	45°
Dee voltage, kV	150	70—100
Wavelength range, m	50—100	25—50
Dee aperture, mm	40—140	80—40
Dee-chamber cladding gap, mm	80	70
Tunable element	Shorting plate	Movable panel
Dee voltage stability, %	None	0,2
Mode of operation	Pulsed	Arbitrary
Vacuum system		
Vacuum chamber volume, m^3	75	25
Chamber pressure, mm Hg	$6 \cdot 10^{-6}$	$1 \cdot 10^{-6}$
Number of high-vacuum, oil-vapor pumps	5	5 (7)
Capacity of a single pump, sec^{-1}	20 000	8000
Extraction and Beam Transport systems		
Azimuthal extent of deflector, deg	103	45
Entrance and exit gaps, mm	8/22	6
Deflector working voltage, kV	40—60	40—60
Azimuthal extent of focussing magnetic channel, deg	34	45
Field gradient in channel, Oe/cm	450	1500
Number of extracted beams	1	2
Number of switching magnets	2	3
Number of working directions	12	16
Extraction efficiency, %	30	30—100
Beams		
Energy of accelerated ions, MeV/nucleon	5—10	1—50
Total energy, MeV	250 Z^2/A	400—625 Z^2/A
Mass-to-charge ratio A/Z	5—7	3,5—25
Energy spread, %	0,5	0,2—0,3

of the flutter as a function of the average magnetic field level at the final radius of the accelerator is shown in Fig. 4. Using these flutter values, the spiral angle of the sectors was chosen with consideration given to the following conditions. With the introduction of helicity, vertical focussing is increased and the allowance for shaping the magnetic field, particularly at high levels, is reduced. However, at large angles, the limits of field regulation are reduced because the quantity ν_z rises to 0.5 with a decrease in the field level. The sector helicity angle was chosen to be 30° so that $\nu_z \leq 0.5$ for ions with energies up to 5 MeV/nucleon at a magnetic field level of 16 kOe.

Thus the magnetic field structure selected for the U-400 cyclotron makes it possible to accelerate ions over a broad A/Z range and with smoothly controlled energy (see Fig. 1) without using flutter-correcting coils.

Magnetic Field Measurements

The increase in accelerator dimensions and the expansion in the range of magnetic field operating levels lead to an increase in the volume of magnetic measurements by almost an order of magntiude in comparison with the volume of measurements on the U-200 cyclotron [4]. In shaping the magnetic field of the U-200 cyclotron, the total number of measured field values was 400,000, which took about 300 h on the whole.

If the previous rate of measurement is retained, the performance of the magnetic measurements would require about 3000 h. This number includes only the time of actual measurement, and does not include the time which would be spent on the fabrication of the measured version of a shim, on the fabrication of equipment, etc. At the present time, work is going on to improve the measuring technique developed for the U-200 cyclotron for the purpose of increasing the rate of measurement by factors of three or four while maintaining, and even increasing, accuracy, and also for the purpose of increasing the reliability and recording speed of the measurements.

Hf-System

A diagram of the arrangement of the basic units of the U-400 accelerator is shown in Fig. 5. Preservation of the old electromagnet yoke makes the use of more than two dees difficult. The choice of frequency range (6-12 MHz) for the two-dee version was decided by the following conditions. First, the use of the amplitude of the accelerating voltage should be most efficient for the acceleration of ions with A/Z =7-12 (the heaviest for which there is the greatest interest). The maximum energy rise experienced by particles per turn in such a system is

$$\Delta E_{max} = 4\bar{Z}_e U_g \sin\frac{n\pi}{8},$$

where n is the order of the accelerating voltage harmonic. Second, the amplitude of the accelerating voltage should be such that breakdown in the chamber is practically completely eliminated for the selected

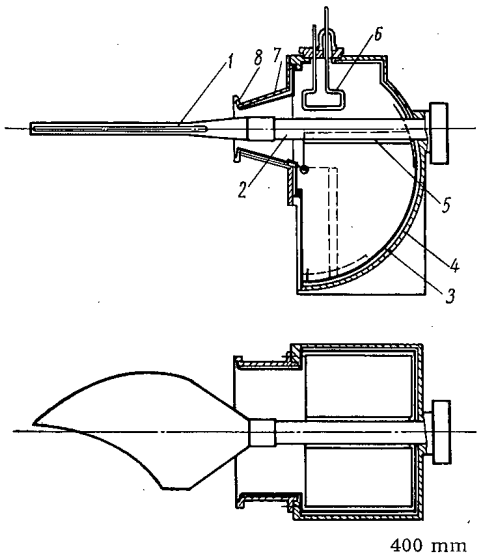

Fig. 6. Model of U-400 cyclotron resonator: 1) dee; 2) stem; 3) resonator housing; 4) copper cladding of resonator; 5) movable panel in maximum frequency position (dashed lines show minimum frequency position); 6) coupling loop; 7) transition fitting; 8) flange.

TABLE 2. Energy and Intensity of Ions to be Accelerated in the U-400 Cyclotron

Type of ion accelerated	Energy, MeV /nucleon	Intensity of internal beam, particles/sec
Ne_{20}^{+2}	6,2	9 м·10^{14}
Ne_{20}^{+3}	14,1	4·10^{14}
Ne_{22}^{+3}	11,6	4·10^{14}
Ar_{40}^{+5}	9,8	6·10^{13}
Zn_{64}^{+7}	7,5	2,5·10^{13}
Kr_{84}^{+8}	5,7	1,8·10^{13}
Kr_{84}^{+9}	7,2	1,3·10^{12}
Xe_{132}^{+12}	5,2	5·10^{11}
Xe_{132}^{+13}	6,1	10^{11}

dee-chamber cladding gap (7 cm); this ensures stable machine operation in both continuous and pulsed modes. Finally, the third condition for the choice of frequency range was that it should be a multiple of the frequency range of the existing "Apatit" generator (f = 3-6 MHz).

On this basis, an accelerator mode in the second-fourth harmonics was chosen for ions with A/Z = 7-12 (see Fig. 1). With a dee voltage amplitude U_g = 100 kV, these ions, accelerating to the final energy, will then complete about 200 revolutions. Increase in the number of revolutions and operation at higher harmonics of the ion rotation frequency require stabilization of the accelerating voltage amplitude to an accuracy of the order of ±0.2%. The frequency of the dee circuit is controlled in the given range by means of a moving panel.

The resonator model with a single rotating panel [5] selected for the U-400 cyclotron makes it possible to achieve changes in the frequency of the dee circuit by a factor of two comparatively simply. A model of the U-400 cyclotron resonator is sketched in Fig. 6. One edge of the rotating panel makes contact with the cladding of the resonator by means of a crimped copper plate, and contact of the second stage is provided by the capacity of the vacuum condenser formed by the shoe and the resonator wall. Measurements of resonator Q and impedance, made with a full-size model, showed that a dee voltage amplitude of 100 kV is provided at any frequency in the assigned range with generator power from 75-100 kW.

Ion Sources

The comparatively large gap between the vacuum chamber covers in the U-400 cyclotron (see Fig. 5) makes it possible to use ion sources in horizontal and vertical arrangements. Horizontally constructed sources are mainly intended for producing ions from elements which are normally only in the solid state because the chamber dimensions are increased in this case by the presence of a vaporizer for the working material, which is located in the immediate vicinity. A vertical opening in the electromagnet yoke permits the use of an ion source in a vertical arrangement [6, 7]; in addition, it can be used for the external injection of a beam of heavy ions from sources operating on other principles [8]. The arrangement of such sources in the accelerator chamber and their operation in the magnetic field of the cyclotron presents some difficulties.

Beam Extraction

Extraction of the beam from the U-400 cyclotron will be accomplished in two ways – by an electrostatic deflector and by charge-exchange of the ions in a thin foil [9, 10]. As experience with the U-200 has shown, the realization of these two methods encounters no fundamental difficulties; however, because of vaporization and erosion of the charge-exchange foils, the extraction of intense beams of heavy ions with $A \geq 40$ by the charge-exchange method is limited.

Thus the increase in energy and the expansion of the range of A/Z ratios of the accelerated ions makes it possible to increase the intensity in beams of ions of standard elements (neon, argon) with mass

$A \leq 40$ because of acceleration in the isochronous mode of ions of the elements at lower charge, or to increase their energy by acceleration of ions with their previous charge, and, finally, to accelerate ions with a mass $A \leq 132$. Table 2 shows the intensity and maximum energy of various heavy ions which will be accelerated in the U-400 cyclotron.

The authors are grateful to G. N. Flerov for his continuous concern with the work and to I. F. Malyshev for valuable advice.

LITERATURE CITED

1. I. A. Shelaev et al., JINR Preprint 9-3988, Dubna (1968).
2. V. S. Alfeev et al., JINR Preprint P-2693, Dubna (1966).
3. I. A. Shelaev et al., JINR Preprint P-9-4233, Dubna (1968).
4. E. G. Imaev et al., JINR Preprint 9-3713, Dubna (1968).
5. T. Johnson et al., IEEE Transactions on Nucl. Science, NS-16, 438 (1969).
6. K. W. Ehlers, Nucl. Instrum. and Methods, 18-19, 571 (1962).
7. T. Tauti et al., JINR Report 9-4368, Dubna (1969).
8. E. D. Donets et al., JINR Preprint P7-4124, Dubna (1968).
9. I. A. Shelaev et al., JINR Preprint P9-4831, Dubna (1969).
10. I. A. Shelaev et al., JINR Report P9-5037, Dubna (1970).

SYSTEM FOR SLOW STEERING OF ACCELERATED BEAM ONTO INTERNAL TARGETS IN THE IHEP 70-GeV ACCELERATOR

V. I. Gridasov, A. A. Kardash,
K. M. Kozlov, O. V. Kurnaev,
V. V. Lapin, S. V. Lobanov,
L. L. Moizhes, K. P. Myznikov,
and A. A. Naumov

UDC 621.384.6

The majority of the physics experiments using counting techniques are performed at the Institute for High-Energy Physics (IHEP) accelerator with beams of secondary particles which are produced at internal targets. There are several targets for each of the operating channels. The position of the targets within the vacuum chamber is selected so as to ensure emergence into the channel of secondary particles covering a broad range of momenta with minimal production angles. In this way, we have succeeded in obtaining high intensity in the extracted beams of secondary particles – up to 10^6 particles per pulse. In the optimum arrangement, the targets are radially displaced by distances of up to ±5 cm with respect to the center of the vacuum chamber. Steering the accelerated beam onto a target is performed during the flat portion of the magnetic cycle of the accelerator. Steering time is 1.5 sec for a field stability of 4×10^{-4} at the 12 KOe level and the relative magnitude of the amplitude of the predominant ripple frequencies of 25, 50, and 150 Hz is $2\text{-}3 \times 10^{-5}$.

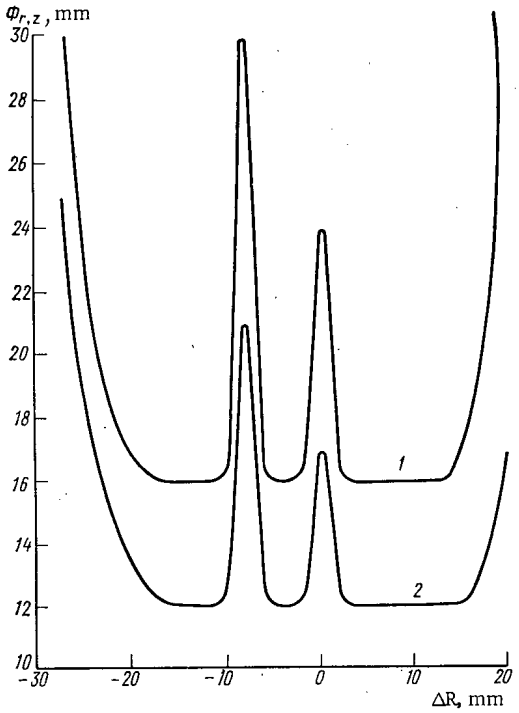

Fig. 1. Radial dependence of horizontal (1) and vertical (2) dimensions of the accelerated beam in a radially focussing section.

For efficient use of secondary particle beams, it is necessary to maximize the extraction time and to eliminate modulation of extracted beam densities. In the IHEP accelerator, increase in extraction time to more than 1 sec is achieved by reducing the beam steering velocity onto the target to 3-5 mm/sec. At such velocities, one can obtain beam intensities sufficiently uniform in time and can eliminate the modulation determined by the ripple of the magnetic field only by introducing feedback from the particle current out of the target into the steering system.

Under these conditions, the method of beam steering to a target by changing the hf acceleration mode [1], which is widely used at accelerators, is completely unacceptable. It does not offer the capability of shifting the beam by distances of ±5 cm from the equilibrium orbit without loss of stability and it does not enable one to eliminate the time structure in the extracted beam. The system described below for steering the accelerated beam onto internal targets is based on artificial excitation of azimuthal asymmetry in the magnetic field of the accelerator. It differs considerably from existing systems [2, 3] in the large

Translated from Atomnaya Énergiya, Vol. 30, No. 6, pp. 520-525, June, 1971. Original article submitted September 14, 1970.

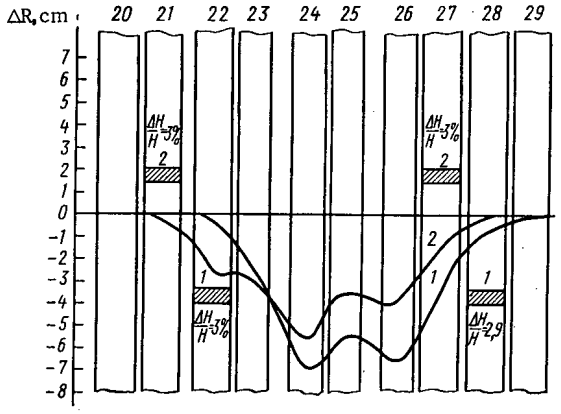

Fig. 2. Shape of orbit distorted by excitation of azimuthal asymmetry of the magnetic field in focussing (1) and defocussing (2) sections in the portion of the accelerator between sections 21 and 29.

working range of radial target positions and thereby provides beam extraction times > 1 sec with a density variation less than 10%.

Properties of Beam Motion During Steering onto Target

Particle dynamics while steering the accelerated beam onto internal targets has been discussed in detail [4]. It was established that the nonlinear components of the magnetic field at 12 kOe give rise to a strong dependence of the frequencies of the radial, Q_r, and vertical, Q_z, betatron oscillations on orbit radius. Because of this, both linear and nonlinear resonances may appear at certain orbit radii. This is aggravated by the fact that the beam moves in a constant magnetic field for a time greater than one second during guidance to the target.

An experimental check completely confirmed this hypothesis. The dependence of the horizontal and vertical dimensions of the accelerated beam on its motion at various radii during the flat portion of the magnetic field with H = 12 kOe is shown in Fig. 1. The beam is completely lost by an inward displacement of 3 cm from the central orbit and by an outward displacement of 2 cm, which corresponds to the theoretical location of integral and parametric resonances. In the space between them, the beam dimensions increase because of the effects of nonlinear resonances. The presence of resonances can reduce the efficiency of the beam–target interaction significantly and can make the time structure of the extracted beams poorer. Consequently, methods which employ artificial expansion (contraction) of the orbit are completely excluded.

It is more reasonable to hold the accelerated beam in the unperturbed region near the central orbit and to carry out steering itself by a method which does not disturb the vertical and radial stability of the beam. For this purpose, a method for exciting local distortions of the orbit was selected. The local orbital distortion, with an extent close to half the wavelength of a betatron oscillaton, was created by excitation of a supplementary field in two sections with a strength up to $\Delta H/H = \pm 3\%$.

The shape of the distorted orbit is shown in Fig. 2. Calculations showed that for distortions corresponding to curve 1, the frequency shift can reach ±0.04 (Fig. 3a) for a distortion amplitude of ±5 cm. With

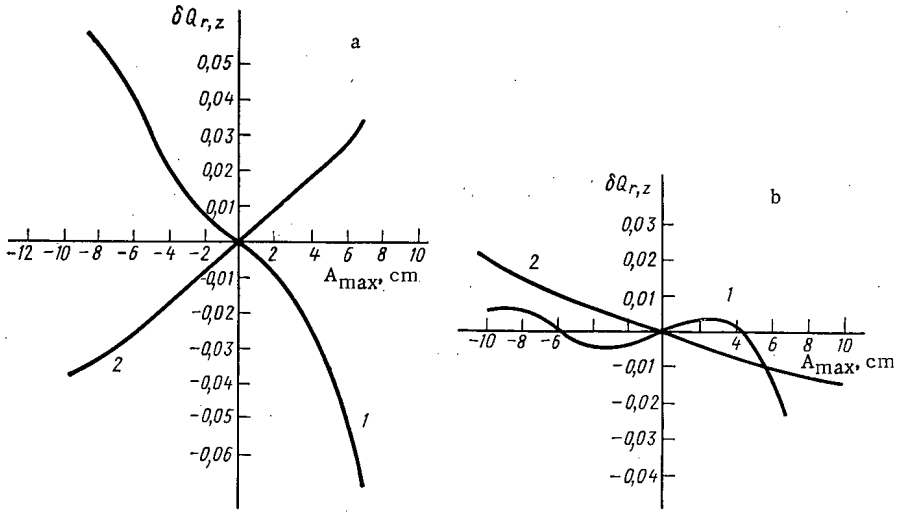

Fig. 3. Shift in frequency of horizontal (1) and vertical (2) betatron oscillations with excitation of azimuthally asymmetric magnetic field in focussing (a) and defocussing (b) sections.

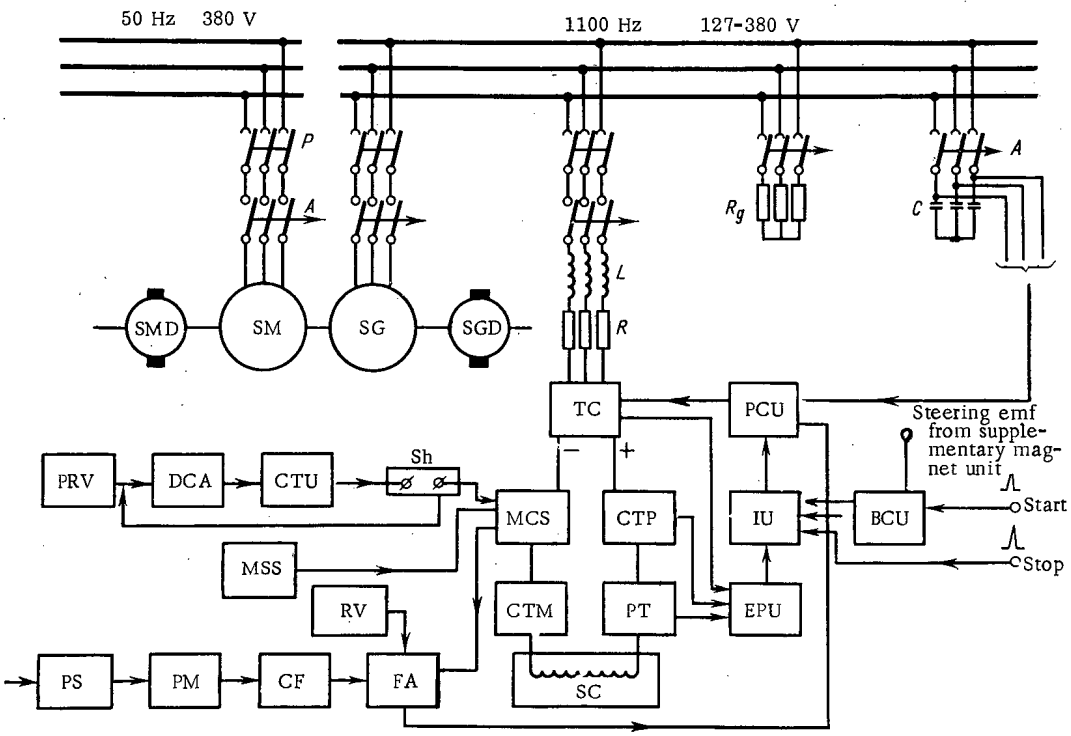

Fig. 4. Block diagram of supply system for supplementary coils: SG) synchronous generator; SGD) synchronous generator driver; SM) synchronous motor; SMD) synchronous motor driver; TC) regulated thyristor converter; SC) supplementary coil of magnet section; PS) secondary particle intensity sensor; PM) photomultipler; CF) cathode follower; RV) reference voltage unit; FA) feedback amplifier; PRV) pulsed reference voltage source; DCA) dc amplifier; CTU) control transistor unit; Sh) stabilization shunt; MCS) magnetic current sensor; MSS) magnetic current sensor supply unit; CTM) current transformer for measurements; CTP) current transformer for protection; PT) Pulsed unit transformer, EPU) electronic protection unit, PCU) phase control unit; IU) inverter units; BCU) bump time position control unit.

excitation of the distortion in defocussing sections, the frequency shifts resulting from changes in gradient and from nonlinear terms of the magnetic field compensate one another so that the total shift becomes negligibly small (Fig. 3b). Thus by creating the orbit distortion in defocussing sections, the target operating region can be expanded to ±5 cm and more.

Intensity modulation in the extracted beams at the frequency of the hf voltage is eliminated by turning off the accelerating field at the time of transition to the flat portion of the magnetic cycle. Beam steering to the target begins only after debunching. Since the effects of resonances are eliminated during steering intensity modulation with time can only be caused by magnetic field ripple. For effective suppression of this phenomenon, a feedback signal proportional to the beam current at the target was introduced and a rapid-response, broad frequency range was provided for the supply system for the supplementary coils in the sections. On the other hand, the current ripple in the supply system itself was confined to levels which did not lead to noticeable modulation of the particle flux density.

Description of System

The current in the supplementary coils of the magnet sections is supplied from regulated thyristor converters which are fed over a three-phase bridge circuit from synchronous induction generators running at a frequency of 1100 Hz and at a power of 260 kW (Fig. 4). Voltage regulation of the thyristor converters is accomplished by means of negative feedback based on a signal from a sensor of accelerated beam current at the target. A scintillation monitor of the intensity of the secondary particles created in the target is used as the sensor. A block diagram of the system for regulation of the beam current at the target is shown in Fig. 5 along with the frequency characteristics [5]. In plotting the logarithmic frequency characteristics (Fig. 5), the following transfer functions of the elements were assumed:

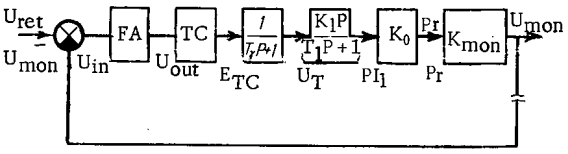

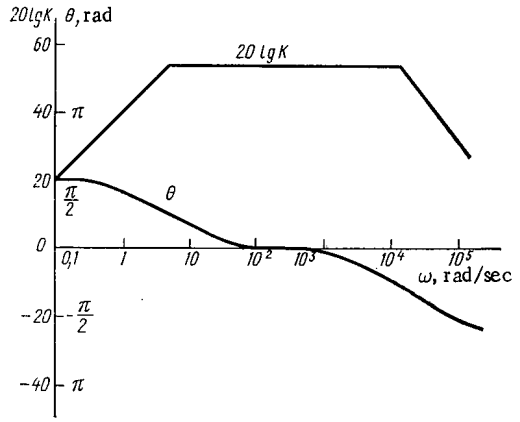

Fig. 5. Block diagram of the control systems for beam current at the target and logarithmic frequency characteristics.

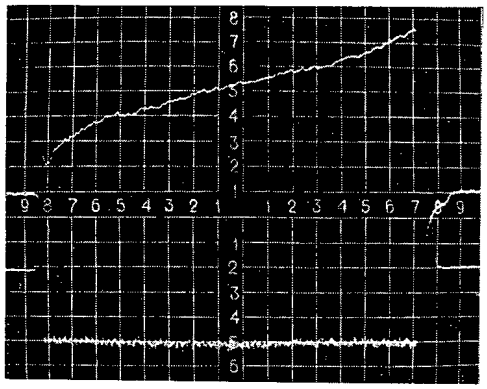

Fig. 6. Oscillogram of the supplementary coil current (upper beam) and signal from secondary particle intensity monitor (lower beam) for slow beam steering onto the target. Sweep scale is 50 msec/div.

a) amplification factor of the feedback amplifier

$$K_{ta} = \frac{U_{out}}{U_{in}},$$

where $U_{in} = U_{ref} - U_{mon}$; U_{ref} is a reference voltage, and U_{mon} is the monitor voltage;

b) transfer function of thyristor converter

$$K_T = \frac{U_T}{U_{out}} = \frac{E_{TC}}{U_{out}} \cdot \frac{1}{T_\gamma \cdot P + 1},$$

where $T_\gamma = \gamma/4\pi f$, γ is the commutation angle, and f is the generator frequency;

c) transfer function for derived current in load

$$K_{PL} = \frac{I_l \cdot P}{U_T} = \frac{K_l \cdot P}{T_l \cdot P + 1},$$

where I_l is the load current, T_l is the load time constant, and K_l is the load factor;

d) beam displacement transfer function

$$K_o = \frac{r}{I_l},$$

where r is the beam displacement from the equilibrium orbit;

e) monitor intensity transfer function

$$K_{mon} = \frac{U_{mon}}{P \cdot r}.$$

For maximum possible expansion of the frequency range determined by the supply voltage frequency of 1100 Hz, the time jitter for pulse formation on cutting in the thyristors was reduced to 10-20 μsec. Cascade thyristors (type PTL-100), which have an intrinsic turn-on time of a few microseconds, are used in the system. The required stability in tying in the control system with the transistors at the moment the 1100 Hz voltage passes through zero is ensured by a filter network which prevents marked distortion of the voltage sine wave from the generators (see Fig. 4).

The transfer functions for the individual elements and for the entire block diagram, which are shown in Fig. 5, ensure effective processing of the variations in the feedback signal caused by instability in the flat portion of the magnetic field in the accelerator and by ripple harmonics in the frequency range 25-600 Hz. This is achieved through the uniformity of the amplification factor and the nearly zero phase shift over the frequency range mentioned. The use of a high-frequency feed (1100 Hz) eliminates amplitude and phase distortions in the handling of feedback signal variations by tube-type converters at the ripple frequency of the accelerator magnetic field.

By replacing the feedback from the beam current sensor with the feedback from the magnetic current sensor in the supplementary coil (see Fig. 4), one can form trapezoidal current pulses with flat or sloped tops which can be used for feeding the beam to a target by a fast displacement of the beam at the target, for orbit corrections in the sections, etc. The stability of the pulse tops, including current ripple, is ~0.1%.

At the leading and trailing edges of the current pulse in the supplementary coil, the feedback circuit is not closed (with respect to beam current or coil current). To reduce the current pulse rise and decay

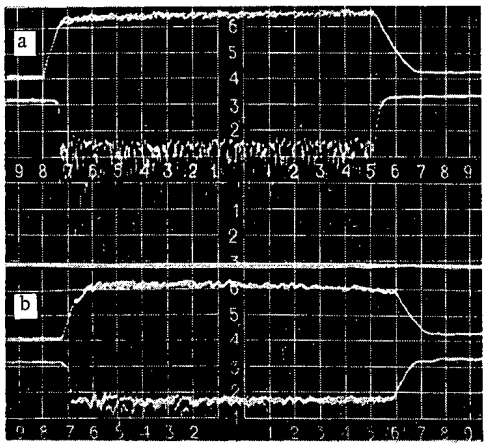

Fig. 7

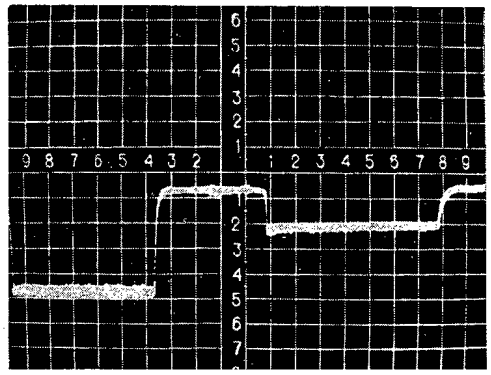

Fig. 8

Fig. 7. Oscillograms of supplementary coil current and secondary particle beam intensity monitor signal in cases of slow beam steering onto a target under the effect (a), and with suppressed effect (b), of nonlinear resonances. Sweep scale is 50 msec/div.

Fig. 8. Oscillogram of signal from secondary particle intensity monitor for slow beam steering sequentially onto two targets in different channels. Sweep scale is 50 msec/div.

times, a voltage is applied to the coil which is several times greater than the effective component of the voltage drop in it. Formation of the leading edge of the current pulse begins with the arrival of a "start" pulse from the overall timing device for the accelerator (see Fig. 4). In this mode, the regulation angle is kept close to zero, which corresponds to the maximum voltage on the coil. Formation of the current decay occurs after the arrival of a "stop" pulse from the overall timing device. In this case a constant regulation angle close to 150° is established in the phase control unit by means of the phase inverter unit, which also ensures the optimum mode for inversion of the magnetic field energy in the supplementary coil. Shortening the lengths of the leading and trailing edges of the current pulse to values which are several times less than the time constant of the supplementary coil circuit (0.2 sec) ensures effective use of the flat portion of the magnetic field for multiple beam deflections onto several internal targets set up at different accelerator azimuths.

RESULTS

Figure 6 shows an oscillogram of the current variation in the supplementary coil (upper beam) which ensures uniform intensity for a deflection 800msec long with a density modulation of approximately 5% (lower beam). Clearly visible in the current variation curve are components with frequencies of 25-150 Hz derived from the ripple in the magnetic field of the accelerator. The greater rate of change in current during the first stage of the beam deflection ensures the formation of an almost rectangular shape for the variation of the secondary particle beam intensity. The average value of the secondary particle intensity during the entire time of beam deflection varies by no more than a few percent. The rise time of the intensity in the oscillogram of Fig. 6 is about 10 msec, and the decay time is about 30 msec.

Deterioration of the time structure in the extracted beam resulting from the effects of nonlinear resonances is shown in Fig. 7a. It is clear that perturbations of the proton beam caused by these resonances lead to modulation of the secondary particle flux density by as much as 80%. An oscillogram illustrating an improvement in beam deflection to the target is shown in Fig. 7b. The improvement was obtained by a correction to the accelerator field gradient which displaced the operating point outside the boundaries where nonlinear resonances had an effect. The remaining beam-steering conditions were the same as for the oscillogram in Fig. 7a.

Figure 8 shows an oscillogram of the monitor signal for sequential extraction of secondary particles into two channels with deflection times of 300 and 350 msec. The monitor recorded secondary particles from

both targets. It is clear that the short rise and decay times for the intensity, equal to 10-15 msec, make it possible to use the flat portion of the magnetic field effectively for sequential operation of several secondary particle channels in a single acceleration cycle.

LITERATURE CITED

1. G. S. Kazanskii et al., Pribory i Tekh. Éksperim., No. 5, 19 (1962).
2. K. P. Myznikov and I. N. Yalovoi, Pribory i Tekh. Éksperim., No. 4, 19 (1963).
3. K. Reich, Progr. in Nuc. Techniks and Instr., II, 163 (1967).
4. V. I. Gridasov and K. P. Myznikov, IFVÉ Preprint 68-60 (1968).
5. V. P. Shipillo, Automated Tube Electric Drive [in Russian], Énergiya, Moscow (1969).

NUCLEAR POWER ENGINEERING AND THORIUM RESOURCES

I. V. Chirkov

UDC 621.039:546.841

Predictions of the development of nuclear power generation are currently based on the presumed exploitation of natural uranium alone. However, other development lines exist, e.g., the development of competitive nuclear power stations equipped with thorium (uranium–thorium), reactors of various types, and the use of the thorium resources, which are probably greater than the uranium resources, in nuclear power generation.

The present article describes the demand for uranium of the expanding nuclear power production, discusses the fundamentals of the use of thorium, reviews briefly the practical application of thorium in reactors with a thorium cycle, and evaluates, in a first approximation (from the viewpoint of a geologist), the possible extent to which thorium can be used in nuclear power engineering.

Nuclear Power Plants and the Demand for Uranium

According to estimates, the power produced by nuclear power stations in all capitalist countries will reach about 25 GW (el.) in 1971 and will amount to 100-125 GW (el.) by 1975. An output of 230-340 GW (el.) is predicted for 1980 from all nuclear power plants. The contribution of nuclear power stations to the total electric energy production of the world will increase from 0.9% to 14% in 1980.

What are the uranium demands of nuclear power generation? The figures have been rather accurately determined for the near future (to 1980) because nuclear reactors making use of thermal neutrons and uranium will play the main role. The total demand for uranium of the capitalist countries will increase by 60-70% by 1974-1975, and the production of uranium must increase approximately four times by 1980, i. e., 62-86 thousand tons of U_3O_8 must be produced per year.

The annual US demand for uranium oxide for 145 GW (el.) output of the nuclear power plants was determined as 34 thousand tons by 1980 [1]; the integral demand amounts to 220 thousand tons. The specific consumption of uranium per GW (el.) of a fixed-power nuclear power station will be reduced from 700-800 t at the present time to 250-300 t at the end of the seventies. The feasibility of this program has been confirmed by contracts confirming the supply of 63 thousand tons of uranium [2].

When the usual 8-10 year reserve is added to the 220 thousand tons of uranium oxide, the sum increases to about 550 thousand tons. All other capitalist countries plan to use nuclear power in this time period and to create an uranium oxide reserve of more than 400 thousand tons. Thus, about 1 million tons of uranium oxide will be needed until 1980. Even with the worldwide development of fast breeder reactors, the uranium demand will amount to several million tons until the year 2000 [3].

Uranium and Thorium Resources

In foreign publications concerning the uranium resources in the interior of the Earth, a distinction is made between secured resources (which correspond to the concept of explored resources, as used in the USSR) and possible additional resources. Both types of resources are classified according to the expenses for their winning and enriching. A classification of the resources into those less expensive than 22, 22-33, and 33-36 dollar/kg U_3O_8 has been generally accepted. Due to the substantial economic disadvantages of nuclear power plants using thermal reactors, uranium resources which are more expensive than 22 dollar/kg will hardly be exploited on a large scale in the near future, though these resources amount

Translated from Atomnaya Énergiya, Vol. 30, No. 6, pp. 526-533, June 1971. Original article submitted September 8, 1970; final version received November 30, 1970.

to several million tons. It is therefore interesting to compare the above-mentioned uranium demand figures with the reserves available in mines from which the material can be extracted at a cost of 11-22 dollar/kg.

According to the latest estimates, the guaranteed U_3O_8 reserves amount to more than 700 thousand tons (more than 590 thousand tons when referred to the metal) and the additional reserves amount to about 700 thousand tons. Thus, the explored resources of inexpensive uranium do not even suffice until 1980. In the capitalist countries which are the main producers of uranium, prospecting and exploration work for uranium was resumed in 1965-1966. The extent of this work can be estimated from the drilling volume which exceeded several times that of the first "uranium boom" period (1955-1959). However, one can hardly expect that the explored reserves of inexpensive uranium will reach several million tons in the near future. Incidentally, the foreign press considers the time of 1980 to 2000 as a period with a shortage of inexpensive natural uranium.

In the overall calculation of the resources of nuclear fuel, it is justifiable to include the uranium used for military purposes. From 1942 to 1968, more than 370 thousand tons of U_3O_8 (i.e., 320 thousand tons of the metal) were won; the major part of this uranium (after partial extraction of the U^{235} isotope) remained in stock, mainly in the USA, in the form of "stockpiled" uranium [4]. This uranium can be used in uranium–plutonium reactors. Noteworthy enough, the price of this uranium amounts to only 2.5-3.0 dollar/kg. This uranium reserve will be used toward the end of the eighties because in the next 10-15 years, thermal reactors can provide the plutonium for the relatively small number of fast reactors. The problem of supplying uranium for nuclear power generation is actually rather acute when thorium is disregarded.

The thorium raw-material base is much greater than that of uranium. According to the latest estimates, the explored, reliably established thorium reserves in the capitalist countries amount to more than 450 thousand tons (calculations referring to the metal) at a cost of 22 dollar/kg ThO_2; the potential additional reserves amount to about 760 thousand tons. Moreover, about 30 thousand tons of thorium were accumulated in the stockpiles of the Canadian uranium plants.

Thus, the thorium reserves are of the same order of magnitude as the uranium reserves. However, these reserves can account for a much greater nuclear power generation, because the specific consumption of thorium per unit of nuclear power obtained with thermal reactors is a fraction of the respective consumption of uranium [1, 2]. If necessary, higher price thorium can be used because the fuel component of the cost of electric energy generated by thorium reactors is small and amounts to about 10-15% [5, 6-8]. This is one of the advantages of thorium over uranium.

It is an important point that practically all thorium sites are complex, in distinction to the majority of the uranium sites. This increases the value of the thorium sites in any well-organized exploitation.

The above-stated data concerning the thorium reserves are minimum estimates; the potentially available reserves are much greater than in the case of uranium, because prospecting and exploration of thorium ores have been conducted on a relatively small scale or, essentially, only sporadically.

In addition to the thorium reserves which can be made available by mining, considerable quantities of this metal (in the form of oxalate, oxides, and various concentrates) have been accumulated (similar to uranium) in some capitalist countries as "strategic reserves." The corresponding data are rarely published.

The thorium reserves of the USA alone amount certainly to thousands of tons, judging from the fragmentary information concerning the amounts purchased by the US Atomic Energy Commission and the reprocessed monazite concentrates and other thorium-containing products. More than 2500 tons of thorium imported in the form of an uranium – thorium concentrate from the Southern part of Madagascar have been piled up in France. These thorium reserves can be used for nuclear power generation.

The world production of thorium (excluding the USSR) amounts (according to the author's estimates) to 700-900 t/year. Only 200-250 t are used up per year, with the main part not being used for the purposes of nuclear engineering but for various magnesium-based alloys for rockets and planes, heat-resistant materials, electronics components, etc.

The relatively low prices for thorium concentrates and products must be taken into account when thorium is evaluated as a competing nuclear fuel. Monazite concentrates, which are one of the thorium sources, were purchased in the last few years by the US AEC and the UAE of Great Britain at a price of 1.5-2.5 dollar/kg of thorium oxide contained in the concentrates; these concentrates were resold to other countries at 5-7 dollar/kg. Canada supplies a thorium which was obtained as a by-product in the processing of uranium ore at a price of 5-7 dollar/kg of thorium oxalate and thorium oxide; the U_3O_8 price of the

concentrates amounts to 13-17 dollar/kg. Undue increases in price of the thorium raw material and thorium compounds need not be expected. In optimistic estimates of the development of nuclear power production, a price of 10-12 dollar/kg is anticipated for thorium oxide [5, 9, 10], whereas a price of 17-22 dollar/kg is predicted for uranium oxide [1, 5, 9, 10].

The prices for isotopes are as follows: Pu^{239} 5-7 (up to 10) dollar/g; U^{235} 11-12 dollar/g; and U^{233} 13-14 dollar/g [5, 6].

Some Principles of the Use of Thorium

The number of people advocating the use of thorium in nuclear power production increases from year to year, and it is assumed that the use of thorium cannot be avoided in the development of long-term programs. Disputed are only the extent and the time of thorium use. Theoretical work and projects have now proved that it is convenient and economically advantageous to use thorium in nuclear power generation [5-18].

The possibility of converting almost all of the thorium into U^{233} (which cannot be obtained from uranium and plutonium) is one of the important advantages of thermal nuclear reactors using thorium. The conversion ratio in thorium converters is close to unity and can reach values of 1.10-1.15 in thermal breeders [3, 5]. This ratio is much smaller (about 0.5-0.6 and up to 0.8 in heavy-water reactors) when uranium–plutonium fuel is used. It has been suggested in some papers [5, 14, 17, 19] that improved thermal breeder reactors using thorium will in the future have better performance characteristics than fast uranium–plutonium breeders and will make ample use of the thorium resources [5, 14, 17, 19]. The low cost of the electric energy produced is in this case a more favorable indicator than the high conversion ratio [17]. The very high energy rate which can be obtained in certain types of thermal thorium reactors makes it possible to reach short duplication times so that these reactors are competitive even with fast uranium–plutonium breeder reactors.

When the thermal load is somewhat increased in conventional thermal water reactors, the thorium-fuel cycle begins to become more economical than the uranium cycle [11]. The use of thorium in nuclear power plants can reduce, by one order of magnitude, the demand in uranium, which results from the uranium-fuel cycle.

Calculations have shown that in the programs for the development of nuclear power generation until 2010 in the West-European countries [9, 10], reactor combinations using simultaneously uranium, thorium, and plutonium will render optimum results. The construction of improved uranium and thorium converters has been recommended. These converters will produce U^{233} and plutonium for the subsequent operation of fast reactors making use of the thorium cycle. A comparison of thermal uranium–thorium breeders and fast uranium–plutonium breeders shows that thermal breeders are advantageous because a low demand for natural uranium (1 million tons) at a very low fuel-component factor is obtained.

In considerations of the prospects of producing cheaper electric energy in the future (of the order of 0.15 cent/kW·h at a fuel rate of 0.01-0.02 cent/kW·h), the calculations are based on the use of powerful nuclear stations with fast uranium–plutonium reactors or thermal thorium reactors [13].

In view of the low critical mass of U^{233} and other "attractive" properties of U^{233}, this material will probably be employed in transportable devices (considerable weight reduction and improved characteristics) and, in addition, in nuclear propulsion systems of outer space rockets [20].

Based upon theoretical considerations, one can assume that the use of thorium and U^{233} in intermediate and fast reactors is at least as promising as the use of uranium and plutonium [5, 12, 21]. For example, it has been proposed in [12] that one use thorium in the blankets of operating and planned fast BN-350, BN-600, and BN-1000 reactors in the USSR, in which Pu^{239} or U^{235} and U^{238} are used in the active zone. One can obtain every day up to 170 kg of pure U^{233} (with about 70 kg free of U^{232} impurities) in a BN-600 reactor. Similar theoretical studies of the application of thorium in fast reactors were made in Great Britain [22]. In the five-year plan for the development of nuclear energy in India (1969-1974), a fast reactor of a similar type has been included as a project [8, 22].

Use of Thorium in Nuclear Reactors

Enriched or natural uranium is used in the majority of modern nuclear reactors. Only in one nuclear power plant (Indian Point, USA) with an output of 292 MW (el.), is thorium used along with uranium in a

pressurized water reactor. This reactor reached its projected output in 1962; the reactor operation has been interrupted several times for removing U^{233}. Nineteen tons of metallic thorium were required for the first charge of this reactor and up to 9.4 t/year were supplied for maintaining the output.

A rather large number of thermal test reactors operating with thorium have been created in the last few years. Some of these reactors are considered to be prototypes of future large-scale nuclear power plants. At the present time, the number of thorium reactors, including experimental devices, is greater than 26 (or about 5% of the total number of reactors in the world). Research on thorium reactors is conducted along several lines.

Various high-temperature reactors of improved design with a gaseous (most often helium) heat carrier and a graphite moderator have become very popular (HTR, HTGR, AVR, Dragon reactors). To date the relatively high price of the fuel elements in the graphite matrix (which reduces the efficiency of the relatively high conversion rate) is the disadvantage of these reactors. Experience in the exploitation of reactors of this type was gained in Pitch Bottom (USA) with the HTGR reactor having an output power of 40 MW (el.), in Winfritt (Great Britain) with the Dragon reactor having an output of 20 MW (el.), and in Jülich (Federal Republic of Germany) with the AVR reactor having an output of 15 MW (el.). A high-temperature reactor with an output of 25 MW (el.) is under construction in Geestahcht in the Federal Republic of Germany [5, 14, 16, 23-25].

The favorable results obtained in the operation of these reactor prototypes made it possible to pass to the design of relatively large nuclear power plants. In Fort St. Vrain (USA) a 330 MW (el.) nuclear power plant of the Pitch-Bottom type has been under construction since 1968 [4, 24]. Based on the Dragon reactor in Winfritt, a huge nuclear power plant with an output of 630 MW (el.) has been projected [25]. The planning for a 300 MW (el.) nuclear power station in which the experience gathered in the operation of the AVR reactor in Jülich is used has been completed in the Federal Republic of Germany. It is assumed that the construction work will be finished in 1974 [16, 23]. Apart from this, design calculations of high-temperature thorium reactors with gas cooling and a power output of 600, 1000, and 1200 MW (el.) have been made in those three countries. It has been stated in the third program for the development of nuclear energy in the Federal Republic of Germany (1968-1972) that the development of thermal thorium high-temperature reactors and fast plutonium reactors must be given priority [16, 23].

The use of thorium in heavy-water reactors (of the HWR, and CANDU types, etc.) is promising [9, 26]. Experiments with thorium as a fuel have been conducted in such reactors during the last few years (USA and Canada). Similar research is under way in the Federal Republic of Germany in relation to a 300 MW (el.) reactor. A liquid fuel, thermal breeder reactor operating with a suspension of uranium and thorium in heavy water (KSTR reactor) is experimentally operated in the Netherlands [9]. A project of creating a huge nuclear power plant with a heavy-water thorium reactor has been developed in India (in collaboration with the USA and Canada) [26]. A new form of spherical fuel elements for thermal heavy-water breeder reactors with a U^{233} conversion coefficient of 1.05 has been patented in Great Britain at the end of 1969; the greatest theoretical conversion rate amounts to 1.3 [27].

A third very promising application of thorium arises in reactors operating with diluted salts (MSR, MSRE, MSBR, and Mosel reactors) [5, 7, 13, 14, 17-19]. The absence of fuel elements, the continuous purification of gaseous fission fragments, the low demands in nuclear fuel, and the possibility of operating the reactor as a breeder (MSBR reactor) with a conversion rate of up to 1.1 are the most attractive properties of this type. Good results in the operation of such a homogeneous reactor have been reported from Oak Ridge (USA) where the 8 MW (thermal) MSRE reactor was put into operation with U^{235} in 1965. The start of the operation of the U^{233} MSRE reactor in October 1968 in Oak Ridge was an important event [17, 18, 28]. This is the first experimental reactor in the world, which has a power of 8 MW (thermal), works with a diluted salt solution, and provided, after one year, the initial data required for the planning of industrial reactors using the Th-U^{233} fuel cycle. Thirty four kg of U^{233} were needed for the initial charge. More powerful (25-50 MW (el.)) prototypes of these reactors have been designed and the calculations for a full-scale reactor with an output of 1000 MW (el.) have been made.

Theoretical and experimental research on the thorium-fuel cycle has been conducted in relation to other types of reactors. For example, since 1964, in Elk River (USA) a boiling-water reactor has been operating with a power of 22 MW (el.) in which a mixed uranium–thorium fuel is employed [29]. It is planned to introduce a new charge consisting of thorium oxide in 1974 into the existing 100 MW demonstration reactor in Shippingport (USA) [30]. The project includes feasibility tests of a light-water thorium breeder reactor.

In the heavy-water uranium reactor Zirus operating in India with an output power of 40 MW, thorium has been irradiated since 1967 in order to obtain U^{233} [31]. Moreover, it is planned to build a small (10 MW) thorium breeder reactor. A nuclear power plant project using the Instinto 300 MW (el.) thorium reactor has been developed in Brazil in collaboration with France [32]. The construction of this power plant will begin in 1972. There exists fragmentary information concerning work on the use of thorium in reactors of other countries, e.g., Denmark, Belgium, Switzerland, Italy, France, Sweden, Peoples Republic of Korea, Japan, and Australia.

Considerable stockpiles of U^{233} have been accumulated in the USA – amounting to 730 kg at the end of 1967 (mainly from the reactors of the nuclear power plants in Indian Point, Elk River, and Pitch Bottom) [29]. It was intended to use 410 kg of this quantity. Obviously, small amounts of this valuable isotope are in existence in other countries.

Thorium Demands for Nuclear Power Generation

The demand for thorium is small at the present time and amounts to 20-30 t/year. The use of thorium was retarded for several decades due to great technological difficulties encountered in the thermal thorium cycle (contamination by protactinium, etc.). Considerable difficulties were encountered in the purification of U^{233} from accompanying isotopes, particularly from U^{232}. Only in the last few years, these difficulties could be overcome in the improvements of nuclear technology. Since research was initiated late, the majority of promising thorium reactors have not yet been thoroughly developed. Difficulties originated also from the need of using highly enriched U^{235} as the initial charge of thorium reactors. As far as the engineering aspect is concerned, improved-design reactors making use of the thorium cycle are only slightly more complicated than conventional uranium reactors. The radiochemical industry for thorium is actually in the initiation stage. The huge uranium industry, which was built up during the 25-30 years of its existence, the high competition by the uranium industry, and its continuous improvement slow down the development of the recently created thorium industry.

When the prospects for the use of thorium are evaluated, one must take into account the recent changes in the competition between uranium and thorium, definitely established development tendencies in nuclear power engineering, and the advantages of thorium over uranium which at the present time can be considered well-established. In future developments of more economical test reactors of improved design and performance, the potential advantages of the uranium–thorium fuel cycle will probably be embodied in large-scale nuclear power plants.

At the present time, there exist no unsurmountable technological difficulties which could prevent the use of thorium. The only problem is the engineering work on thorium reactors in relation to questions of economy and the uranium competing with the thorium. The above-stated data concerning the practical use of thorium, which began in the last few years in reactors of several countries, and the construction projects of industrial nuclear power plants using thorium corroborate the theoretical forecasts of the advocates of thorium. By the middle of the seventies, there will probably exist at least 5-6 operating industrial nuclear power plants making use of uranium–thorium reactors with a total power output of 2000-2300 MW (el.).

Though it is by no means clear to what extent, in what ratio to uranium, or at what rate the demand for thorium will grow, one can give at the present time a first approximation of the corresponding figures. The times and the scale on which fast uranium–plutonium breeders will be introduced cannot have any deciding influence upon the use of thorium, because from an economical viewpoint, thorium remains competitive.

In an approximation calculation, whose results are stated in the table, the total fixed power of nuclear power plants is assumed as 2000 GW (el.) by the end of the current century. The rate at which the power of nuclear power plants employing thorium grows is very moderate, but is higher than the growth rate of nuclear power plants using uranium; the growth rate exceeds that of uranium-using plants by 1.5-20%, with the growth decreasing by the end of the time period considered, because fast plutonium reactors, in which inexpensive U^{238} is used, will gain increasing importance after the eighties.

Data concerning the operating and projected nuclear power plants using thorium and uranium–thorium mixtures as the fuel were considered in the calculations of the thorium demand of nuclear power generation. At the present time, 60-200 t/GW (el.) are required for the charges of thermal converters

TABLE 1. Approximate Thorium Demand until the Year 2000

Year	Total fixed power of all nuclear power plants, GW (el.)	Nuclear power plants using thorium, % of the total fixed nuclear power	Fixed power of nuclear power plants using thorium, GW (el.)	Demand for thorium, t: average value per GW (el.) for a five-year period	Demand for thorium, t: annual	Demand for thorium, t: total for the period considered
1971	25	1,5	0,4	116	50	50
1972	40	1,5	0,6		70	120
1973	75	1,2	0,9		110	230
1974	100	2,0	2,0		230	460
1975	115	2,0	2,3		260	720
1976	160	2,2	3,5	94	340	1 060
1977	200	2,3	4,6		440	1 500
1978	250	3,0	7,5		690	2 190
1979	270	3,5	9,5		910	3 100
1980	300	4,0	12,0		1 100	4 200
1981	340	4,5	15,3	87	1 300	5 500
1982	390	5,0	19,5		1 800	7 300
1983	450	5,5	24,7		2 100	9 400
1984	510	6,0	30,6		2 700	12 100
1985	580	6,5	37,7		3 300	15 400
1986	640	7,5	48,0	76	3 900	19 300
1987	700	9,0	63,0		4 900	24 200
1988	780	11,5	89,7		6 700	30 900
1989	860	13,0	111,8		8 400	39 300
1990	950	14,0	133,0		10 000	49 300
1991	1050	15,0	158,0	71	11 500	60 800
1992	1150	16,0	184,0		13 100	73 900
1993	1270	17,0	216,0		15 200	89 100
1994	1400	17,5	245,0		17 600	106 700
1995	1500	18,0	270,0		19 300	126 000
1996	1600	18,5	296,0	67	20 600	146 600
1997	1700	19,0	323,0		22 100	168 700
1998	1800	19,5	351,0		23 700	192 400
1999	1900	20,0	380,0		25 500	217 900
2000	2000	20,5	410,0		27 100	245 000

and breeders; the demands for thorium for the mixed uranium–thorium cycle of fast reactors are much lower and amount to 25-60 (up to 100)t. Moreover, during the 20-30 year operation span of a nuclear power plant, up to 50% of the initial charge is burnt and approximately the same amount of thorium must be kept in rotation for radiochemical conversion. The thorium consumption figures refer to the minimum values and were calculated for improved thermal converter and breeder reactors to be used from the seventies, with a partial transition to fast uranium–thorium breeders predicted for the eighties.

Naturally, the extent to which thorium will be in demand is insignificant compared to the demand for uranium (which exceeds the demand for thorium by one order of magnitude). However, thorium can replace at least 500-800 thousand tons of natural uranium.

The above figures concerning the thorium demand during 30 years may actually be lower if the recommendations of the Oak Ridge National Laboratory (USA) are obeyed, i.e., when a large number of thorium reactors are built as the most economical reactors of the seventies. A more rapid introduction of thorium in nuclear power generation is possible when the use of thorium in conventional power reactors is increased by the nineties, while the large-scale industrial introduction of fast breeder reactors is continued. In this case, a shortage of inexpensive natural uranium may result earlier and at an increased scale.

Whatever the state of the raw material base of thorium may be in relation to the thorium demand of nuclear power generation, one can foresee for the near future an expansion of the exploration and prospecting work on thorium ore, along with a tendency to improve the prospecting methods. It is generally accepted that ten years or more pass between the discovery of a site and its industrial exploitation. Increased thorium prospecting and a gradual growth of the output of the mining and converting enterprises are inevitable, particularly in view of the probable growth of the thorium demand in nonnuclear branches of industry.

* * *

The following conclusions can be drawn from what has been said above:

1. The rapid development of nuclear power generation during the last few years causes a demand for uranium measuring millions of tons. Thus, there is the risk that the explored or potential resources of cheap uranium will be exhausted unless the uranium is replaced by the equivalent thorium or fast breeder reactors are introduced on a large scale in industry.

2. Thorium can be fully equivalent to or even more efficient and economical than uranium. The use of thorium leads to a substantial (several times) reduction of the uranium consumption and eliminates the need for processing expensive ores. The resources and reserves of thorium are numerically almost the same as those of uranium, but are a more promising source of nuclear fuel, because the specific consumption of thorium per unit power generated in a nuclear power plant is much smaller. The price of the thorium raw materials is two to three times lower than the price of natural uranium.

3. Difficulties in technology and engineering, which until recently have prevented the large-scale use of thorium in nuclear technology, are only temporary and are being overcome at the present time.

4. The possibility of obtaining an almost complete reproduction of the fuel in thermal converters, i.e., the possibility of converting almost all of the thorium into U^{233}, is one of the important advantages of reactors using thorium. The great extent to which the fission nuclei are used in the thorium cycle makes it possible to transform converters of improved design into thermal breeders (with a conversion ratio as high as 1.10-1.15); these breeders will be able to provide very cheap electrical energy in the next few years.

5. Thermal thorium converters and thermal breeders have a simpler design than fast breeders. They can therefore form a transition from the conventional reactors to the more economical fast reactors of the future.

Thermal thorium converters and breeders will be competitive with the uranium–plutonium breeders in the future.

6. The use of thorium in fast breeder reactors (with a conversion ratio as high as 1.4-1.5) is obviously not less promising than the use of uranium and plutonium. For example, it is possible to use thorium in the reproduction zone in order to obtain pure U^{233} in the uranium–plutonium BN-350 reactor which is currently under construction in the USSR and in the BN-600 and BN-1000 reactors which have been planned.

7. The principal problem of thorium, its competition with uranium, is currently solved in favor of thorium. This has been proved by calculations concerning the technological and economical aspects in the optimization of long-term programs for the development of nuclear power production as well as by the actual use of thorium in test reactors of many types and in the projects of industrial nuclear power generation.

8. Approximate calculations have shown that thousands of tons of thorium will be required for nuclear power production as early as in 1980; in the ensuing decades, the demand for thorium will reach several ten thousand tons.

There is reason to assume that these estimates indicate the minimum figures, and the actual "substitution" of uranium by thorium can be greater than the 4:1 ratio (by the year 2000). It is safe to say at the present time that the demand for thorium will be considerable in the near future.

9. The increased demand for thorium will necessarily expand geological work related to the prospecting of thorium resources, will increase the productivity of the mining and processing enterprises, will improve the methods of enriching complex ores, and will lead to a reprocessing of thorium-containing concentrates and tailings in order to extract thorium.

In conclusion, the author expresses his gratitude to A. I. Leipunskii, S. M. Feinberg, and V. M. Murogov for their advice and to D. Ya. Surazhskii, A. P. Zefirov, N. M. Sinev, G. M. Lyamkin, D. I. Skorovarov, and B. I. Yakushenkov and to his co-workers for useful advice and critical remarks in the preparation of the manuscript.

LITERATURE CITED

1. Atomic Energy Clearing House, 17, No. 46, 42 (1967).
2. Atomic Energy Clearing House, 15, No. 21, 9 (1969).

3. A. I. Leipunskii et al., Atomnaya Énergiya, 25, 380 (1968); S. M. Feinberg, Atomnaya Énergiya, 25, 363 (1968).
4. D. Bell, Canad. Mining and Metallurg. Bull., 60, No. 666, 450 (1967).
5. Utilization of Thorium in Power Reactors. Technical Reports Series, No. 52, IAEA, Vienna (1966).
6. L. Lang, Nucl. Appl., 5, No. 5, 302 (1968); Atomnaya tekhnika za rubezhom, No. 9, 22 (1969).
7. S. V. Bryunin, Atomnaya tekhnika za rubezhom, No. 9, 11 (1969).
8. V. V. Batov, Atomnaya tekhnika za rubezhom, No. 3, 3 (1970).
9. I. Went, Report No. 163 presented by the Netherlands during the 7th Congress of the World Energy Conference [in Russian], Moscow, August 1968.
10. P. Margen, Nuclear Engin., No. 147, 669 (1968); Atomnaya tekhnika za rubezhom, No. 4, 8 (1969).
11. S. M. Feinberg, Report No. SM-105/42 presented by the USSR during the Symposium on the Economic Aspects of Nuclear Fuel (Gottwaldov, Chek. Soc. Sov. Rep., 1968).
12. A. I. Leipunskii, V. M. Murogov, and M. F. Troyanov, Report of the Conference of Experts on the Use of Thorium (Vienna, 1966), MAGATÉ Vienna (1967).
13. A. Weinberg, Kernenergie, No. 7, 181 (1968); Atomnaya tekhnika za rubezhom, No. 6, 3 (1969).
14. Kerntechnik, 10, No. 8/9, 424 (1968); Nucleonics Week, 9, No. 45, 7 (1968).
15. V. S. Smirnov, Atomnaya tekhnika za rubezhom, No. 10, 3 (1969).
16. H. Krämer, Kerntechnik, 11, No. 9/10, 497 (1969).
17. M. Rosental et al., Nucl. Engin., No. 159, 420 (1969); Atomnaya tekhnika za rubezhom, No. 12, 3 (1969); Chem. Engin., 75, No. 23, 48 (1969).
18. E. Bettis and R. Robertson, Nucl. Appl. and Technol., 8, No. 2, 190 (1970).
19. Scient. American, 218, No. 6, 44 (1968).
20. J. Spacecraft and Rockets, 4, No. 12, 1592 (1967).
21. Nucl. Engin., No. 148, 741 (1968).
22. Nucl. News, 11, No. 5, 17 (1968).
23. Atomwirtschaft, 14, No. 3, 128; No. 4, 171 (1969); Appl. Atomics, No. 667, 4 (1968).
24. Electrical World, 170, No. 10, 27 (1968).
25. R. Saunders, Atompraxis, 2, 96 (1969).
26. Atomic Energy Austral., 11, No. 2, 14 (1968); J. Brit. Nucl. Energy Soc., 7, No. 4, 278 (1968).
27. Electrical Review, 185, No. 21, 765 (1969).
28. Nucl. Engin., No. 150, 901 (1968); Chem. Eng. News, 47, No. 24, 77 (1969).
29. Nucleonics Week, 7, No. 19, 3 (1966).
30. Nucleonics Week, 10, No. 10, 1; No. 37, 4 (1969).
31. Nucl. India, 5, No. 5, 6; No. 11-12, 6 (1967); Nucleonics Week, 10, No. 34, 7 (1969).
32. Atomwirtschaft, 13, No. 11, 518 (1968).

DETERMINATION OF THE DYNAMIC CHARACTERISTICS OF FUEL CELLS*

I. I. Morozov and V. P. Kaz'min

UDC 621.039.546

Investigations of the stability of operation of boiling reactors and steam generators of nuclear energy installations give evidence that non-equilibrium processes in the walls of the fuel channels can substantially influence the position of the limit of stability, the value of the required choking, etc. The influence of heat exchange on the reactor stability is expressed by the equation of the energy balance, while the value of the fluctuation of the thermal flux in this equation depends on a certain complex quantity, considering the thermal inertia of the wall and expressing its dynamic characteristics.

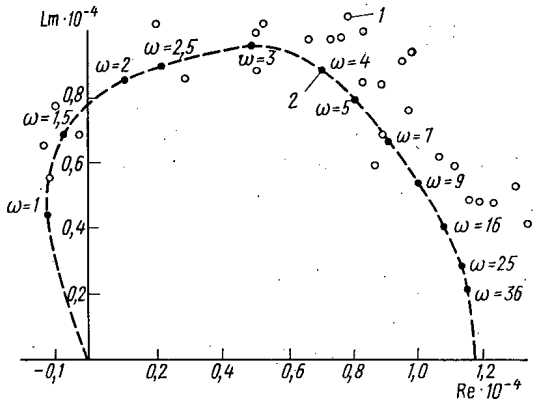

Fig. 1. Frequency characteristic of a tubular fuel cell $F_1(\omega)$: 1) experimental points; 2) calculated points.

An experimental method is proposed for determining the frequency characteristics of the wall of the heater, which is illustrated with a tubular fuel cell as an example. The essence of the method consists of studying the harmonic oscillations of the consumption and measuring the temperature fluctuations of the liquid (and, consequently, the fluctuations of the thermal flux). The set of points $|\delta q|/|\delta \dot{G}|$, considering the phase shift, represent one of the frequency characteristics of the wall of the heater, with a knowledge of which all the remainder can be determined. Investigations of a tubular fuel cell (see Fig. 1) indicated satisfactory agreement between the calculated and experimental frequency characteristics and the practical possibility of their determination.

THE VISCOSITY OF HEAVY WATER AT HIGH PRESSURES IN THE 100-275°C TEMPERATURE RANGE†

N. A. Agaev, A. M. Kerimov, and Azad Abas-Zade

UDC 621.1.013

The results of an experimental study of the viscosity of heavy water at pressures of 1-1200 kg/cm^2 and temperatures of 100-275°C, including measurements near the saturation line, are given in this paper.

*Translated from Atomnaya Énergiya, Vol. 30, No. 6, p. 534, June, 1971. Original abstract submitted July 22, 1969; revision submitted November 16, 1970; final revision submitted January 30, 1971.

†Translated from Atomnaya Énergiya, Vol. 30, No. 6, pp. 534-535, June, 1971. Original abstract submitted September 15, 1969; revision submitted November 27, 1970.

TABLE 1. Viscosity of Heavy Water at High Pressures at Various Temperatures ($\times 10^{-5}$ N·sec/m^2)

Pressure, kg/cm^2	Temperature, °C											
	100,00	108,82	117,00	125,00	136,94	150,00	159,12	175,00	200,00	225,00	250,00	275,00
51	32,9	30,1	27,0	25,8	23,4	21,1	19,7	17,7	15,4	13,7	12,1	—
101	33,0	30,3	28,0	26,0	23,5	21,3	19,9	17,9	15,6	13,8	12,3	11,1
201	33,4	30,7	28,4	26,2	23,7	21,5	20,2	18,1	15,9	14,1	12,6	11,4
301	33,7	31,1	28,7	26,5	24,0	21,8	20,4	18,4	16,1	14,3	12,9	11,7
401	34,1	31,4	29,0	26,7	24,3	22,1	20,6	18,7	16,4	14,6	13,1	11,9
501	34,5	31,8	29,3	27,0	24,6	22,3	21,0	19,0	16,6	14,8	13,3	12,2
601	34,9	32,1	29,7	27,3	24,9	22,6	21,2	19,2	16,8	15,0	13,5	12,4
701	35,3	32,5	30,0	27,6	25,2	—	21,4	19,5	17,1	15,2	13,7	12,6
801	35,6	32,9	30,4	27,8	25,5	—	21,7	19,7	17,3	15,4	13,9	12,8
901	—	33,3	30,6	28,1	25,7	—	21,9	19,9	17,5	15,7	14,1	12,9
1001	—	33,6	31,0	28,4	26,0	—	22,2	20,2	17,7	15,8	14,3	13,1
1101	—	34,0	31,3	28,7	26,2	—	22,4	20,4	17,9	16,0	14,5	13,3
1201	—	34,5	31,6	29,0	25,5	—	22,7	20,6	18,1	16,2	14,7	13,5
Saturation line*	32,7	30,0	27,8	25,7	23,3	21,0	19,6	17,6	15,3	13,5	12,1	11,0

*Viscosity data near the saturation line were obtained at a pressure 1 kg/cm^2 greater than the saturation pressure.

The measurements were done using an experimental instrument for determining the viscosities of liquids and gases at high pressures. The heavy water was 99.8 at. % pure. Experiments were performed along isotherms; measurements were made two or three times at each temperature–pressure point, with an experimental reproducibility of ±0.1 to 0.2%.

The maximum relative experimental error was ±1%; the Reynolds number did not exceed 500 in the experiments.

Shown in Table 1 are experimental values for the coefficients of dynamic viscosity of heavy water at high pressures and near the saturation line.

These values deviate from those in the literature by not more than 1-2%.

SIMULTANEOUS DETERMINATION OF LEAD, COPPER, AND ZINC IN SAMPLES OF POLYMETALLIC ORES AND PRODUCTS OF THEIR PROCESSING BY AN ACTIVATION METHOD

L. V. Navalikhin, V. A. Kireev,
Yu. N. Talanin, and G. S. Nikonorov

UDC 543.53

A rapid method of determining the content of lead, copper, and zinc in samples of polymetallic ores using 14 MeV neutrons was described. The lead content is determined by measuring the induced activity of the isotope Pb^{207m}. Cyclic irradiation of the samples and measurement of the induced activity are used. The time of irradiation and measurement is 4 sec, exposure 0.7 sec. The number of cycles and all the operations within a single cycle are set and regulated by a system of automatic control. The value of the

Translated from Atomnaya Énergiya, Vol. 30, No. 6, p. 535, June, 1971. Original abstract submitted August 12, 1970.

induced activity is measured with a rapid–slow coincidence spectrometer. The interfering influence of large contents of oxygen in the sample is considered simultaneously by measuring the activity of the isotope N^{16}.

The copper and zinc contents are determined according to the induced activity of the isotopes Cu^{62} and Zn^{63}, respectively. The measurements with a coincidence spectrometer are performed twice: the first 8-10 min after irradiation, the second after 35-40 min. Such a method permits combination of high output of the analyses with sufficient accuracy of the results obtained. A consideration of the possible influence of large contents of iron is performed by measuring the activity of the isotope Mn^{56} in the region of 0.845 MeV 50-60 min after irradiation of the sample.

An expression was obtained permitting selection of the optimum conditions of measurements for the quantitative analysis of binary mixtures of radioactive isotopes, differing only in half-life, and an estimation of the measurement error.

The calculated sensitivity of the determination of lead is 0.1%, and for copper and zinc $(3\text{-}5)\cdot 10^{-2}$%. The mean square error of the determination does not exceed ±20% and depends on the content of the components to be analyzed.

The output of the analyses for all three elements is 20-25 samples per shift. No more than 1 min is required to determine lead alone, which permits the use of the method in assembly-line production at condensation enterprises.

DISTRIBUTION OF NEUTRONS EMITTED FROM A POINT SOURCE AND SLOWED DOWN IN A SYSTEM OF TWO MEDIA WITH A PLANE INTERFACE

I. A. Kozachok, V. V. Kulik and V. I. Pirogov

UDC 539.125.523

We consider the problem of finding the steady-state distribution of neutrons emitted by a point monoenergetic source and slowed down in two media separated by a plane boundary. The problem is formulated in terms of a differential equation which has a much broader range of applicability than the age approximation. In particular it is valid even for hydrogenous media.

The problem is solved in cylindrical coordinates. The boundary between the media is the plane $z = 0$, and a source of unit strength is placed at the point $z = z_0$, $\rho = 0$. The initial system of equations has the form

$$\left(\frac{\partial}{\partial t_i} - \lambda_{si}^2 \frac{\partial^2}{\partial t_i^2} - \Delta\right) \frac{\xi_i v}{l_{si}} N_i = \delta_{i1} \frac{\delta(\rho)}{2\pi\rho} \delta(z - z_0)\, \delta(t_1), \quad i = 1, 2. \tag{1}$$

Here the subscripts 1 and 2 refer to media in the half-spaces $z > 0$ and $z < 0$ respectively; N is the neutron density, t is the modified neutron age, λ_s^2 is a constant, v and l_s are the neutron velocity and mean free path, and ξ is the average logarithmic energy loss of a neutron in an elastic collision with a nucleus.

The boundary conditions on the interface follow from requiring the continuity of the neutron density and the normal component of the neutron current for all energies:

$$N_1 = N_2;\ \langle D_1 \rangle \frac{\partial N_1}{\partial z} = \langle D_2 \rangle \frac{\partial N_2}{\partial z} \quad \text{for} \quad z = 0. \tag{2}$$

Translated from Atomnaya Énergiya, Vol. 30, No. 6, p. 536, June, 1971. Original abstract submitted July 14, 1970.

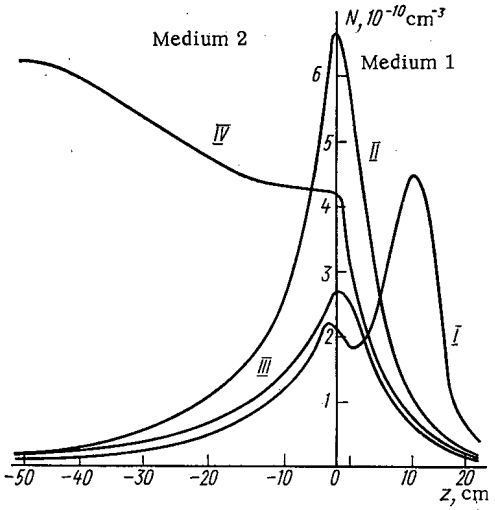

Fig. 1. Distribution of moderated neutrons in a system of two media: H_2O (1) and SiO_2 (2). I) $z_0 = 12$ (N × 2); II) $z_0 = 2$; III) $z_0 = -8$; IV) $z_0 = -48$ (N × 20).

Here

$$\langle D_i \rangle = \frac{\int \frac{l_{si}^2\, du}{3\xi_i (1-\mu_i)}}{\int \frac{l_{si}\, du}{\xi_t}}, \quad i = 1, 2,$$

where u is the lethargy and μ is the average cosine of the scattering angle in a collision of a neutron with a nucleus.

The solution of the problem posed has the form

$$N_1 = n_1(\rho, z - z_0, t) - n_1(\rho, z + z_0, t) + C_1(\rho, z, z_0, t); \; N_2 = C_2(\rho, z, z_0, t), \quad (3)$$

where n is a solution of the original equation for an infinite medium, and C_1 and C_2 are expressions which depend on the form of the integrals and can be obtained numerically.

Figure 1 shows the neutron distribution from a monoenergetic source (E = 5.44 MeV) slowed down to the indium resonance energy (E = 1.44 eV) for various positions of the source.

OPTIMIZATION OF THE SHAPE OF A SHADOW SHIELD AGAINST NEUTRONS FROM A SURFACE SOURCE BY THE MONTE CARLO METHOD

V. L. Generozov and V. A. Sakovich

UDC 621.039.538.7

We present the results of optimizing the shape of a shadow shield against monoenergetic neutrons from a surface source by using the Monte Carlo method to compute the dose and its first derivatives with respect to the varied shield parameters.

The optimization was performed for cylindrical and disk surface sources of 8 MeV neutrons with cosine angular distributions. The generator of the axially symmetric shadow field was approximated, as in [1], by a stepped line with the height of each step subjected to variation. The original shield was a slab of polyethylene 30 cm thick. We sought the minimum neutron dose averaged over a circular shielded region coaxial with the source and 13 m from it. The weight of the shield was kept constant.

The method of gradient programming [2, 3] was used for the optimization. The weight of the shield and the derivatives of the weight with respect to the varied parameters were computed from geometric relations. The neutron doses at certain points in the shielded region were found by using the Monte Carlo method to compute the "local flux" [4]. The derivatives of the neutron dose with respect to the varied parameters were determined simultaneously with the calculation of the dose by following the method proposed in [5].

In tracing random neutron histories the anisotropy of elastic neutron scattering and the energy loss in inelastic scattering were taken into account. The error in the dose calculation after tracing 4000 histories was about 5%. The corresponding error in the calculation of the derivatives of the dose was 10-30%.

Translated from Atomnaya Énergiya, Vol. 30, No. 6, pp. 536-537, June, 1971. Original abstract submitted June 11, 1970; revision submitted February 10, 1971.

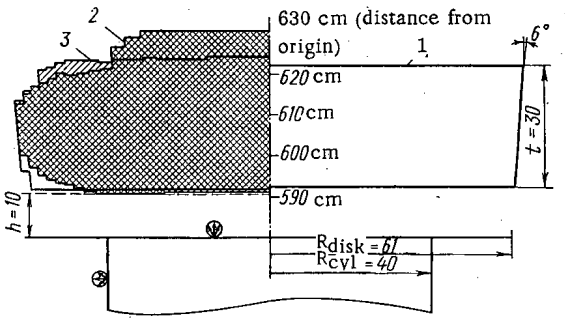

Fig. 1. Optimized shape of a polyethylene shield against neutrons from a surface cosine source: 1) initial shape of shield; 2) final shape of shield for cylindrical surface source after 11 iterations; 3) final shape of shield for disk source after four iterations.

Eleven iterations in the optimization of the shield against neutrons from a cylindrical source reduced the dose by 25%. In the optimization of the shield against neutrons from a disk source four iterations reduced the dose by 35%.

The initial shape of the shield and the optimized shape are shown in Fig. 1. The method proposed for optimizing the shape of a shadow shield permits substantial refinement of the shield shape even for small differences in doses, and can take account of geometric limitations arising in actual construction.

LITERATURE CITED

1. V. L. Generozov and V. A. Sakovich, Atomnaya Énergiya, 28, 175 (1970).
2. R. Sheffield, Convair Fort Worth Report MR-N-186 (NARF-57-62T).
3. W. Cranford and R. Miller, TID-6302.
4. V. G. Zolotukhin and S. M. Ermakov, in: Problems in the Physics of Reactor Shielding [in Russian], D. L. Broder et al., editors, Atomizdat, Moscow (1963).
5. M. Z. Brainina et al., Zh. Vychisl. Matem. i Matem. Fiz., 7, No. 4 (1967).

NEUTRON THRESHOLD DETECTOR RH^{103}

I. L. Lomonosov, E. I. Firsov, and N. G. Cherenda

UDC 539.1.074.88

The reaction $Rh^{103}(n, n')Rh^{103m}$ is characterized by a very low threshold, and the excitation function has a sharp rise in the 500-keV neutron energy region; consequently, the use of Rh^{103} as a threshold detector makes it possible to expand the range of spectral measurements of fast neutrons from reactors to an energy region extending down to 500 keV. It is most convenient to use the technique developed for detecting low-energy emitters [1] to measure the Rh^{103} activity.

An aqueous solution of the complex compound triethylenediamine rhodium nitrate was used as the irradiation target. The activity was measured by recording the conversion electrons with a single-channel liquid scintillation counter having an FEU-42 photomultiplier and a dioxan scintillator. The counting efficiency was computed theoretically with allowance for the experimentally determined scintillation efficiency. The Rh^{103} activity was identified by the decay curve in the spectral pulse-height range corresponding to an electron energy of 35 keV.

The paper considers the possible effect of Rh^{103} adsorption on the walls of the irradiation vessel and on the walls of the counting chamber because of the low rhodium concentration in the solution and the chemical inequivalence of the Rh^{103} before and after irradiation of the solution. On the basis of numerous measurements for various holding times in the irradiation vessel and counting chamber, it was concluded that the possible effect mentioned does not appear.

Translated from Atomnaya Énergiya, Vol. 30, No. 6, p. 537, June, 1971. Original abstract submitted May 18, 1970; abstract submitted July 31, 1970.

Integral fast-neutron spectra measured in the vertical channel of an IRT-2000 reactor with a set of threshold detectors are presented. The flux density of neutrons with energies above 500 keV obtained with the rhodium detector by the integral flux method was $2.1 \cdot 10^{12}$ neutrons/cm^2·sec at a reactor power of 2 MW. Thus the actual neutron spectrum at the point of measurement produces a flux value in the energy range under consideration which exceeds the flux value corresponding to a fission spectrum by 20%. The error in the flux measurement is estimated to be 10%.

LITERATURE CITED

1. I. I. Lomonosov and L. D. Soshin, Tritium Measurement [in Russian], Atomizdat, Moscow (1968).

EFFECTIVE CROSS SECTIONS OF PROTON AND ALPHA PARTICLE TRACKS IN IONIC CRYSTAL

D. I. Vaisburd, A. A. Vorob'ev, and L. A. Melikyan

UDC 539.121.72.75:539.2 :539.16.04:535.535.343.2

Effective transverse sizes of proton (1-6 MeV) and alpha particle (4-25 MeV) tracks in monocrystalline NaCl were determined from the transformation kinetics of electron color centers. The crystals are irradiated at room temperature (see insert a in Fig. 1) until an F_2-center density of 10^{17} cm^{-3} is reached. The crystal is next irradiated at low temperature and practically all the F_2-centers are transformed to F_2^+ and (v_a^+, F_1)-centers consisting of an anionic vacancy and an adjacent F_1-center. Irradiation at room temperature quickly reestablishes the original F_2-center concentration at the expense of electron capture by F_2^+ and (v_a^+, F_1)-centers. The regeneration of one F_2-center takes only $\varepsilon_0 = 2 \cdot 10^2$ eV. Their yield is a factor of 10^3 greater than the initial concentration. This effect has been previously discovered and studied.* The simplicity of the mechanism and the high yield of this process make it useful in determining the effective transverse sizes of tracks.

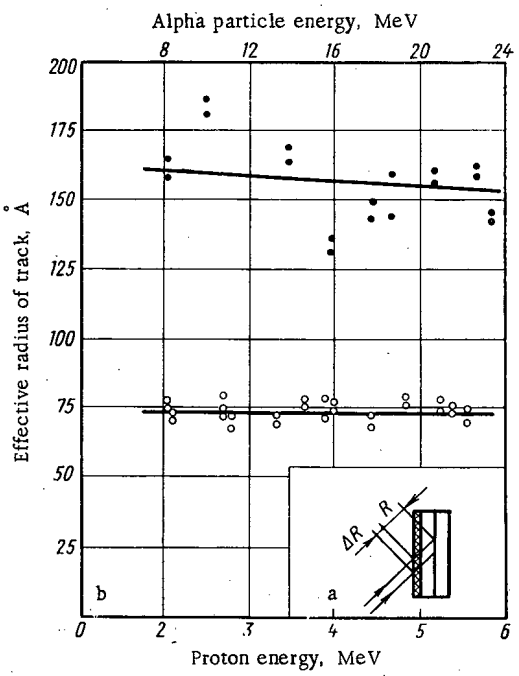

Fig. 1. a) Diagram showing crystal irradiation; b) the dependence of the effective radius of the proton and alpha particle tracks on their energy.

In the general case the F_2-center concentration (n) obeys the following law

$$n = N\{1 - (1/q)\ln[(e^q - 1)e^{-x} + 2]\}. \quad (1)$$

where N is the saturation level of the regenerated center concentration; $x = \Omega\nu$, where Ω is the effective volume of the track and ν is the instantaneous track concentration; $VET = dE/d\Omega$ where $q = N\varepsilon_0/VET$ is the energy transfer per unit volume in the track. In particular, if $N\varepsilon_0 \ll VET$ then every particle in the effective volume of its track regenerates practically all the F_2-centers up to the limiting concentration N. Then

*D. I. Vaisburd et al., Fiz. Tverd. Tela, 12, 2788 (1970).

Translated from Atomnaya Énergiya, Vol. 30, No. 6, pp. 538, June, 1971. Original abstract submitted July 15, 1970.

$$n = N[1 - \exp(-\Omega v)]. \quad (2)$$

This case is realized for $N < 10^{17}$ cm^{-3} in proton tracks and for $N < 2 \cdot 10^{17}$ in alpha particle tracks. It was this case that was used for the experimental determination of effective volumes Ω, effective cross sections $\sigma = \Omega/R$ (where R is the particle range), and effective radii $r = \sqrt{\sigma/\pi}$ of proton and alpha tracks (see Fig. 1).

The effective radius of a track, measured in this way, implies that the width of the radial distribution of the energy transfer per unit volume in a track is at the level of $4.5 \cdot 10^{19}$ eV/cm^3. At this level of energy transfer the radius of a 1-6 MeV proton track is (74 ± 5) Å while a 4-25 MeV alpha particle track equals (155 ± 15) Å.

LETTERS TO THE EDITOR

MINIMIZATION OF THE COEFFICIENT OF VARIATION OF ENERGY RELEASE IN A SLAB REACTOR WITH A REFLECTOR

E. G. Sakhnovskii

UDC 621.039.51

In the presentation paper, by using methods in optimal control theory, we show that by shaping the fuel we can attain a minimum (equal to unity) coefficient of variation of energy release in a homogeneous slab reactor with reflector, but not for all values of its critical size and maximum allowable uranium concentration in the core.

We consider a slab symmetric reactor with core of half-width R and infinite reflector. We assume that the structural materials (excluding the moderator with continuous properties) are distributed homogeneously both in the core ($0 \geq r \leq R$) and in the reflector ($R \leq r < \infty$). We state the problem on the fuel distribution in the core as follows. We wish to minimize the functional

$$J = \frac{\max\limits_{0 \leqslant r \leqslant R} [\Phi(r)\, u(r)]}{\frac{1}{R}\int\limits_0^R \Phi(r)\, u(r)\, dr} \tag{1}$$

under the technological and heat-engineering constraints

$$0 \leqslant u(r) \leqslant u\max,\ \Phi(r)\, u(r) \leqslant q\max. \tag{2}$$

In (1) and (2), $\Phi(r)$ is the thermal-neutron flux; $u(r)$ is the ratio of the macroscopic absorption cross sections of the uranium and the structural materials; and u_{max} and q_{max} are given constants.

Assuming $\max [\Phi(r)u(r)] = A \leq q_{max}$, we rewrite the functional (1) in the form

$$J = \frac{A}{W} R \quad \left(W = \int\limits_0^R \Phi u\, dr\right), \tag{3}$$

where W (with accuracy up to a multiplier) is the reactor power. If A and W are assumed given, then the optimization problem under consideration is obviously equivalent to the problem of minimizing the critical size R of a reactor with constraints $0 \leq u(r) \leq u_{max}$, $\Phi(r)u(r) \leq A$. A solution of this problem for a two-region reactor without a reflector was obtained in a two-group approximation in [1]. For a reactor with a reflector, a solution was obtained in a one-group approximation in [2], where it was shown that the reactor core with minimum critical size can consist of regions of two and only two types: with $u = u_{max}$ and $u = A/\Phi$. From the form of the functional (1) it follows directly that $\min J = 1$ and that it is attained for $u(r) = A/\Phi(r)$ everywhere in the core; it is easy to verify that such a distribution satisfies the necessary Weierstrass condition [1] of a strong minimum of the functional (3).

We now obtain an explicit expression $u(r)$ for the reactor model under consideration. (The possibility of loading the fuel according to the law $\Phi u = \text{const}$ was indicated earlier by Wilkins [3].) We write the one-group equation of diffusion in the form

$$\Phi'' + \alpha^2(r)\,\Phi = 0,\ \alpha^2(r) = \begin{cases} \dfrac{u/u_0 - 1}{L_0^2} & \text{for } 0 \leqslant r \leqslant R \\ -1/L_*^2 & \text{for } R \leqslant r < \infty, \end{cases} \tag{4}$$

Translated from Atomnaya Énergiya, Vol. 30, No. 6, pp. 539-540, June, 1971. Original letter submitted June 30, 1970.

where the constants L_0 and L_* are the diffusion lengths (neglecting absorption in uranium) in the core and in the reflector, respectively; $u_0 = 1/(\eta - 1)$ is the exact lower bound of the values u_{max}; η is the effective number of neutrons produced in the absorption of one neutron in uranium. Assuming in Eq. (4) that $u(r) = A/\Phi(r)$ and using the usual conditions at the points $r = 0$, R, and ∞, we obtain

$$\Phi(r) = \begin{cases} \dfrac{A}{u_0}\left(1 - \dfrac{\operatorname{ch} r/L_0}{\operatorname{ch} R/L_0 + \dfrac{DL_*}{D_*L_0}\operatorname{sh} R/L_0}\right) & \text{for} \quad 0 \leqslant r \leqslant R; \\ \dfrac{A}{u_0}\dfrac{\dfrac{DL_*}{D_*L_0}\operatorname{sh} R/L_0}{\operatorname{ch} R/L_0 + \dfrac{DL_*}{D_*L_0}\operatorname{sh} R/L_0}\exp\left(-\dfrac{r-R}{L_*}\right) & \text{for} \quad R \leqslant r < \infty, \end{cases} \tag{5}$$

where D and D_* are the diffusion coefficients in the core and in the reflector, respectively. From (5), it follows that

$$u(r) = u_0\left(1 - \frac{\operatorname{ch} r/L_0}{\operatorname{ch} R/L_0 + \dfrac{DL_*}{D_*L_0}\operatorname{sh} R/L_0}\right)^{-1} \tag{6}$$

and that it is a monotonically increasing function of r.

Therefore

$$\max_{0 \leqslant r \leqslant R} u(r) = u(R) = u_0\left(1 + \frac{D_*L_0}{DL_*}\operatorname{cth} R/L_0\right) \tag{7}$$

and is a monotonically decreasing function of R, with

$$\lim_{R \to \infty} u(R) = u_0\left(1 + \frac{D_*L_0}{DL_*}\right). \tag{8}$$

From the inequality (2), we have

$$\max_{0 \leqslant r \leqslant R} u(r) \leqslant u_{max} \tag{9}$$

Hence from Eq. (7) it also follows that for $R < R_*$, where

$$R_* = \frac{L_0}{2}\ln\frac{\dfrac{DL_*}{D_*L_0}\left(\dfrac{u_{max}}{u_0} - 1\right) + 1}{\dfrac{DL_*}{D_*L_0}\left(\dfrac{u_{max}}{u_0} - 1\right) - 1}, \tag{10}$$

since the condition (9) is not satisfied, the reactor cannot be of the one-region type with $u = A/\Phi$ everywhere in the region $0 \leq r \leq R$.† Thus, for $R < R_*$ the optimum (in the sense of the minimum) functional (1) will be a two-region reactor with $u = A/\Phi$ for $0 \leq r \leq h$ and $u = u_{max}$ for $h \leq r \leq R$, with the point h being determined by the condition that u(r) be continuous [1]; the minimum coefficient of variation of energy release in this case will be greater than unity. We note that R_* decreases with increasing u_{max}; however, it has as its lower boundary the value

$$R_{cr} = \frac{1}{\alpha_{max}}\arctan\frac{D_*}{L_*D\alpha_{max}}, \tag{11}$$

which is the absolute minimum critical size of the reactor model being considered, and is attained for loading of the entire core according to the law $u = u_{max}$ [it is of course assumed that the heat-engineering constraint (2) is satisfied].

Furthermore, from Eq. (8) [or (10)] it follows that for

$$u_{max} < u_0\left(1 + \frac{D_*L_0}{DL_*}\right) \tag{12}$$

the inequality (9) is no longer satisfied for all values of R and, hence, in this case, it is impossible to shape the fuel in order to attain min J = 1.

†A similar situation holds in the problem of minimizing the critical size. Earlier, in the problem of minimizing the critical mass [4], the violation of the inequality (9) at the point r = 0 also was asserted essentially by the form of the optimal solution.

We also note that for $u = A/\Phi$ everywhere in the core, the critical size is related to the power as $R = W/A$. Therefore the minimum R for which we can plot the given power W will be attained for $A = q_{max}$.

In conclusion we note that if we consider functionals of the form

$$J = \frac{\max [\Phi(r)\, u(r)]}{\frac{1}{V}\int\limits_{(V)} \Phi(r)\, u(r)\, dV} \tag{13}$$

in the multigroup approximation (taking into account fission in only one thermal group), then independently of the reactor geometry, $\min J = 1$ is attained for $u(r) = A/\Phi(r)$ everywhere in the core of volume V.

The author thanks Yu. V. Petrov for helpful discussion of the work.

LITERATURE CITED

1. T. S. Zaritskaya and A. P. Rudik, At. Énerg., 22, 6 (1967).
2. É. G. Sakhnovskii, At. Énerg., 29, 201 (1970).
3. The Reactor Handbook, Vol. 1, US Atomic Energy Commission (1955).
4. B. P. Kochurov, At. Énerg., 20, 243 (1966).

CALCULATION OF HEAT TRANSFER UNDER CONDITIONS OF BUBBLE BOILING

V. F. Prisnyakov

UDC 536.24:536.42

The total amount of heat transferred from a heating surface to a boiling liquid can be represented as the sum of the heat q" carried by bubbles of vapor and the heat q' removed by the liquid as a result of convection and mixing.

The quantity q' is given by the formulas for free convection [1] in which the effect of mixing is taken into account by means of a correction factor $\varkappa' = 1.25$ [2]. Such an assumption has little effect on the accuracy of the calculations since under conditions of well-developed boiling q" is much larger than q', while under conditions of weak boiling the effect of bubbles of vapor on free convection is reduced [2] (a single dash denotes liquid and two dashes vapor). Consequently, going over to the Peclet number $Pe'_* \sim q'$, we obtain

$$Pe'_* = \varkappa' C' N'_T \, Ja^{1+\nu}. \tag{1}$$

The amount of heat removed by vapor bubbles is given by the expression

$$q'' = nfVr\rho''$$

or, in dimensionless parameters, by

$$Pe''_* = \frac{4}{3}\pi \bar{n} \bar{f} \bar{R}^3. \tag{2}$$

The radius at which the bubbles detach $\bar{R} = R/R_*$, the frequency at which they appear $\bar{f} = f/f_*$, and the density of vapor formation centers $\bar{n} = nR_*^2$, can be found by means of the relationships [3]:

$$\bar{R}^3 - \frac{3}{2}\zeta_\sigma \sin\Theta \bar{R} - \frac{8}{27}\left(\frac{1+\cos\Theta}{\pi}\right)^2 \zeta_R \vartheta \, Ja^4 = 0; \tag{3}$$

$$\bar{f} = \left[\frac{\pi}{4}\left(\frac{Ja}{Re_*}\right)^2 + \frac{9}{16}\pi\frac{\bar{R}^2}{Ja^2}\right]^{-1}; \tag{4}$$

$$n = n_{max}\left\{0{,}5 + \Phi_0\left[\varepsilon\left(1 - \frac{e^{m_{cp}} - 1}{e^m - 1}\right)\right]\right\}. \tag{5}$$

Since $\bar{n}$ and $\bar{R}$ are the functions of the Jakob number Ja and the physical parameters, it follows that the dependence of $Pe_* = Pe'_* = Pe''_*$ on Ja can be found from the set of equations (1)-(5). The calculations are quite cumbersome and will not be reproduced here, since the more simple approximate solution given below is sufficiently accurate for most design calculations. We approximate (1) over the entire range of variation of the product Pr'Gr (Gr ~ Ja) by a relationship having an exponent $\gamma = 1/3$, which greatly simplifies the final results without detracting from the accuracy:

$$Pe'_* = \varkappa N_T \, Ja^{4/3}. \tag{6}$$

This expression along with (2)-(5) yields an equation for the Peclet number Pe_*:

$$Pe_*^3 - \left(\varkappa N_T Ja^{4/3} + \frac{64}{27}\bar{n}\bar{R}Ja^2\right) Pe_*^2 + \frac{4}{9}\cdot\frac{Ja^4}{\bar{R}^2} Pe_* - \frac{4}{9}\cdot\frac{\varkappa N_T Ja^{16/3}}{\bar{R}^2} = 0. \tag{7}$$

From the solution of this equation we may readily go over to the criterion $Nu_* = Pe_*/Ja$, which determines the heat-transfer coefficient in the presence of boiling. Introducing the following dimensionless quantities:

Translated from Atomnaya Énergiya, Vol. 30, No. 6, pp. 540-542, June, 1971. Original letter submitted March 13, 1970; revision submitted November 23, 1970.

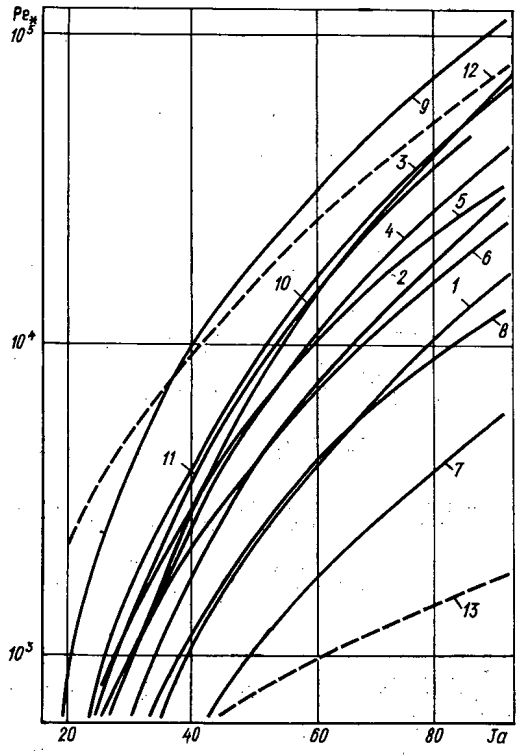

Fig. 1. Pe_* as a function of Ja: 1) S. S. Kutateladze's formula [1]; 2) formula obtained by E. K. Averin, V. M. Borishanskii, F. P. Minchenko, and G. I. Bobrovich (see [1]); 3) formula obtained by V. M. Borishanskii and F. P. Minchenko (see [1]); 4) formula in [5]; 5, 6) formulas in [6, 7]; 7, 8, 9) formula in [4] for different values of the coefficient (respectively, maximum 0.0173, intermediate 0.013, and minimum 0.006); 10) formula in [8]; 11) formula in [9] for fD = 0.1556 m/sec for water at 100°C; 12, 13) calculation from formula (7) for heating surfaces of the 7th and 14th smoothness classes respectively.

$$\Lambda=\frac{Pe_*\overline{R}}{Ja^2}=\frac{Nu_*^2\overline{R}}{Re_*\,Pr'};\quad s=\varkappa N_T\frac{\overline{R}}{Ja^{2/3}}$$

$$\eta=\overline{n}\overline{R}^2,$$

Eq. (7) reduces to the universal equation

$$\Lambda^3-\left(s+\frac{64}{27}\eta\right)\Lambda^2+\frac{4}{9}\Lambda-\frac{4}{9}s=0, \tag{8}$$

the solution of which is readily obtained.

These results lead to the formulas obtained by other authors (correct to a constant factor). Under conditions of well-developed bubble boiling and large values of η (< 0.5) the quantities Λ and η are interrelated approximately by $\Lambda = 2.5\,\eta$ or, in terms of Pe_* and Ja:

$$Pe_*=2{,}5\overline{n}\overline{R}Ja^2.$$

In the case of small Jakob numbers, for which $\overline{R} \approx$ const and $\overline{n} \approx Ja$ [3], this expression yields a relationship similar to that obtained in [4]: $Pe_* \approx Ja^3$ or $Nu_* \sim Pe_*^{2/3}$. For large Jakob numbers, when $\overline{R} \sim Ja^{4/3}$ and $\overline{n}$ is only weakly dependent on Ja [3], we obtain relationships that accord with most formulas describing heat exchange in the presence of boiling: $Pe_* \sim Ja^{10/3}$ or $Nu_* \sim Pe_*^{0.7}$ ($\alpha \sim q^{0.7}$). In the case of small values of η the quantity Λ is effectively dependent only on s: $\Lambda = 1.1s$. Consequently,

$$Pe_*=1{,}1\varkappa N_T Ja^{4/3},$$

i.e., under conditions of weak formation of vapor, heat transfer is determined by natural convection and mixing. The exponent of the Jakob number Ja thus varies from 4/3 to 13/3, which includes the values obtained in all known formulas for heat transfer in the presence of boiling.

Curves 1-11 in the figure are calculated from the most well-known formulas; curves 12 and 13 correspond to the limits of the smoothness classes most usually encountered in practice, i.e., from class 7 (curve 12) to class 14 (curve 13). The curves for the remaining surfaces (smoothness classes 8-13) lie between these limiting curves, as do the curves computed from other formulas.

Results calculated from our formula (for h_m equal to $2.4\cdot10^{-7}$ m and $5\cdot10^{-7}$ m; smoothness classes 10 and 13) are also in satisfactory agreement with the experimental data given in [10, 2, 11, 12].

Notation

R and V denote the radius and volume of a bubble at detachment; γ is an exponent equal to 1/3 or 1/4 depending on the product Pr'Gr; C' = f(Pr'Gr); Φ_0 is the Laplace probability integral; ζ_σ is the surface tension [3]; ζ_R is the bubble drag coefficient, which depends on the rate of growth of the bubble [3]; h is the height of heating surface micro-irregularities; $\varkappa = 0.4$;

$$R_* = \sqrt{\frac{\sigma}{q(\rho' - \rho'')}}; \quad f_* = a' R_*^{-2}; \quad \vartheta = \frac{\rho' a'^2}{\sigma R_*};$$

$$\mathrm{Pe}_* = \frac{qR_*}{r\rho'' a'}; \quad \mathrm{Nu}_* = \frac{\alpha R_*}{\lambda'}; \quad \mathrm{Ja} = \frac{c'\rho''\Delta T}{r\rho''};$$

$$\mathrm{Ja}_s = \frac{c'\rho' T_s}{r\rho''}; \quad \mathrm{Ja}_\beta = \frac{c'\rho'}{\beta r \rho''}; \quad \mathrm{Re}_* = \frac{\mathrm{Pe}_*}{\mathrm{Pr}'};$$

$$N_T' = q^\nu n^{\frac{1-3\nu}{2}} A^{3\nu-1} \nu'^{-2\nu} R_* \mathrm{Pr}'^{\nu} \mathrm{Ja}_\beta^{-\nu}; \quad N_T = \sqrt[3]{qR_*^3 \beta r \rho'' (\nu'\lambda')^{-1}}; \quad m = \frac{r\rho''}{p_s}\left(1 + \frac{\mathrm{Ja}_s}{\mathrm{Ja}}\right)^{-1};$$

the suffix "m" indicates the mean height of the micro-irregularities [3]. The rest of the notation is conventional.

LITERATURE CITED

1. S. S. Kutateladze, Fundamentals of the Theory of Heat Exchange [in Russian], Mashgiz, Moscow (1962).
2. C. Rallis and H. Sawurek, Intern. J. Heat Mass Transfer, 7, 1051 (1964).
3. V. F. Prisnyakov, Inzh.-Fiz. Zh., 19, No. 5, 912 (1970); PMTF, No. 5, 143 (1970); At. Énerg., 29, 46 (1970).
4. W. Rohsenow, Trans. ASME, 74, 969 (1952).
5. B. K. Averin and G. N. Kruzhilin, Izv. AN SSSR Otdelenie Tekh. Nauk, No. 10, 131 (1955).
6. D. A. Labuntsov, Izv. AN SSSR Otdelenie Tekh. Nauk, Seriya Énergetika i Transport, No. 1, 58 (1963).
7. D. A. Labuntsov, Teploénergetika, 19, No. 12 (1959).
8. N. G. Styushin and L. M. Élinzon, Inzh.-Fiz. Zh., 16, No. 1, 54 (1969).
9. V. I. Tolubinskii, Izv. Vuzov. Énergetika, No. 1, 15 (1959).
10. R. Gaertner, Trans. ASME, 84, No. 1, 52 (1954).
11. R. Vachon et al., Trans. ASME, 90, No. 2, 24 (1968).
12. A. Hatton and J. S. Hall, Proc. Third Int. Heat Transfer Conference (Chicago, 1966).

USE OF RESISTANCE THERMOMETERS IN NUCLEAR REACTORS

É. Ya. Gorodetskaya, A. I. Kits, and V. Ya. Kotel'man

UDC 621.039.564

Resistance thermometers are widely used to measure temperatures in nuclear reactors. References [1-5] discuss the action of nuclear radiation on the materials used to make resistance thermometers. Reference [4] describes the influence of fluxes of fast neutrons (10^{19} neutrons/cm^2) on the resistances of platinum, copper, and nickel. It was found that as a result of irradiation the resistivity of platinum increases by 1% (at 30°C), that of copper by 20% (at 150°C), and that of nickel by much less than 1% (at 240°C).

The resistances of nickel and platinum thermometers increased on irradiation by integral fluxes of fast neutrons of $2 \cdot 10^{19}$ neutrons/cm^2 at 100°C [2], and the thermometers indicated temperatures 3.7 and 2.6°C higher than the nominal values, respectively. Annealing after cessation of irradiation reduced the deviations, but did not completely return the calibration of the thermometers to normal.

The unavoidable changes in resistance thermometers irradiated by thermal neutrons are due to changes in the chemical composition of the material of the thermosensitive element. Different materials used to make resistance thermometers undergo different changes of properties. For example, in copper wire irradiated by a flux of $3.1 \cdot 10^{22}$ neutrons/cm^2 the quantity of copper decreased by 10%, and in a flux of 6.2 10^{22} neutrons/cm^2 it decreased by 20%. In the first case, about 5% nickel and 5% zinc were formed, and in the second case 10% nickel and 10% zinc. In platinum wire irradiated by fluxes of $3.1 \cdot 10^{22}$ and $6.2 \cdot 10^{22}$ neutrons/cm^2, the quantity of platinum decreased by about 2 and 4% respectively [3].

Calculations of the changes in resistance of the thermometers on irradiation showed [5] that copper resistance thermometers undergo changes 10 times greater than platinum thermometers and 16 times greater than nickel thermometers; this agrees well enough with the experimental data. It was also shown [4] that it is inadvisable to use platinum resistance thermometers in integral fluxes of thermal neutrons of up to 10^{22} neutrons/cm^2 and temperatures up to 100°C.

To investigate the characteristics of resistance thermometers of contemporary design [6] under irradiation, we tested 10 platinum resistance thermometers (R_0 = 100 Ω, class 2, GOST 6651-59). The thermometers consisted of platinum windings in ceramic insulation channels of sintered alumina. The channels with the windings were filled with powdered alumina and sealed by glaze. Then the thermometers

TABLE 1. Changes in Insulation Resistance of Thermometers*

Thermometer	Insulation resistance, MΩ		Thermometer	Insulation resistance, MΩ	
	before irradiation	after irradiation		before irradiation	after irradiation
1	500	20	6	500	20
2	500	5	7	500	50
3	500	5	10	500	5
4	500	5			

*The resistance permitted by State Standard GOST 6651-59 is 2 MΩ at 20°C for a humidity of 98%.

Translated from Atomnaya Énergiya, Vol. 30, No. 6, pp. 542-543, June, 1971. Original letter submitted March 20, 1970.

were placed in a protective jacket of Steel Kh18N9T and irradiated by a flux of $6 \cdot 10^{18}$ neutrons/cm^2 with $E > 1$ MeV or a flux of $3 \cdot 10^{19}$ neutrons/cm^2 with energies $E < 0.4$ MeV at 280°C. The resistance of the thermometer was measured before and after irradiation at about 0°C (R_0) with the aid of an MOD-49 dc bridge of Class 0.05. After irradiation we found an increase in resistance of about 0.05%, which is within the permissible deviation from the nominal value for platinum resistance thermometers of the second class. This small increase in the thermometer resistance can be explained by the continuous annealing of the thermosensitive element, and also by the fact that impurity atoms are not formed under such comparatively small integral fluxes of thermal neutrons. This is also confirmed by the results in [3].

One of the main characteristics of resistance thermometers is the resistance of the insulation between the thermosensitive element and the protective jacket. Nuclear radiation, by acting on the insulating material, reduces this resistance. According to [4], the resistance of ceramic insulation of alumina is reduced a hundredfold from 10^{10} to 10^8 Ω when it is irradiated by a flux of up to $3.5 \cdot 10^{18}$ neutrons/cm^2 ($E > 1$ MeV), at 400°C. Further increase in the integral flux does not lead to a fall in the insulation resistance. We measured the insulation resistances of seven resistance thermometers after irradiation by fluxes of $6 \cdot 10^{18}$ neutrons/cm^2 ($E > 1$ MeV) and $3 \cdot 10^{19}$ neutrons/cm^2 ($E < 0.4$ MeV). The results are listed in Table 1.

From our analysis of the published data and our experiments we can draw the following conclusions.

1. Platinum resistance thermometers with ceramic insulation made of alumina can be used to measure temperatures in nuclear reactors.

2. It is desirable to use resistance thermometers in integral fluxes of thermal or fast neutrons of up to 10^{19} neutrons/cm^2 and at temperatures ensuring continuous annealing, i.e., not below 280°C. Further research is needed to study the possibilities for the use of resistance thermometers at high integral fluxes and lower temperatures.

LITERATURE CITED

1. N. F. Pravdyuk, A. N. Ivanov, and K. P. Dubrovin, At. Énerg., 25, 233 (1968).
2. V. A. Krivtsov, G. I. Gushchin, and A. A. Fraktovnikova, Teplofizika Vysokikh Temperatur, 4, 279 (1966).
3. W. E. Browning and K. E. Miller, Theoretical Changes in the Compositions of Thermocouples under the action of Radiation: Symposium of Temperature Gages in Objects of the New Technology, translated from the English under the supervision of A. N. Gordov [Russian translation], Mir, Moscow (1965).
4. J. F. Kircher and R. E. Bowman, Effects of Radiation on the Materials and Elements of Electronic Circuits: translated from the English under the supervision of V. N. Bykov and S. P. Solov'eva [Russian translation], Atomizdat, Moscow (1967).
5. C. Ross, Comm. and Electronics, No. 61, 58 (1962).
6. Thermocouples and Resistance Thermometers: Coordinated Catalog, ONTIPribor., Moscow (1965).

THE TRANSITION-REGION FUNCTION FOR BERLYLLIUM AND SOME EXAMPLES OF ITS USE

V. N. Bogomolov and L. A. Chernov

UDC 621.039.5

For certain practical problems (measurement of integral characteristics of the neutron spectrum in a reactor, measurement of spatial distribution of resonance neutrons, etc.), the method used is to represent the neutron spectrum in a reactor with a low degree of poisoning by means of a simplified model based on the rather crude assumption that the real spectrum can be divided into the Maxwell spectrum and the moderation spectrum $\sim 1/E$.

The transitional part of the spectrum, linking these two, in the region (2-40)kT (where k is the Boltzmann constant and T the neutron temperature in degrees Kelvin), as shown in [1-5], does not vary much with the moderator temperature provided that $\Sigma_a(kT)/\xi\Sigma_s < 0.2$.

Then the neutron energy distribution can be written in the simple form

$$\Phi(E) = \frac{E}{(kT)^2} e^{-E/kT} + \lambda \frac{\Delta(E/kT)}{E}. \quad (1)$$

Here $\Delta(E/kT)$ is the transition-region function, and the quantity λ, which characterizes the ratio between the fluxes of thermal and epithermal neutrons, is easily found experimentally [5]. Detailed derivations of the expression for λ, with the mathematical apparatus used, can be found in the literature [1, 2].

Since the form of the transition-region function does not vary much with the moderator temperature [3], the function $\Delta(E/kT)$ can be calculated even from a single experimental spectrum. We have found the function $\Delta(E/kT)$ for beryllium. For this purpose, from the experimental neutron spectra we subtracted the Maxwell distribution $M(E/kT)$, which approximates them at thermal energies. The experimental spectrum was normalized to the Maxwell spectrum for an equal number of absorptions of a thin 1/v-detector in the neutron energy region 0.01-0.1 eV. The resulting function $\Phi'(E) = \Phi(E) - M(E/kT)$ was divided by the

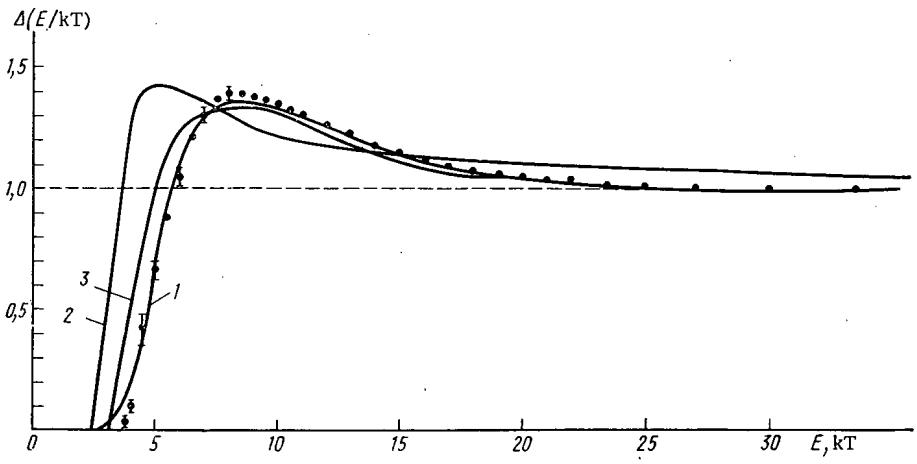

Fig. 1. Transition-region functions for beryllium (1), water (2) [2], and graphite (3) [3]. •) Experimental points for beryllium.

Translated from Atomnaya Énergiya, Vol. 30, No. 6, pp. 543-545, June, 1971. Original letter submitted June 15, 1970.

quantity λ, which is obtained automatically in measurements of the neutron spectra by the time-of-flight method and in the above-mentioned normalization. The normalization enabled us to find the function $\Phi''(E) = 1/E$ for $E > 30kT$. The transition-region function $\Delta(E/kT) = E\Phi''(E)$ averaged over several experimental neutron spectra for beryllium was found to be close to the transition function for graphite (see Fig. 1).

The discrepancy between the vanishing points of the transition-region function for beryllium and graphite is due to the peculiarities of the interaction of neutrons with these substances and to experimental errors.

Westkott [5] suggests several analytical relations which fairly accurately fit the experimental and theoretical data. The function Δ_4, suggested as a basis in [5], after slight modifications, fairly accurately fits the curve of the experimental transition-region function for beryllium (see Fig. 1) and has the form

$$f(E/kT) = \left[1 - \frac{0.29}{1 + \left(\frac{E}{14.5kT}\right)^5} + \left(\frac{4.9kT}{E}\right)^8\right]^{-1}. \quad (2)$$

The initial neutron spectra were measured at the center of a beryllium block about 240 mm in diameter, placed at the center of a thermal uranium–beryllium reactor with material buckling $B^2 = 1.625 \cdot 10^{-3}$ cm^{-2}. The spectra were measured by the time-of-flight method with a mechanical velocity selector. The spectrometer had a resolution of about 20 μsec/m.

Activation measurements revealed that in this beryllium block, in the central part with a diameter of about 100 mm the radial distributions of activation density of a 1/v-detector and the cadmium ratio are constant. These results suggest that the size of the block is large enough so that the function $\Delta(E/kT)$ refers to pure beryllium.

The transition-region functions obtained in the measurements were used to calculate the effective limiting energy for cadmium for a thin 1/v-detector, given [2] by

$$E_{Cd} = 4\left\{\int_0^\infty \Delta(E/kT)\, E_2\left[\sum\nolimits_a^{Cd}(E)\, d^{Cd}\right] E^{-3/2} dE\right\}^{-2}. \quad (3)$$

The concept of the limiting energy of cadmium is used in activation measurements, and, in somewhat modified form, in measurements of reactivity coefficients in work with specimens.

For cadmium with thickness $d^{Cd} = 0.5$ mm and $\sum_a^{Cd}(E)$ taken from [6], we obtained $E_{Cd} = (0.576 \pm 0.006)$ eV, which is somewhat greater than the effective limiting energy of cadmium for a thin 1/v-detector as found in the literature. For example, for $d^{Cd} = 0.5$ mm, Bekurz and Wirtz [2] give $E_{Cd} \approx 0.56$ eV. The slight discrepancy can be explained by the difference between the functions $\Delta(E/kT)$ used to calculate E_{Cd}. The same authors [2] plot E_{Cd} versus the thickness of the cadmium, using the function $\Delta(E/kT)$ for D_2O.

The effective limiting energy of cadmium can be found experimentally if we measure the neutron specimen within a hollow space surrounded by cadmium. This experiment was performed. We paid special attention to securing "neutron-tightness" of the whole beam extraction channel. Therefore the whole of the experimental extraction channel, including the luminous surface, was lined with 0.5 mm of cadmium.

From the spectrum obtained, $\Phi^{Cd}(E)$, by means of the relation

$$\int_{E_{Cd}}^\infty \frac{dE}{E\sqrt{E}} = \int_0^\infty \Phi^{Cd}(E)\frac{dE}{\sqrt{E}}, \quad (4)$$

the right-hand side of which was integrated numerically, we obtained the value $E_{Cd} = (0.572 \pm 0.006)$ eV. The resolution of the spectrometer used for the measurements of $\Phi^{Cd}(E)$ was about 15 μsec/m.

Using the transition-region function for beryllium, we can obtain the limiting energy of the neutron moderation spectrum in beryllium for a thin 1/v-detector. The calculation was based [2] on the relation

$$E_{lim} = 4\left[\int_0^\infty \Delta(E/kT)\frac{1}{E}\frac{dE}{\sqrt{E}}\right]^{-2} = \mu kT. \quad (5)$$

The value obtained, $\mu = 3.9 \pm 0.4$, is somewhat higher than the expected value ($\mu = 3.6 \pm 0.4$ for D_2O and $\mu = 3.4 \pm 0.3$ for graphite [2]).

The neutron spectra in beryllium, used to obtain $\Delta(E/kT)$, had a neutron temperature difference of about 50°K.

In conclusion, the authors thank I. D. Shorinova for helping in processing the data on a computer.

LITERATURE CITED

1. N. S. Shapiro, in: Thermalization of Neutrons [in Russian], Atomizdat, Moscow (1964), p. 403.
2. K. Bekurtz and K. Wirtz, Neutron Physics [Russian translation], Atomizdat, Moscow (1968).
3. M. Coats, Neutron Time-of-Flight Methods, Euratom, Brussels (1961).
4. M. Poole, Symposium on Neutron Time-of-Flight Methods, Tuly, Saclay (1961).
5. C. Westkott, Effective Cross Sections for Well-Moderated Thermal Reactor Spectra (3rd ed. d), Report No. AECL 1101 (1960).
6. Bulletin of the Information Center on Nuclear Data, No. III (Appendix), Atomizdat, Moscow (1967).

THERMODYNAMICS OF EXTRACTION OF Pu(IV) FROM NITRIC ACID SOLUTIONS BY TRI-n-BUTYL PHOSPHATE (TBP)

A. S. Solovkin

UDC 66.061.5:546.799.4

We have shown [1] that zirconium in the monomer state is extracted from nitrate media by solutions of TBP in kerosene and xylol in the form of $Zr(NO_3)_4 \cdot 2TBP$, $Zr(OH)(NO_3)_3 \cdot 2TBP$, and $Zr(OH)_2(NO_3)_2 \cdot 2TBP$. Literature data based on spectrophotometry [2] states that in the TBP phase Pu(IV) nitrate may exist in hydrolyzed form, i.e., as $Pu(OH)(NO_3)_3$.

According to calculations (based on the method in [1]), from nitrate media Pu(IV) is extracted into TBP solutions in kerosene in the form of $Pu(NO_3)_4 \cdot 2TBP$ and $Pu(OH)(NO_3)_3 \cdot 2TBP$. Thus the relation between the partition coefficient D, the composition of the aqueous phase, and the TBP concentration in the diluent can be written as follows:

$$D = C_a^q \left(K_0^0 \cdot \gamma_{Pu^{4+}} \cdot M'_{Pu^{4+}} \cdot a^4_{NO_3^-} + K_1^0 \cdot \gamma_{Pu(OH)^{3+}} \cdot M'_{Pu(OH)^{3+}} \cdot a^3_{NO_3^-}\right).$$

Here C_a^q is the active TBP concentration in the diluent phase, $\gamma_{Pu^{4+}}$ and $\gamma_{Pu(OH)^{3+}}$ are the activity coefficients of the Pu^{4+} and $Pu(OH)^{3+}$ ions in the aqueous phase, the $M_i^!$ are the fractions of the respective ions in the aqueous phase, and $a_{NO_3^-}$ is the activity of NO_3^- ions in the aqueous phase [3]. The value of C_a^q was calculated from Eqs. (8.7) and (8.8) in [3]; in extraction from mixtures of $HNO_3 + NaNO_3$, for the ionic strength F due to the extracted electrolytes the value was $m_S = ([H^+][NO_3^-])^{1/2}$ [4]. In calculating C_a^q and K_i^0, the degree of dissociation of HNO_3 in the aqueous phase in the presence of $NaNO_3$ and the concentration of NO_3^- ions were found with allowance for association of the $NaNO_3$ [3]. The calculation of $M_i^!$ (by the method in [1]) was based on the following values for the thermodynamic equilibrium constants of the reaction $Pu^{4+} + iOH^- \rightleftharpoons Pu(OH)_i^{4-i}$: $\beta_1^0 = 0.17$*, $\beta_2^0 \approx 0.6$,† and $\beta_3^0 \approx 3.2$.† The thermodynamic equilibrium constants of the reactions $Pu^{4+} + 4NO_3^- + 2TBP \rightleftharpoons Pu(NO_3)_4 \cdot 2TBP$ and $Pu(OH)^{3+} + 3NO_3^- + 2TBP \rightleftharpoons Pu(OH)(NO_3)_3 \cdot 2TBP$ were found to be $K_0^0 = 380$ and $K_1^0 = 4.8 \cdot 10^4$.

*Calculated by A. S. Solovkin and A. I. Ivantsov from the data in [10].

†Calculated from data on extraction of Pu(IV) by TBP at low HNO_3 concentrations (0.5-1.0 M) from solutions with and without $NaNO_3$.

TABLE 1. Thermodynamic Parameters Necessary for Calculating k_i^0 (T = 25°C)

Composition of aq. phase	γ_{H^+}	$\gamma_{NO_3^-}$	$\gamma_{Pu^{4+}}$	$\gamma_{Pu(OH)^{3+}}$	$\gamma_{Pu(OH)_2^{2+}}$	$\gamma_{Pu(OH)_3^+}$
0,5*M* HNO_3	0,827	0,632	0,0083	0,040	0,23	0,59
1,0*M* HNO_3	0,961	0,603	0,0062	0,039	0,19	0,51
2,0*M* HNO_3	1,297	0,613	0,0093	0,0355	0,195	0,44
3,0*M* HNO_3	1,930	0,658	0,0194	0,051	—	—
4,0*M* HNO_3	2,707	0,721	0,052	0,094	—	—
0,5*M* HNO_3 + 1,5*M* $NaNO_3$	1,40	0,435	0,0105	0,034	0,18	0,45
2,0*M* HNO_3 + 2,0*M* $NaNO_3$	3,12	0,468	0,123	0,072	—	—
1,0*M* HNO_3 + 3,0*M* $NaNO_3$	3,38	0,400	0,100	0,063	—	—

Note: If the HNO_3 concentration in the aqueous phase is ≥ 2M, hydrolysis of Pu(IV) by the second and third stages has practically no influence on $M_i^!$. For $Pu(OH)^{3+}$, $Pu(OH)_2^{2+}$, and $Pu(OH)_3^+$, the values of $\rho_+^!$ and r_+ [3] are respectively equal to 0.0513, 0.0443, 0.026, and 1.28, 1.62, 1.96 Å.

Translated from Atomnaya Énergiya, Vol. 30, No. 6, pp. 545-547, June, 1971. Original letter submitted June 30, 1970.

TABLE 2. Comparison between Experimental and Theoretical Values of D for Extraction of Pu(IV) from HNO_3 Solutions

HNO_3 concentration in aq. phase, mole/liter	TBP concentration in organic phase, vol.%	C_a^q	$M'_{Pu^{4+}}$	$M'_{Pu(OH)^{3+}}$	D		Source
					calculated	experiment	
0,5	20	0,232	0,41	0,0436	0,60	0,47	[7]
0,5	30	0,45	0,41	0,0436	1,16	0,81	[9]
0,91	19	0,159	0,81	0,035	1,74	1,30	[6]
0,99	30	0,23	0,91	0,0305	2,85	2,90	[8]
1,0	20	0,147	0,91	0,0305	1,82	1,45	[7]
1,0	19	0,1455	0,91	0,0305	1,79	1,50	[6]
1,28	19	0,105	0,92	0,0274	2,31	2,20	[6]
1,41	19	0,094	0,95	0,0265	2,80	2,37	[6]
2,0	20	0,055	0,9778	0,0222	3,60	3,83	[7]
2,0	30	0,08	0,9778	0,0222	5,3	6,3	[8]
2,0	30	0,08	0,9778	0,0222	5,3	6	[9]
2,2	19	0,044	0,9794	0,0206	4,07	3,90	[6]
3,0	19	0,020	0,9845	0,0155	5,67	6,80	[6]
3,0	20	0,0205	0,9845	0,0155	5,81	5,80	[7]
3,0	30	0,0325	0,9845	0,0155	9,2	11	[9]
3,0	30	0,0325	0,9845	0,0155	9,2	16,0	[8]
4,0	19	0,0090	0,9875	0,0125	13,4	11,5	[6]
4,0	20	0,0091	0,9875	0,0125	13,57	10,26	[7]
4,0	30	0,0145	0,9875	0,0125	21,6	21,5	[8]
4,0	30	0,0145	0,9875	0,0125	21,6	20	[9]

TABLE 3. Comparison between Experimental and Theoretical Values of D for Extraction of Pu(IV) from Mixed Solutions in HNO_3 + $NaNO_3$

Composition of aq. phase	C_a^q	$M'_{Pu^{4+}}$	$M'_{Pu(OH)^{3+}}$	$[NO_3^-]$, g-ion/liter	X	D	
						calculated	experiment [6]
0,5*M* HNO_3 +1,5*M* $NaNO_3$	0,144	0,58	0,0563	1,70	0,028	5,5	~ 6
1,0*M* HNO_3 +3,0*M* $NaNO_3$	0,05	0,90	0,10	2,64	0,136	20,5	~ 19,5
2,0*M* HNO_3 +2,0*M* $NaNO_3$	0,027	0,938	0,062	2,80	0,26	16,1	~ 14,8

Note: X is the concentration of undissociated HNO_3 molecules in the aqueous phase.

The thermodynamic parameters necessary for calculating k_i^0 are listed in Table 1. Tables 2 and 3 compare the experimental and theoretical values of D. The calculated values of D agree with the experimental values within ±15% (from Table 2 it follows that the experimental values of D obtained by different authors in the same conditions frequently disagree by 15-20% or more). If the equilibrium concentration of HNO_3 in the aqueous phase is greater than 4.5M, the calculated values of D are greater than the experimental values, and the difference rapidly increases ("avalanche-fashion") as the HNO_3 concentration increases in the range 5-6M, in agreement with the ideas in [5] of "avalanche-like" formation of complexes of the type $Me(NO_3)_6^{2-}$ ($Me = U^{4+}$, Np^{4+}) in these conditions. Apparently Pu^{4+} behaves like these metals. The calculated values of D agree with the experimental values also for joint extraction of uranyl nitrate and Pu(IV) from HNO_3 solutions. For example, according to Best et al. [6], when Pu(IV) is extracted from 1M aqueous solution of HNO_3 with 0.027M uranyl nitrate (uranyl nitrate concentration in organic phase, 0.087M) by a 19 vol.% solution of TBP in kerosene, the experimental value of D is equal to 0.90 and the calculated value 1.09.

It is interesting to note that the fraction of Pu(IV) extracted in the form of $Pu(NO_3)_4 \cdot 2TBP$ rapidly falls as the acidity of the aqueous phase decreases – from 0.386 at 4M HNO_3 to 0.022 at 1M HNO_3, and to 0.016 for the system 0.5M HNO_3 + 1.5M $NaNO_3$.

In conclusion, we must emphasize that when the HNO_3 concentration in the aqueous phase is less than 4M, extraction of Pu(IV) can be represented without invoking ideas of formation of complexes of the $Pu(NO_3)_i^{4-i}$ ($i \leq 6$) type in the system $H_2O - HNO_3(NaNO_3) - Pu(IV)$.

LITERATURE CITED

1. A. S. Solovkin, Zh. Neorgan. Khim., 15, 1914 (1970).
2. J. Woodhead, J. Inorg. Nucl. Chem., 26, 1472 (1964).

3. A. S. Solovkin, Salting Out and Quantitative Description of Extraction Equilibria [in Russian], Atomizdat, Moscow (1969).
4. A. S. Solovkin, Zh. Neorgan. Khim., 16, 272 (1971).
5. A. G. Rykov, V. Ya. Vasil'ev, and N. B. Blokhin, Radiokhimiya, 12, 711, 717 (1970).
6. G. Best, H. McKay, and P. Woodgate, J. Inorg. Nucl. Chem., 4, 315 (1957).
7. A. M. Rozen and É. I. Moiseenko, in: Extraction: Theory, Application, and Apparatus [in Russian], Gosatomizdat, Moscow (1962), p. 235.
8. J. Codding, W. Haase, and F. Heuman, Industr. and Engng Chem., 50, 145 (1958).
9. M. Germain, D. Gourisse, and M. Sougnez, J. Inorg. Nucl. Chem., 32, 245 (1970).
10. S. Rabidean, J. Amer. Chem. Soc., 79, 3675 (1967).

DETERMINATION OF THORIUM CONCENTRATION WITH THE AID OF CASCADE EMISSION

G. S. Semenov, A. P. Grumbkov, and V. P. Kuptsov

UDC 550.3.835.08:553.495

To determine thorium concentrations, several methods are currently being used, including gamma spectrometry with the aid of the ThB (288 keV), MsTh(II) (907 keV), and ThC" (582 and 2620 keV) lines [1-4].

Whereas most methods require delicate chemical preparation of the specimen, and neutron activation analysis requires complex equipment (a nuclear reactor), the gamma spectrometric method is quite simple. From the photopeak intensities of the gamma lines mentioned, the quantity of thorium in the specimen can be determined to within $5 \cdot 10^{-4}\%$.

However, the method has certain shortcomings, as follows.

1. If the emitter (Th, U–Ra, and K^{40}) is of mixed composition, we get interference from neighboring intense gamma lines of radium.

2. Measurements on the 2.62 MeV line are inefficiently performed [4, 5] by current production-line instruments, leading to reduction in output and increased difficulty in the analyses.

The above drawbacks can be overcome if in the gamma-spectrometric measurements of thorium concentration we can increase the efficiencies of the scintillation detectors, which are proportional to the volume and the square of the solid angle. Therefore increasing the volume of the crystal and using nearly 4π geometry permits us to raise the efficiency. In addition, such a detector will make it possible to use the effect of summation of cascade gamma quanta of ThC", with energies of 0.582 and 2.62 MeV [1, 6], to determine the thorium content. Cascade gamma quanta of thorium were registered by a scintillation detector consisting of a crystal of sodium iodide with a well and an FÉU-49 photomultiplier. The sample measurement geometry, which was nearly 4π, permitted registration of the cascade gamma lines without a special electronic

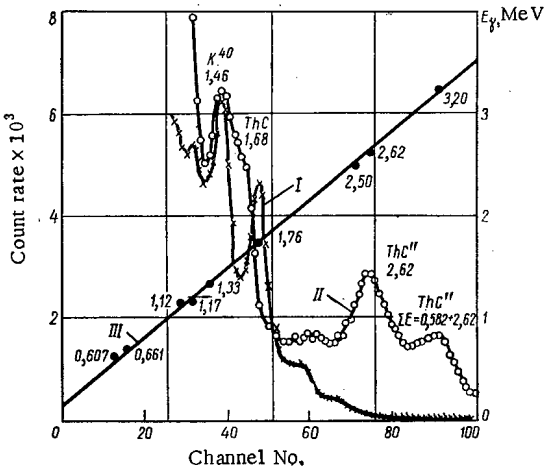

Fig. 1. Instrumental-spectra of equilibrium uranium ore (I) and mixed thorium–uranium ore (II). (III) Energy calibration.

Translated from Atomnaya Énergiya, Vol. 30, No. 6, pp. 547-548, June, 1971. Original letter submitted May 25, 1970.

circuit, purely by means of the physical effect of summation of their scintillations which arise simultaneously in the crystal. The use of a large (2.4 dm^3) scintillator with a well greatly increased the probability of simultaneous registration of both gamma quanta in a cascade.

The energy resolution of the crystal (12% for Cs^{137}) enabled us to separate the photopeaks of ThC" at 2.62 and 3.2 MeV. With a lower threshold of 2.4 MeV, the detector registers only the photoabsorption of the 2.62 MeV quanta in the cyrstal, while photoabsorption of the 0.58 cascade quanta is nearly equal to unity, since the crystal is nearly "black" for this line. In the case of gamma spectrometry in a nearly 4π geometry, the use of the usual energy range (2.4-2.8 MeV [3]) may lead to a marked reduction in the number of pulses corresponding to cascade gamma quanta. To avoid this, the upper limit of the range should be at least 3.8 MeV. We can also use discrimination of the lower level only, but in this case some increase of the background count is likely owing to the muon component of the cosmic rays with energies above 3 MeV, and this will lead to a reduction in the effect/background ratio. The use of a broad "window", in which the relative contributions of other emitters are reduced, gives a marked rise in the stability of solution of the system of equations, which permits reduction of errors and thus reduces the threshold of sensitivity to $1.0 \cdot 10^{-4}$% Th, allowing the sample weight to be cut to 200 g.

This method of summing the cascade gamma quanta of thorium was tested in laboratory conditions with thorium ores and sources with thorium concentrations ranging from $5 \cdot 10^{-4}$ to $20 \cdot 10^{-2}$%.

Figure 1 plots the instrumental spectra of equilibrium uranium ore and mixed thorium–uranium ore.

The method was also tested with natural thorium ores with concentrations of $0.2 \cdot 10^{-3} - 1.6 \cdot 10^{-3}$ wt. % (according to chemical analysis data).

A thorium concentration meter can be assembled from units of standard commercial nuclear-physics apparatus. It can be used in geological surveys to study alluvial placer deposits, because we know the relation between the thorium contents of fluvial and marine alluvial deposits and the ores of heavy metals such as gold, molybdenum, tin, tungsten, titanium, the zirconium mineral group, etc. [4, 7]. A thorium concentration meter can be used to determine the concentrations of artificial radioisotopes with cascade gamma lines (Co^{60}, Sc^{46}, Na^{24}, Na^{22}, etc.) in a mixture of several emitters with gamma lines of similar energies.

The authors are obliged to V. V. Matveev and V. L. Shashkin for helpful consultations and observations.

LITERATURE CITED

1. K. Sigban, Beta and Gamma Spectrometry [Russian translation], Fizmatgiz, Moscow (1959).
2. Methods of Determining Radioactive Elements in Minerals: Handbook [in Russian], Gosgeoltekhizdat, Moscow (1961).
3. V. L. Shashkin, Methods of Analysis of Natural Radioactive Elements [in Russian], Gosatomizdat, Moscow (1961).
4. A. L. Yakubovich, Rapid Analysis of Minerals with Scintillation Apparatus [in Russian], Gosatomizdat, Moscow (1963).
5. V. A. Zelentsev, Pribory i Tekhnika Éksperimenta, No. 6, 204 (1967).
6. N. A. Vartanov and P. S. Samoilov, Practical Methods of Scintillation Gamma Spectrometry [in Russian], Atomizdat, Moscow (1964).
7. Methodological Instructions for the Use of Radiometric Methods for Surveys and Prospecting of Ores of Nonradioactive Elements [in Russian], Second Edition, Nedra, Moscow (1965).

MEASUREMENT OF NEUTRON SPECTRA IN FAST REACTORS

Yu. A. Kazanskii

In November 1970 the International Atomic Energy Agency held an international Conference at the Argonne National Laboratory (United States of America) on the measurement of neutron spectra in fast reactors and their interpretation. Eighteen specialists from Great Britain, Belgium, Italy, the Netherlands, the USSR, the United States, France, and the Federal Republic of Germany took part in the conference. Fourteen reports were heard; these were discussed in detail at unofficial evening meetings. The reports may be divided into the following groups: a) programmes for spectrometric studies; b) a hydrogen proportional counter; c) the time-of-flight method; d) other methods for measuring neutron spectra (an Li^6 semiconductor spectrometer, a scintillation spectrometer with NE-213, etc.).

The reports of M. Wiener (United States) and Yu. A. Kazanskii (USSR) dealt with programs of work on the study of neutron spectra in fast reactors. It is assumed that detailed information on the neutron spectra obtained in simply constructed homogeneous assemblies will make it possible to verify systems of multi-group constants and calculation methods and make them more precise. The measurement of neutron spectra in physical assemblies simulating fast power reactors will make it possible to obtain more exact information on certain reactor characteristics and to verify them (critical mass, multiplication factor, coefficient of reactivity of various materials, temperature effects, etc.).

Spectral measurements are, of course, no substitute for integral experiments on critical assemblies. However, the spectral measurements will help in understanding the reasons for the existing discrepancies between measured and calculated integral characteristics. From some considerations raised at the conference, particularly in M. Wiener's report, it appears that a solution of the problems involved requires spectrum measurements accurate to 4% or less in the 10 keV to 1 MeV neutron energy range.

The reports of E. Bennett (United States), A. Broomfield (Great Britain), and A. Léridon (France) were devoted to methodological questions involved in the use of a hydrogen proportional counter and some of the results obtained with this instrument. At present it is possible, by using a proportional counter with hydrogen and methane, to measure "smooth" spectra to within ±7-8% or less in the energy range from 50 keV to 1 MeV and to within ±10-12% in the 10-50 keV range. In the energy range below 10 keV the accuracy is ±20-30%. It is believed that the required accuracy (approximately 5%) can be achieved in the 50 keV to 1 MeV energy range. However, this would require painstaking and methodical work, including, in particular a careful determination of the shape of the spectrometer curve, taking account of effects such as the wall effect and the inductive effect and the influence of distortion of the field in the vicinity of points of attachment of the wire. In addition, it is necessary to measure more precisely how the amount of energy spent in creating ion vapors varies as a function of the energy of carbon recoil nuclei and protons. In order to obtain the necessary accuracy, the energy scale of the spectrometer must be carefully determined with an error of no more than 2%. Some phenomena still remain unexplained. (For example, the positions of minima and maxima in measured spectra do not always coincide with the calculated values.)

The time-of-flight method for investigating the spectra of neutrons escaping from critical assemblies was discussed in the reports of E. Wotekamps (Federal Republic of Germany), Ku. A. Kazanskii (USSR), C. Preskitt (United States), D. Sanders (Great Britain), W. Jjoen (Netherlands), and A. Schmitt (France). The method has already been used in Great Britain (the VERA and ZEBRA assemblies), the United States (STSF), and the Federal Republic of Germany (SUAK). In the near future, conditions suitable for making

Translated from Atomnaya Énergiya, Vol. 30, No. 6, pp. 549-550, June, 1971.

such measurements will be established at the Argonne National Laboratory (ZPR-6), the USSR Institute of Physics and Power (BFS), and the Netherlands (STEK). The time-of-flight method makes it possible to obtain the spectra of neutrons escaping from fast critical assemblies, ranging in energy from hundreds of electron volts to several MeV. Despite its relative complexity and high cost, this method is the best from the point of view of energy resolution, and in the energy range below several keV it is the only differential method available. The accuracy of this method is estimated at about 10% in the range of neutron energies from 1 keV to 1 MeV. The largest share of the error is contributed by the determination of the detector efficiency (from 5 to 10% for an Li^6 detector), the statistical accuracy, and the background in the low-energy range (below about 1 keV). Thus, on the STSF assembly the statistical accuracy, when the deduction for the background is taken into account, is less than about 15% for energies of several hundred electron volts. The interpretation of neutron spectra measured by the time-of-flight method gives rise to some problems which have not yet been thoroughly studied (the perturbation of the measured spectrum by the extraction channel, the absence of the leakage-neutron spectra from the spectra of neutrons inside the reactor, the absence in the spectra of neutrons of subcritical and critical reactors, the influence of the heterogeneity of the assembly on the formation of the neutron spectrum). As the discussions showed, the extraction channel does not affect the measured neutron spectrum if the channel diameter is less than 7-8 cm. The effects of the heterogeneity can be taken into account fairly well in calculations using the transport approximation. (This was shown in C. Preskitt's report.)

The reports of W. Paterson (Great Britain), E. Straker (United States), and A. Fabry (Belgium) dealt with the possibilities of measuring neutron spectra with an Li^6 semiconductor spectrometer, a scintillation spectrometer with NE-213, a scintillation pair spectrometer, the method of filters, etc. Perhaps the most interesting is the Li^6 semiconductor spectrometer, which can be used to cover a wide range of energies, from 5 keV to several MeV. This spectrometer can compete successfully with the hydrogen proportional counter.

A comparison of the measured and calculated spectra in fast physical assemblies was discussed in the reports of E. Bennett, A. Broomfield, and C. Preskitt. Comparison of the theory with a series of measurements on ZPR assemblies revealed systematic discrepancies, which cannot be explained by measurement errors, nor, probably, by an heterogeneous effect. The discrepancies are observed chiefly in the neighborhoods of strong resonances (sodium, iron, oxygen). A comparison of measured spectra on ZEBRA assemblies with the calculations also showed poor agreement in the neighborhood of strong resonances. In addition, the ratio of calculated and measured fluxes over broad energy intervals points to a systematic overestimate of the calculated fluxes in the 3-30 keV neutron energy range. An additional indication in this direction is the U^{238}/Pu^{239} fission cross section ratio, which was found to have calculated values 10-15% lower than the experimental values. An analysis of the measurement results obtained in the STSF showed that the measured neutron spectrum contains more neutrons in the low-energy range (approximately 3 keV) than the calculated spectrum does.

The conference showed, first of all, that today there are genuine possibilities for studying neutron spectra in fast physical assemblies with the necessary accuracy; secondly, that analysis of existing experimental data points to a need for more precise calculation methods and group cross sections (especially in the vincinity of strong resonances); and, thirdly, that effective calculation methods must be developed in order to utilize the vast store of information contained in measured spectral distributions.

THE LEIPZIG CONFERENCE AND EXHIBITION ON NUCLEAR INSTRUMENTATION OF THE COUNCIL FOR MUTUAL ECONOMICAL ASSISTANCE

L. N. Krylov

The Third "Atoms for Peace" Exhibition of Nuclear Instrumentation of the Council for Mutual Economical Assistance (Comecon) was inaugurated on the Leipzig Fair grounds in the fall of 1970. A Conference on Radioisotopic Devices and Laboratory Instrumentation was held concurrently with the Exhibition. Nearly 150 representatives of Member Countries of the Comecon participated in the Conference and more than 100 papers were read. All papers were divided into three groups according to their subject: 1) radioisotopic instruments for industrial radioisotopic laboratories, 2) nuclear medical instruments and techniques, 3) radiation monitors and nuclear radiation detectors.

The group on radioisotopic instruments dealt mainly with analytic and spectrometric instruments, radiation measurement, and isotopic instrument design. W. Ditch (GDR) reported on the effective use of analytic instruments for the determination of silver density in photographic emulsions. Simple and reliable x-ray radiation measuring instruments with integral pulse selection allow a considerable saving of silver. Soviet x-ray radiation measuring instruments exhibited were the "Ferrite" iron analyzer and the portable "Gipnos" analyzer for molybdenum ores in natural deposits with an abundance of more than 0.02%.

A. V. Dolenko et al., (USSR) described the results obtained with the MAK 1 gamma-resonance equipment at deposits of tin and reported on the new ALOK-1 automatic cassiterite analyzer for laboratory use.

O. K. Nikolaenko et al., (USSR) described the K-1 "Kislorod" single-element neutron activation analyzer, its construction, analytic techniques, and some practical results. The oxygen detection sensitivity with a neutron flux of $6 \cdot 10^8$ n/sec was $3 \cdot 10^{-4}$%. An oxygen determination sensitivity of 10^{-5}% has been obtained with a second neutron activation analyzer described by B. G. Egiazarov et al., (USSR). The instrument includes a computing device for calculating the content. The same paper also described the equipment of a general-purpose activation analysis laboratory with scintillation and semiconductor spectrometers, a 1024-channel analyzer, and computer interface units for programmed data processing. As reported by V. Kapisovski (Czechoslovakia), an 1VM-7040 [IBM-7040, ASK] computer has been used for peak approximation and nonlinearity correction on a gamma spectrometer with a 5.3-cm^3 Ge(Li) semiconductor detector.

Electronic devices for spectrometric systems were extensively represented both at the Conference and at the Exhibition. Among them were portable (weighing less than 10 kg) battery powered AI-256-6 and AI-1024-6 multichannel analyzers (S. S. Kurochkin, L. N. Sineva, et al., USSR) with economical ferrite-core memories (5 W power consumption) and MTA-512B and MTA-521M (M. Blazovski, Hungary), laboratory multichannel analyzers with 10-msec memory access time and 4- and 25-MHz analog-digital conversion frequencies. The MTA analyzers are fitted with digital stabilizers.

Laboratory spectrometric systems with semiconductor detectors are the "Langur" system (Yu. P. Sel'dyakova et al., USSR), the BSD-268 set (Rumania), a set of GDR units (J53-B field-effect transistor preamplifier, VA-V-88 preamplifier, VA-V-100 amplifier-analyzer, etc.). These systems have the following parameters: noise 1-2 keV (zero detector noise), gain stability 0.01-0.02% per °C, nonlinearity 0.1%, expander level instability 0.01-0.05% per °C. The "Langur" system includes seven cryostats with 250 μm beryllium windows for housing the semiconductor detectors.

Translated from Atomnaya Énergiya, Vol. 30, No. 6, pp. 550-552, June, 1971.

K. Broj (Czechoslovakia) described an automatic measuring system for a large number of samples (up to 200) with a two-channel spectrometer whose logic uses Tesla integrated circuits. Also exhibited were RUST-2 (Poland) general-purpose portable radiation meters for alpha, beta, gamma and neutron radiation, and special-purpose instruments for geological prospecting such as UPR-01 (Czechoslovakia) radiation meters with STS-8 counters, RP-20 radiation meters with scintillation counters (Czechoslovakia), and SRP-68 scintillation meter using integrated circuits (described by L. N. Krylov, USSR). The fundamental error of prospecting instruments is 10% with a measuring range of $3 \cdot 10^3$ pulses/sec (Czechoslovak instruments) and 10^4 pulses/sec (SRP-68).

At the radiation detector session H. Michel (GDR) reported on a new method of reception of gas-discharge detector pulses using the electromagnetic radiation of the discharge. Most of the papers presented at this session dealt with semiconductor detectors. In describing Si(Li) semiconductor detectors manufactured in the GDR, K. Schwerdt stated their resolution as 10 keV (at 300°K) and 3 keV (at 77°K) for Cs^{137} beta particles and 0.7 keV at the 59.5 keV line (Am^{241}) using a cooled field-effect transistor preamplifier. J. Chwaszczewska (Poland) reported on the development of semiconductor implantation detectors made of n-silicon of practically any quality. F. Kasak (Czechoslovakia) noted the particular features of growing large Ge(Li) detectors with high resolution (2.4 keV for Co^{60}).

The Conference noted the widespread use of radioisotopic instruments. I. Kubalek reported that in Czechoslovakia densitometers, thickness gauges, level gauges, etc., for use under strenuous operating conditions are designed on the basis of a system of Tesla units. The detector units use ionization chambers with MOS transistor preamplifiers. T. Pecurar (Rumania) described a system of 12 radioisotopic instruments including several level gauges (from a differential level gauge with an accuracy of ±0.1 mm used in glass production to a 12-channel instrument for blast furnaces), a combined densitometer–humidity gauge with digital readout, etc. The RTRNM thickness gauge (F. E. Leitis et al., USSR) with the detector and source located on the same side is based on measuring beta radiation reflected from air behind the measured material. The instrument measures thicknesses of 2-30 g/m^2 with an accuracy of 1.5% The "Orimet" thickness gauge (Czechoslovakia) is used to measure coatings on both sides of tape in the range 3-300 g/m^2 (J. Kuba, Czechoslovakia).

V. V. Terekhov (USSR) noted that optimum control of industrial processes requires not only thickness gauge readings but also statistical data processing. This function is provided by the SAK-1 statistical quality analyzer.

Different measuring methods are used in a tracking liquid-level gauge (H. Ruder, GDR) for up to 30 m range and in the scintillation level gauge, the RSUR-1 regulator (I. I. Kreindlin et al., USSR), operating in the 500 mm range and using a linear source so that an absorber-corrector is not needed.

Radioisotopic instruments are widely used for measurements in gaseous media. The "C-Meter" instrument (A. Unchkovsky, Czechoslovakia) measures gas flow rates of less than 1 m/sec to within ±5%. The IZV-1 instrument (N. V. Ryabov et al., USSR) has been designed for monitoring dust contents of 0.5 mg/m^3 and more in air in mines, and is based on the measurement of alpha particles.

A prominent place in the discussions of the group on nuclear medical instruments and techniques occupies the application of nuclear devices in diagnosis and analysis: liquid scintillation counters for spectrometry of C^{14} and H^3 labeled samples (L. Steenbeck, GDR), multichannel accumulators in scintillography (H. A. Altenbrunn, H. Nauber, I. Markwart, GDR). New results and techniques were reported in the use of radioactive isotopes for medical purposes. Several papers dealt with the advances in nuclear medical instrumentation in Hungary. A. Billing (Hungary) described special-purpose computing units manufactured by the "Gamma" factory which prepare the accumulated data for computer processing (background subtraction, division of the number of pulses by a given number).

Special attention has been devoted at the Conference to radiation monitoring techniques. New thermoluminescent radiation monitors based on LiF, type DTM-1 and DTM-2 (Poland), have a measuring range of $0.1\text{-}10^4$ rad and an accuracy ±5%; the VA-M-65 radiation meters (H. Linemann at el., GDR) operate within the range $0.5\text{-}10^3$ rad. Of great interest was the report of W. Stolz (GDR) on the development of "Doona-Lum" radiation monitors using LiF phosphors for measurements in the millirad region down to 1 mrad.

Narrow-range (0.003-3 R) dosimetry with uniform energy characteristics from 15 keV to 3 MeV can be accomplished with personal radiation monitors using ionization chambers (A. Archakov, V. Nosenko, USSR). Ionization chamber monitors can be made very small such as, for example, the "Aldo" (Poland)

pocket monitor that audibly signalizes that the allowable dose has been exceeded and whose dimensions are 137 × 70 × 25 mm. The instrument has three thresholds 0.03, 0.3, and 3 R and a tolerance of ±10% in the 0.04-1.5 MeV energy range.

The VA-J-100 roentgenometer (GDR) uses two counters to provide a very wide measuring range from 0.015 mR/hr to 250 R/hr in the energy interval from 0.15 to 2 MeV. The VA-J-100 is built in a new standardized shockproof case (7 g) employed also for other portable instruments (195 × 165 × 82 mm, 3 kg).

The scintillation method is preferable to the ionization method in radiation monitors for both continuous and pulsed x-ray or gamma radiation (M. I. Arsaev et al., USSR). The DRG-1 (0.1-300 μR/sec, 30-3000 keV), DRG-3 (0.01-1000 μR/sec, 20-3000 keV), and the pulsed DRGI-1 (0.1-100 μR/sec, 15-1250 keV) radiation monitors have miniature detectors and simple dc amplifiers. Their accuracy is ±10% and their hardness dependence is 15-20%. In this connection it is interesting to note photosemiconductor scintillation detectors described by I. Fitz (GDR) that form a combination of an organic scintillator and photoresistance. The measuring range of a simple roentgenometer of such type is $1\text{-}10^3$ rad/hr with an accuracy of ± 5%.

Dörschel and Birgit (GDR) discussed a method of personal neutron dosimetry ($0.1\text{-}10^4$ rad) in which fission fragments are observed under a microscope in a number of materials after chemical etching. A system of emergency neutron dosimetry used in nuclear installations of the GDR has been described by W. Schmitt. The emergency set includes activation detectors, fission fragments detectors, and a LiF radiation monitor.

The REM-2 recombination chamber (Poland) connected to an Ecco-616 or VA-J-15 electrometer is used for measuring equivalent doses of mixed radiation. The instrument operation is based on the proportional dependence of the ion collection efficiency of a chamber operating in the column recombination region on the radiation quality factor. The error in effective dose values is ±30%.

The problem of air contamination in mines by radon fission products has been discussed by K. P. Markov et al., (USSR). The type 2413-01 portable monitor for periodical testing weighs 4 kg and has a "latent energy" measuring range of $10^4\text{-}10^7$ MeV/liter, while the automatic type RKAZ-01 monitor operates continuously in the range $6.5 \cdot 10^3\text{-}6.5 \cdot 10^6$ MeV/liter (Rn concentration from $5 \cdot 10^{-12}\text{-}5 \cdot 10^{-8}$). Methods and instruments for quantitative analysis of beta-active inert gases have been discussed by L. V. Artemenkova et al., (USSR) who reported a sensitivity of 10^{-11} Ci · liters^{-1}/pulses · sec^{-1} for some isotopes. I. Moravek, I. Pietrik, and É. Hladky (Czechoslovakia) described a threshold system for automatic monitoring of the beta activity of reactor coolants.

Papers were also read dealing with general aspects of instruments for the measurement of dose rates, and radioactive contamination of the air, water, and surfaces (R. Ott, D. Hermann, E. Meiwald, E. Stranze, GDR) and with special demands presented to radiation monitors in nuclear power stations (K. Willun, GDR).

Both the Conference and Exhibition reflected the advances in nuclear and isotopic instrument design as well as the growing specialization in this field of the member countries of the Comecon.

The proceedings of the Conference are scheduled to be published in the beginning of 1971.

INTERNATIONAL CONFERENCE ON LASER PLASMA

G. V. Sklizkov

An international conference whose topic was heating solid plasma to thermonuclear temperatures by laser radiation and the use of laser plasma for injection purposes was held in November 1970 in Moscow. More than 350 Soviet and 40 foreign scientists from England, German Democractic Republic, Italy, Canada, Rumania, USA, France, Federal Republic of Germany, Czechoslovakia, and Japan participated in the Conference. The 42 papers read at seven sessions were devoted mainly to two subjects: 1) heating of plasma by laser radiation (gas dynamics and kinetics of nonequilibrium plasma states, interaction of laser radiation with superdense plasma, plasma heating for thermonuclear fusion purposes) and 2) the behavior of laser plasma in magnetic fields and its utilization for filling magnetic traps, application of multiply charged laser plasma as ion source for accelerators and in spectroscopy. A system of review papers was accepted at the Conference. All more interesting papers were read by the authors in the form of brief reports.

The Conference was inaugurated by Academician N. G. Basov who noted the prospects of laser plasma in various thermonuclear applications.

The application of lasers for creating pulsed thermonuclear reactions has been discussed in review papers by O. N. Krokhin (FIAN, USSR), A. A. Vedenov et al., (I. V. Kurchatov IAE), P. P. Pashinin (FIAN), J. Bobin, F. Floux, and G. Tonin (Limeil, France), and R. Pease and I. Spalding (Callem, England). From these reports follows that with pulsed heating of a solid mixture of deuterium and tritium without the application of containment methods the Lowson condition $n\tau \geq 10^4$ (at $T = 10^8$ °K) is satisfied with a laser energy of $\sim 10^5$ J, pulse duration 10^{-9} sec, and an initial density of 10^{23} cm^{-3}. To increase $n\tau$ one must use more elaborate targets with inertial containment by a heavy body. No such models (mathematically substantiated) have been presented to the Conference.

O. N. Krokhin discussed the conditions for using the inertial containment mode for creating physically favorable thermonuclear reactions. The parameters characterizing the conditions of inertial heating were evaluated. Various schemes were considered using cumulative effects in gas dynamic heating conditions.

Estimates for gaseous targets of relatively low density and laser pulses of several tens of nanoseconds indicated that to provide a positive thermonuclear yield the laser energy has to be the same order of magnitude. Inertial containment by a heavy shell and "freezing" of thermal conductivity by a magnetic field is presupposed. Similar calculations were performed in Limeil (France) where it was intended to set up a magnetic field by a compression shell producing 10^7 G in a characteristic volume of several millimeters. At the same time it is also possible to "contain" alpha particles. It is thus seen that the problem of obtaining $n\tau \geq 10^{14}$ is apparently technically realizable and it is hoped that the energy yield can be increased by increasing the laser energy and using more intricate targets.

One should note the reports that reflected the research programs in topics discussed at the Conference.

Bobin, Floux, and Tonin reported that a yield of $\sim 3 \cdot 10^4$ neutrons per laser pulse of 60 J and 3.5 nsec duration has been observed in the interaction of laser radiation with solid deuterium targets. Much attention is devoted in Limeil to a theoretical and experimental investigation of nonlinear absorption of high-intensity light in plasma. Theoretical estimates indicate that nonlinear absorption in CO_2 lasers is considerably greater than in neodymium lasers. It is assumed that nonlinear absorption is a necessary condition for favorable thermonuclear reactions to occur.

R. Pease and I. Spalding (Callem, England) discussed inertial containment of laser plasma. It has been established that the laser energy necessary for an energetically favorable thermonuclear reactor using

Translated from Atomnaya Énergiya, Vol. 30, No. 6, pp. 552-554, June, 1971.

a D-T mixture of normal density at $T \approx 10^4$ eV is of the order 10^8-10^9 J. The energy needed for initiating the "burning," of the mixture can be significantly reduced by providing burning conditions that can be realized at the expense of high electron thermal conductivity. The energy can also be reduced by preliminary fuel compression (e.g., in a laser-produced shock wave) or by using a heavy shell of high Z.

I. Spalding cited estimates of the energy required to heat plasma of a density 10^{17} cm^{-3} confined by a toroidal magnetic trap. Assuming anomalous absorption of laser radiation in plasma, the energy amounts to $\approx 10^8$ J for CO_2 lasers. In the case of periodic ($\sim$100 Hz) injection in a stellarator the laser radiation energy is abour 10^5 J at 10^4 GW.

Physical properties of laser plasma were discussed in papers by A. Haught and W. Fader (United Aircraft Corp., USA), G. Tonin and J. Bobin (Limeil, France), I. Fabre (École Polytechnique, France), W. Millard (Callem, England), and others. A. Haught described the results of a detailed analysis of the physical properties of plasma in a magnetic field of open-trap configuration. The feasibility of using laser plasma for high-efficiency injection into thermonuclear devices has been proved both theoretically and experimentally. Experiments have been made on the diagnosis of injected plasma by SHF transmission and laser radiation scattering methods, as well as with the aid of diffraction, probe, spectroscopic, and mass spectrometric techniques. The target was a 10-50 μ lithium hydride particle heated by a laser with an energy of nearly 10 J. It was established that the disagreement between theoretical and experimental results concerning plasma expansion asymmetry is due to inhomogeneous recombination and not to the effect of nonhydrodynamic radial acceleration. A. Haught also suggested the use of laser plasma as a target for trapping a fast atom beam.

W. Fader described the results of an experimental investigation of the process of injection of laser plasma in a mirror trap with 8-kOe field at the minimum which agree with the simple hydrodynamic model of plasma interaction with a magnetic field. It has been found that plasmas with a density $3 \cdot 10^{13}$ cm^{-3} and temperature 100 eV can be contained for 150 μsec.

G. Tonin and I. Fabre investigated the dynamics of the development of plasma clusters under conditions of relatively high densities and short times when the effect of instabilities is negligible. The field intensity reached 300 kG (Tonin) and 50 kG (Fabre). The occurrence of a reflected shock wave and magnetic back pinching of the plasma has been observed.

P. P. Pashinin (FIAN, USSR) suggested the use of a strong magnetic field for reducing the dispersion and transverse thermal conductivity in the process of heating of a long gaseous cylinder bounded by a solid shell.

W. Millard (Callem, England) reported on a run of experiments on the injection of beryllium plasma into the Proto-Cleo stellarator. The neodymium laser used for these injections generated 25-nsec pulses of 15 J. The plasma density was 10^{13} cm^{-3} at a temperature of 5 eV and $2 \cdot 10^{11}$ cm^{-3} at 30 eV. At a density $4 \cdot 10^{11}$ the containment time was several milliseconds. Detailed measurements proved that the first to form in a laser plasma were chiefly positive beryllium ions with a temperature 500 eV. After some time the ion temperature fell to 5 eV. This effect is explained by charge transfer among ions and neutrals in 10^{-4} sec.

On investigations of the behavior of laser plasma in magnetic fields reported H. Schwartz (Hartford Pólytechnic Institute, USA), G. A. Askar'yan et al., (FIAN, USSR), G. G. Dolgov-Savel'ev and V. N. Karnyushin (Novosibirsk, USSR), and M. P. Bedilov (Tashkent, USSR).

Progress in the design of high-power lasers was discussed in several papers.

In a review report P. N. Kryukov and Yu. V. Senat-skii (FIAN) discussed basic problems encountered in the design of high-power neodymium-glass lasers. The authors achieved an angle-averaged radiation brightness of 10^{19} W/cm$^2 \cdot$sr. Present laser techniques make it possible to attain light powers of up to 10^{12} W and energy concentrations in matter of up to 10^7 J/cm^3 at an energy release rate of more than 10^{17} W/cm^3. Two lasers delivering pulses in sequence can be used to increase absorption of laser radiation in the target. The second and fourth laser harmonics also can be used for plasma heating to increase high-density absorption. Provisional experiments indicate that the converters have sufficient strength and that the conversion efficiency exceeds 50%. The main factor that limits laser energy in 10^{-9}-10^{-11} sec pulses is the destruction of glass as a result of self-focussing. A significant effect on performance arises from radiation reflected from the target which for a duration of 10^{-11} sec is comparable to the primary beam.

S. Yamanaka (Osaka Univerisity, Japan) reported on a program of research and application of high-power lasers in plasma heating. Japanese workers built a neodymium-glass laser with a maximum energy of 120 J and a divergence of 10^{-3} rad. The laser can be operated in three modes with respective pulse durations of $3 \cdot 10^{-8}$, 10^{-9}, and 10^{-11} sec. The laser energy is limited by destruction of the active rods which takes place at 15 J/cm^2 in rods with platinum and 400 J/cm^2 in platinum-free glass. The surface destruction threshold was 30 J/cm^2. The laser is used for the following investigations: 1) injection of plasma into existing thermonuclear devices, 2) investigation of plasma instabilities in a magnetic field, 3) heating of laser plasma in order to create a "minimal thermonuclear explosion." Of particular interest is the communication of S. Yamanaka about a $PoCl_3$:$ZnCl_4$ liquid amplifier that provided a gain of about 20 at 10 MW in a short-pulse mode.

Ions with an energy of 400 eV were recorded by probe methods in heating a LiH particle by laser; in case of carbon targets the ion energy exceeded 1 keV. Single neutrons were observed in the course of heating of a LiD particle.

R. Sigel and S. Witkovsky (Max Planck Institute, Hartsching, FGR) reviewed the results of an investigation of laser plasma properties. One should take notice of the four-channel device for measuring temperature from plasma x-ray radiation and of the advanced technique of preparing solid deuterium targets. Temperatures of 700 eV were attained with a 30-J, 30-nsec laser beam. The radiation flux on the target was then equal to $1.5 \cdot 10^{13}$ W/cm^2.

W. Keiser and H. Puell (FGR) reviewed the work on plasma heating conducted at the Higher School of Engineering in Munich. The obtained theoretical results are in good agreement with experimental data. The experiments were made with three materials: lithium deuteride, polyethylene, and carbon. A temperature of 320 eV has been obtained with 1 GW laser power and a light flux density of $5 \cdot 10^{12}$ W/cm^2. For carbon and LiD targets the maximum expansion energy was 13 and 3.5 keV respectively.

G. V. Sklizkov et al., studied the initial stage of motion of laser plasma in gas dynamic expansion conditions. They measured the time dependence of jet pressure during the laser pulse.

Several papers dealt with theoretical aspects of interaction of high-power light beams with dense plasma. P. Kaw (Princeton, USA) reported the results of a theoretical study of parametric instabilities near the critical frequency. P. P. Volosevich et al., and I. V. Nemchinov studied the initial stage of plasma heating and the effect of re-emission on heating. N. G. Basov, O. N. Krokhin, S. D. Zakharov et al., studied the theoretical and experimental aspects of high-temperature plasma heating by plasma radiation of ultrashort duration.

The use of laser plasma for producing a large number of ions with a charge of more than 20 has also been reported at the Conference. Of special interest are the theoretical studies of O. N. Krokhin, Yu. V. Afanas'ev et al., concerning the kinetic and hydrodynamic processes in multiply ionized laser plasma.

Yu. P. Raizer (Moscow) and A. Engelhardt (Quebec, Canada) discussed gas heating by continuous radiation including CO_2-laser radiation.

The Conference once more confirmed the possibilities of high-power lasers in thermonuclear research, in plasma physics, and in other physical and astrophysical applications. The organization of such a representative conference reflects the growing interest on the part of theoretical and experimental workers in high-temperature laser plasma.

SYMPOSIUM ON NEW DEVELOPMENTS IN PHYSICAL AND BIOLOGICAL DETECTORS OF RADIATION

V. I. Ivanov

In November 1970 the International Atomic Energy Agency held a symposium in Vienna on new developments in physical and biological detectors of ionizing radiation. Approximately 160 specialists from 28 countries and four international organizations took part in the work of the symposium.

In recent years there have been a number of advances in scientific research and practical developments in the field of ionizing-radiation detectors designed for radiation dosimetry. The transition ionization chambers and photodosimeters have been superseded by new solid-state detectors. These are chiefly semiconductor and luminescent detectors.

At the Vienna symposium a large number of reports were devoted to luminescent methods. These included surveys and program reports (F. Allix, United States; J. Jones et al., England), results concerning new luminophore compositions (G. Webb et al., United States; G. Portal et al., France; T. Hashizume et al., Japan), and reports on improvements in existing detectors and techniques for recording their readings (D. Uran, Yugoslavia; L. Better-Jensen, Denmark, and others). The reports dealt mainly with the dosimetric properties of the detectors, and very little attention was devoted to the mechanism of luminescence.

Special attention was given to questions concerning the use of thermoluminescent detectors (TLD) for determining the equivalent dose of mixed gamma and neutron radiation. One of the interesting ideas (F. Attix, United States) consists in using a mixture of different TLDs with an Li^6/Li^7 isotope ratio such that the dosimeter readings will be proportional to the equivalent dose for the case of simultaneous irradiation with gamma quanta and thermal neutrons. Such a dosimeter has low sensitivity to higher-energy neutrons, but on the surface of the human body it will be capable of recording the thermal neutrons produced by the interaction of primary neutrons with biological tissue. The variation of the albedo as a function of the energy of neutrons impinging on the body is such that the dosimeter readings in the case of irradiation with gamma rays and reflected thermal neutrons will be proportional to the equivalent dose of mixed radiation in a range of primary-neutron energies from thermal energies to 10 keV. For higher neutron energies it was proposed (V. V. Kúz'min, I. P. Mysev, and A. D. Sokolov, USSR) that TLDs should be used with luminophores which are highly sensitive to heavy charged particles. The hydrogenous material in which the luminophore is dispersed is used as the sensitive element of a dosimeter for measuring the equivalent dose of neutrons in the energy range from 10 keV to 10 MeV.

There were three reports on exoelectronic dosimeters. Although exoelectronic emission has long been known, the first publications concerning the use of this phenomenon for dosimetry appeared relatively recently. Because of the complexity of recording low-energy exoelectrons, the unsatisfactory reproducibility of the readings, and other undesirable features, exoelectronic dosimeters have not yet been used in practice. Although the discussion of these questions included some pessimistic comments concerning prospects for the use of exoelectronic dosimeters, there was also an interesting report by A. I. Beskorskii et al. (USSR) proposing a variant of exodosimetry using manganese-activated calcium sulfate for practical applications.

K. Becker and a group of other American scientists presented a study which dealt with increasing the sensitivity of a beryllium oxide emitter by heat-treating its surface and embedding atoms of platinum, palladium, and gold. They obtained encouraging results: doses of less than 1 mr were measurable with a reproducibility of 2-5%.

Translated from Atomnaya Énergiya, Vol. 30, No. 6, pp. 554-555, June, 1971.

With regard to semiconductor detectors, the most interesting reports were those concerning the use of detectors with internal amplification. American scientists used such a detector for making plutonium measurements in vivo. A. Peiret-Lavine et al. (France) used silicon detectors operating in cascade for soft x-ray spectrometry. The dosimetric characteristics of silicon diffusion-drift detectors of gamma radiation and spectrometric characteristics of germanium detectors with radiation defects were considered in two Soviet reports (E. L. Stolyarova et al.).

A survey report by V. I. Ivanov (USSR) presented studies conducted by Soviet scientists on the dosimetric use of such phenomena as the rotation of the polarization plane in optically active solutions (S. V. Starodubtsev, V. V. Generalova, et al., USSR), the specific temperature distribution in a calorimetric solid under irradiation with a mixture of gamma rays and neutrons (B. A. Briskman and V. L. Savina, USSR), and the occurrence of potential differences when electrodes separated by some distance in a vacuum are subjected to irradiation (N. D. Rozenblyum, M. G. Mittel'man, et al., USSR).

Reports by R. Hosemann (Federal Republic of Germany) and V. I. Ivanov (USSR) dealt with the dosimetric use of direct-charge detectors (DCD), known in the literature as "irradiation elements." These detectors have not come into widespread practical use because they did not seem capable of competing with other methods. The Soviet report dealt with new patterns of behavior of DCDs which opened up broader possibilities for their use (e.g., for use as threshold detectors of photon radiation).

Other reports from the Soviet Union dealt with a tissue-equivalent spherical proportional counter (I. M. Dmitrievskii, Yu. D. Lysak, and V. V. Frolov), the measurement of fast-neutron spectra with threshold detectors (E. A. Kramer-Ageev et al.), ionization chambers with liquid dielectrics (V. I. Ivanov, E. D. Kleshchenko, and V. V. Frolov), and the comparison and analysis of parameters of clinical spectrometers for human-body radiation (G. A. Fedorov, I. E. Konstantinov, et al.).

Some of the reports were devoted to track detectors, based on the appearance of damage tracks when charged particles pass through certain insulators. Such detectors can be used in neutron dosimetry in accident situations. The recorded damage tracks appear only in cases of irradiation with particles having sufficiently high values of linear energy loss, which makes them practically insensitive to photon radiation. The interpretation of the tracks requires a cumbersome procedure, and this limits the applicability of track detectors in dosimetric practice. In some reports it was demonstrated that the tracks could be counted by a special apparatus which facilitates the dosimetry.

One meeting of the symposium was devoted to methods of calibrating dosimetric detectors, obtaining more precise values of conversion factors, selecting the materials for the detector walls, determining the dosimetric characteristics of instruments, and comparing the results of the measurements made. Some interest was aroused by the report of Yu. O. Kostyleva and I. O. Mysev (USSR), which discussed in detail the conditions required for electron equilibrium when thin-walled detectors designed for measuring exposure doses were calibrated in a beam of photons. The authors calculated a first approximation to the necessary conditions for accurate measurements.

A number of reports were devoted to biological detectors of radiation. The method which attracted the most attention involved chromosome aberrations, the frequency of which depends on the dose, the nature of the radiation, and the biological characteristics of the organism. Most of the authors suggested that doses could be estimated from an analysis of chromosome disturbances in the lymphocytes of the peripheral blood in the human organism. The standard dosimeter suggested in such cases is a cell culture which has been incubated and irradiated in vitro. It is still too early to speak of a perfected precise procedure for measuring doses on the basis of biological effects, but scientists from Bulgaria (S. Todorov and D. Teslev) and Yugoslavia (M. Traikovic et al.) presented specific examples of the use of biological dosimetry in cases of accidental and chronic irradiation.

The symposium was well organized, and the number of reports was not excessive, so that it was possible to devote considerable time to useful discussions.

WIDEBAND CRUCIFORM RADIO TELESCOPE RESEARCH

*Trudy #38 of the P.N. Lebedev Physics Institute**

Edited by **D. V. Skobel'tsyn**
Director, P.N. Lebedev Physics Institute
Academy of Sciences of USSR, Moscow

Translated from Russian

Concentrating on both construction and operation of radio telescopes, this volume deals with such specific problems as the weight of the structure, loads imparted by the wind, and the means for taking them into account. The tracking system and other components are also described, and the versatility of the instrument is demonstrated in observations of the solar supercorona and measurement of radio wave frequencies. This volume is an invaluable reference source for radio astronomers and engineers called upon to design their radio telescopes. Contributions are based on work done at the Lebedev Physics Institute, recently lauded by *Physics Today* for "the quality and imaginativeness" of its work.

CONTENTS: Control system for the east-west array of the DKRT-1000 cruciform radio telescope, **Yu. I. Alekseev** • Directional diagram frequency control in a wide band antenna array with cophasal signal summation at an intermediate frequency, **I. A. Alekseev and S. N. Ivanov** • Electrical beam control in a wideband antenna array with zoned phase inverters with frequency change, **Yu. P. Ilyasov and S. N. Ivanov** • Use of remote preamplifiers in meter-range antenna arrays, **R. D. Dagkesamanskii, S. N. Ivanov, and Yu. P. Plyasov** • Resolution of correlation arrays, **Yu. P. Ilyasov and Yu. P. Shitov** • Response of multielement correlation arrays to several sources, **Yu. P. Shitov** • Rigidity of a parabolic reflector loaded by its own weight (vertical position), **P. D. Kalachev** • Evaluation of the rigidity of a parabolic reflector loaded by its own weight (symmetrical loading), **P. D. Kalachev** • Investigation of the solar wind and brightness distribution of radio emission sources during observation of their scintillations, **V. V. Vitkevich** • Observations of scintillation of radio sources on inhomogeneities in interplanetary plasma, **T. D. Antonova, V. V. Vitkevich, and V. I. Vlasov** • Observations of the solar supercorona in 1964-1965 and the C character of scattering inhomogeneities in the supercorona, **V. F. Bedevkin and V. V. Vitkevich** • Measurement of the polarization of the total radio emission flux of the crab nebula at 3.3 and 1.6 cm, **V. A. Udal'tsov** • Increasing radiometer reliability. An automatic volume control system for transistorized radioastronomical detectors, **V. N. Brezgunov and V. A. Udal'tsov** • A modification of the interference method for polarization measurements of plane-polarized radiation, **V. A. Udal'tsov** • Selection of optimum parameters of radio telescope servosystems with allowance for wind disturbance, **G. G. Basistov** • Plasma escape from the sun, **M. V. Konyukov** • Amplitude fluctuations during propagation of electromagnetic waves in media with random characteristics, **V. I. Shishov** • A possible mechanism of nonequilibrium solar radio emission by decay electrons, **N. G. Basov and V. V. Vitkevich** • Radio wave frequency and propagation time in a spherically symmetrical gravity field, **B. M. Chikhachev** • A method for measuring the gravitational shift of radio wave frequency in an artificial earth satellite experiment, **B. M. Chikhachev.**

CB Special Research Report
Approx. 190 pages 1969 $22.50

*Place your continuation order today for books in this series. It will ensure the delivery of new volumes **immediately** upon publication; you will be billed later. This arrangement is solely for your convenience and may be cancelled by you at any time.

PLENUM PUBLISHING CORPORATION
Plenum Press • Consultants Bureau • IFI/Plenum Data Corporation
227 WEST 17th STREET, NEW YORK, N. Y. 10011

In United Kingdom: Plenum Publishing Co. Ltd., Donington House, 30 Norfolk Street, London, W.C. 2.